RADIATION FIELD SHAPING THROUGH LOW TEMPERATURE THERMAL-SPRAY IN RADIOTHERAPY

JACOBUS GERT VAN DER WALT

Thesis submitted in fulfilment of the requirements for the Degree

DOCTOR TECHNOLOGIAE:

ENGINEERING: MECHANICAL

in the

Department of Mechanical Engineering
Faculty of Engineering, Information and Communication Technology

at the

Central University of Technology Free State

Supervisor: Prof DJ de Beer, D TECH (Mech. Eng.)
Co-supervisor: Prof M Truscott, Ph. D. (Microbiology)
Co-supervisor: Dr FCP du Plessis, Ph. D. (Medical Physics)

BLOEMFONTEIN
July 2009

DECLARATION WITH REGARD TO INDEPENDENT WORK

I, JACOBUS GERT VAN DER WALT, identity number [redacted] and student number 8721979, do hereby declare that this research project submitted to the Central University of Technology Free State for the Degree DOCTOR TECHNOLOGIAE: ENGINEERING: MECHANICAL, is my own independent work; and complies with the Code of Academic Integrity, as well as other relevant policies, procedures, rules and regulations of the Central University of Technology Free State; and has not been submitted before to any institution by myself or any other person in fulfilment (or partial fulfilment) of the requirements for the attainment of any qualification.

_____ _____

SIGNATURE OF STUDENT **DATE**

ACKNOWLEDGEMENTS

First of all I would like to give praise to my Heavenly Father for giving me the mental and physical ability to complete this study.

I would like to thank my supervisor Prof. Deon de Beer and co-supervisors Prof. Michele Truscott and Dr. Freek du Plessis for their help, advice and time.

I would also like to say thank you to my brother, Mr. Karel van der Walt for his help in developing electronic circuitry as well as software for my research project.

Without a grant from the National Research Foundation and funding from the CUT Innovation Fund this research would not have been possible. Thank you to these institutions.

Last but not least I would like to thank my colleagues, friends and family for their help, support and motivation in this undertaking.

ABSTRACT

Superficial cancerous lesions are commonly treated through low energy X-ray or electron radiation in radiotherapy. The treatment units that produce the radiation are equipped with square, rectangular and round applicators of different sizes. These applicators attach to the treatment units and define the radiation field size applied during treatment. An applicator is chosen to fit the shape of the cancerous lesion on the patient as closely as possible. Since cancerous lesions are irregular in shape, there will always be an area of healthy tissue between the edge of the lesion and the edge of the standard field shape. This healthy tissue will be irradiated along with the lesion during treatment which is undesirable since the cancer wound heals through reparative growth of the surrounding healthy tissue after treatment. Traditional techniques that were developed to shield this healthy tissue and thus shape the radiation field to the shape of the lesion present various shortcomings.

This study introduces a new thermal-spray process for producing radiation field shaping shields which overcomes most of the shortcomings encountered with the traditional field shaping techniques. Since none of the commercially available thermal-spray equipment could be used to produce field shaping shields, new thermal-spray equipment was designed and fabricated tailor made to the application. Different techniques to determine the contours of the treatment area on the patient were investigated. These included a patient contact technique using a plaster bandage impression and a non-contact technique using 3D laser scanning. From the plaster bandage impression a plaster model can be produced onto which a high density low melt material such as Wood's alloy can be thermally sprayed to produce a field shaping mask. A model can also be produced from the 3D laser scanning data through laser sintering (LS) in nylon polyamide powder or through computer numerical controlled (CNC) milling in a block of low density polyurethane. The thermal-spray technique was evaluated by

comparing the field shaping ability of radiation shields produced through the technique to the field shaping ability of shields produced through the traditional techniques. Radiographic film was used for this purpose and the results are presented in the form of isodensity charts. The required thicknesses of thermal-sprayed field shaping masks to shield radiation of various energies were also determined. The thicknesses were determined through radiation transmission measurements of known thicknesses of sprayed sheets of Wood's alloy. X-ray imaging showed that there were no defects present within thermal-sprayed layers of Wood's alloy that may negatively affect the shielding ability of masks produced through the technique.

UITTREKSEL

Oppervlakkige kankeragtige letsels word algemeen behandel deur middel van lae energie X-straal of elektron bestraling in radioterapie. Die behandelingseenhede wat die bestraling produseer is toegerus met vierkantige, reghoekige en ronde toedieners van verskillende groottes. Hierdie toedieners koppel aan die behandelingseenhede en definieer die bestralingsveldgrootte wat toegedien word tydens behandeling. ‘n Toediener word gekies om die vorm van die kankerletsel op die pasiënt so goed as moontlik te pas. Aangesien kankeragtige letsels onreëlmatig in vorm is, sal daar altyd ‘n area van gesonde weefsel tussen die rand van die letsel en die rand van die standaard veldvorm wees. Hierdie gesonde weefsel sal saam met die letsel bestraal word wat ongewens is aangesien die kankerwond genees deur regenererende groei van die omliggende gesonde weefsel na behandeling. Tradisionele tegnieke wat ontwikkel is om hierdie gesonde weefsel af te skerm en dus die bestralingsveld te vorm volgens die vorm van die letsel het verskeie tekortkominge.

Hierdie studie stel ‘n nuwe termiese-sproei proses bekend vir die vervaardiging van straling veldvormingskerms wat die meeste van die tekortkominge ondervind met die tradisionele veldvormingstegnieke oorkom. Aangesien geen van die kommersieel beskikbare termiese-sproei toerusting gebruik kan word om straling veldvormingskerms te vervaardig nie, is nuwe termiese-sproei toerusting ontwerp en vervaardig wat pasgemaak is vir die toepassing. Verskillende tegnieke om die kontoere van die behandelingsarea op die pasiënt te bepaal is ondersoek. Dit sluit in ‘n pasiënt kontak metode deur gebruik te maak van ‘n gipsverband afdruk en ‘n nie-kontak metode deur gebruik te maak van 3D laserskandering. Van die gipsverband afdruk kan ‘n gips model vervaardig word waarop ‘n hoë digtheid lae smeltpunt materiaal soos Wood se allooi termies gesproei kan word om daardeur ‘n veldvormingsmasker te vervaardig. ‘n Model kan ook vervaardig word vanaf die 3D laser skanderingsdata deur laser-sintering (LS) in nylon poliamiede poeier of deur rekenaar numeries-beheerde (RNB) freesmasjinering in ‘n blok lae digtheid poliuretaan. Die termiese-

sproei tegniek is geëvalueer deur die veldvormingsvermoë van stralingsafskerms vervaardig deur die tegniek te vergelyk met die veldvormingsvermoë van afskerms wat deur die tradisionele metodes vervaardig is. Radiografiese film is vir die doel gebruik en resultate word getoon in die vorm van iso-digtheidskaarte. Die nodige diktes van termies-gesproeide veldvormingsmaskers om straling van verskillende energië af te skerm is ook bepaal. Die diktes is bepaal deur stralingstransmissiemetings van bekende diktes van gesproeide plate van die allooi te neem. X-straalafbeelding het getoon dat daar geen defekte teenwoordig is in termies-gesproeide lae van Wood se allooi wat die afskermingseffek van maskers wat deur die tegniek vervaardig is negatief sal beïnvloed nie.

TABLE OF CONTENTS

CHAPTER 4

BREAST CANCER AND TREATMENT THEREOF

CHAPTER 9

EVALUATION OF THE THERMAL-SPRAY TECHNIQUE

ADDENDUM A2

ISODENSITY CHARTS

ADDENDUM A3

ISODENSITY CHARTS

ADDENDUM B1

REQUIRED THICKNESS OF THERMAL-SPRAYED MASKS

LIST OF FIGURES

LIST OF TABLES

LIST OF ABBREVIATIONS

APS	Atmospheric plasma spraying
BCC	Basal cell carcinoma
CAD	Computer aided design
CAM	Computer aided machining
CCD	Charged-coupled-device
CNC	Computer numerical control
CT	Computer tomography
DCIS	Ductal carcinoma in situ
FSD	Field-to-source distance
Gy	Gray
HVOF	High velocity oxy-fuel
LCD	Liquid crystal display
LCIS	Lobular carcinoma in situ
LED	Light emitting diode
LPPS	Low pressure plasma spraying
LS	Laser sintering
MU	Monitor units
PET	Polygon editing tool
RE	Reverse engineering
RF	Radio frequency
RP	Rapid prototyping
SAD	Source-to-axis distance
SCC	Squamous cell carcinoma
SDD	Source-to-diaphragm distance

SSD	Source-to-skin distance
TNM	Tumour node metastasis
VPS	Vacuum plasma spraying

CHAPTER 1

INTRODUCTION

1.1 Foreword

Skin and breast cancer have profound effects on the lives of many people everyday, not only physically but also emotionally. This project combines the study fields of engineering, radiotherapy and nuclear physics in an attempt to lend support in the ongoing fight against this crippling disease.

1.2 Problem statement

Superficial cancerous lesions are commonly treated by means of low energy X-ray or electron radiation in radiotherapy. The treatment units that produce the radiation are equipped with standard applicators of different sizes. These applicators attach to the treatment units and are used to define the treatment field sizes. An applicator is selected to fit the size of the lesion as closely as possible. The problem with the applicators is that those available are only able to produce square, rectangular or round field shapes while the lesions are irregular in shape. There will thus always be an area of healthy tissue between the edge of the lesion and the field's edge that will be unnecessarily irradiated during treatment. This problem becomes even worse when the lesion is large and situated across a curved area of the patient's body. Considering the fact that the treatment-end of the applicator that comes into contact with the patient's body during treatment is flat, there could be a considerable stand-off between the applicator and the patient's skin at the field's edges. This is especially problematic with

electron treatments since the electrons scatter past the edges of the treatment field with a stand-off resulting in a larger area being irradiated than intended. Existing methods of shaping the radiation fields are either too time consuming or do not accurately shape the radiation fields according to the cancer affected areas.

1.3 Hypothetical resolution

Some of the problems with existing field shaping techniques for low energy radiation in radiotherapy can be resolved by producing field shaping masks by means of low temperature thermal-spray. The equipment necessary for thermal-spray can be fabricated from affordable components with available tools.

1.4 Purpose of the study

The purpose of the study is to develop the necessary equipment as well as work procedures in order to implement an improved field shaping technique for low energy radiation in radiotherapy.

1.5 Importance of the study

Radiation field shaping masks produced through the thermal-spray technique is likely to show improvement over the existing methods of shaping radiation fields in terms of accuracy and production time. Should the thermal-sprayed masks prove to be more successful, patients with superficial cancerous lesions will benefit through an improvement in the quality of treatment they receive. The technologists that will produce the masks will also benefit by saving time.

1.6 Methodology

The methodology was as follows:

a) Gather information on existing field shaping techniques for low energy radiation in radiotherapy.
b) Gather information on existing thermal-spray equipment.
c) Design and construct the necessary equipment for low temperature thermal-spray.
d) Investigate what techniques could be used to determine the contours of the treatment area on the patient.
e) Determine what techniques could be used to produce thermal-sprayed field shaping masks according to the gathered contour information.
f) Evaluate the thermal-spray radiation field shaping technique through comparison with traditional field shaping techniques.
g) Determine the mask thicknesses required for effective shielding of different radiation energies through measurements.
h) Test thermal-sprayed masks for internal defects that may negatively influence the shielding ability of masks produced through the technique.

The composition of the thesis is represented in Figure 1.1 through a flowchart.

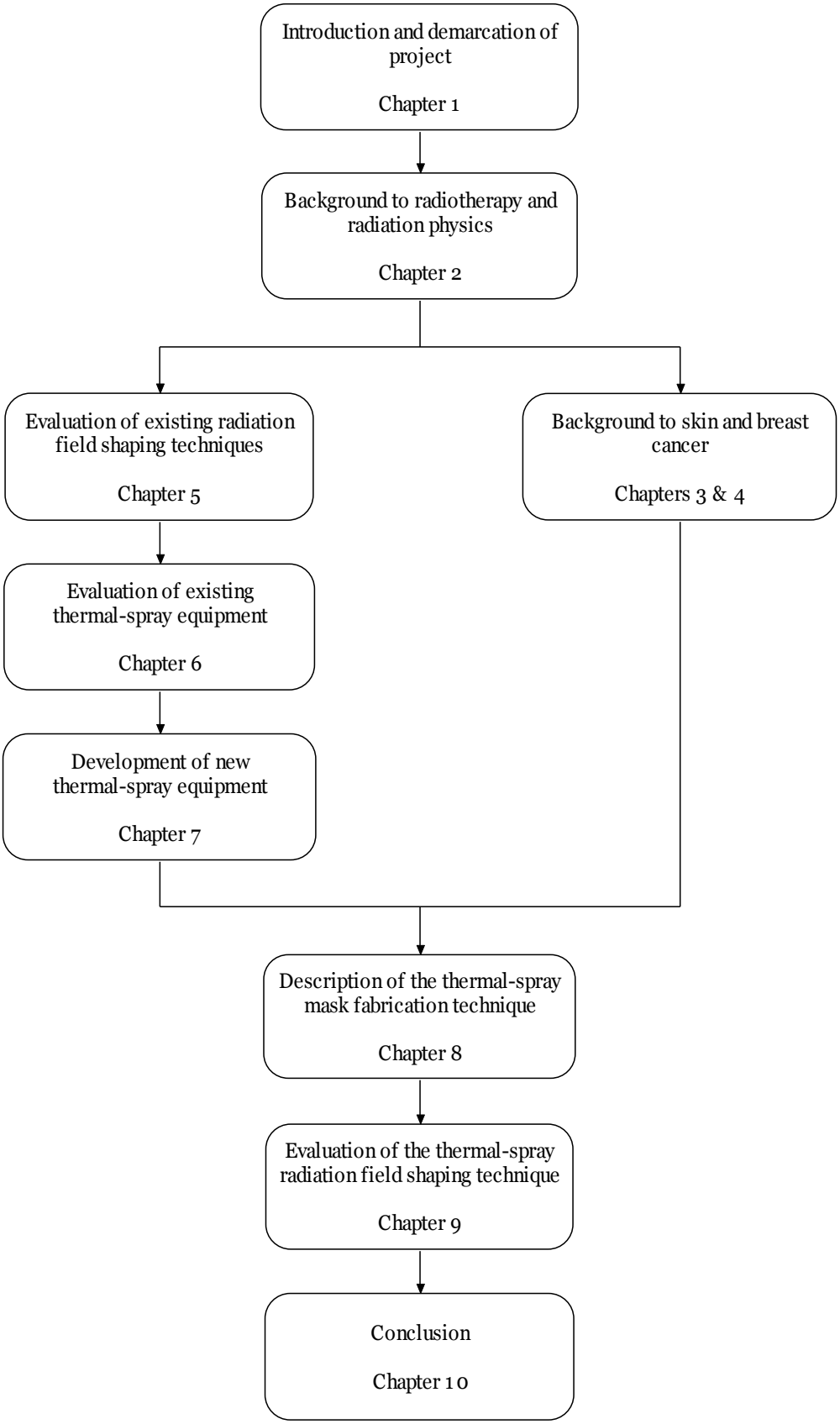

Figure 1.1 Flowchart of the composition of the thesis

CHAPTER 2

RADIOTHERAPY AND RADIATION PHYSICS

2.1 Introduction

The first patient with cancer was treated a mere four weeks after the publication of the momentous discovery of X-radiation by Wilhem Roentgen in 1895. Much progress has been made in the intervening time, but it is nonetheless humbling to recognize how far-seeing physicians and scientists at the turn of the century were to enlist the miracles of X-radiation in the battle against this most feared of human diseases [49, p. 1].

2.2 Radiotherapy

This section presents the reader with a brief explanation of what cancer is and how ionizing radiation is used in the treatment of the disease.

2.2.1 Normal and malignant growth

Cancer can be described as a pathological variation of normal growth. The mechanism through which growth takes place is by division and multiplication of cells within the body. The rate of growth varies widely from the foetus where growth is very rapid then gradually diminishes until adulthood. Cells divide and multiply at different rates within different tissues in the body. The lining of the epithelium of the intestine and the epidermis of the skin are for instance replaced continuously. Other organs such as the liver and kidney have a much lower

replacement rate. Nerve and muscle cells are all present at birth and can never be replaced if damaged later in life. Cell division and multiplication are under strict control and only take place where cells need to be replaced during the normal functioning of the body or to repair damaged tissue. Malignant cells are under no such controlling constraints and as a result multiply without taking the needs of the body into consideration [51, p. 11]. Examples of this lost of control is shown through the negative effect skin and breast cancer have on patients as explained in Chapters 3 and 4.

2.2.2 The biological effect of radiation on tissue

Ionization[1] is produced in living cells whenever X-rays or other types of ionizing radiation are absorbed in the body during radiation treatment. This ionization causes physical and chemical changes within cells which will interfere with the functioning of the cells. Both normal and cancerous cells are affected alike by these changes. If the radiation damage to the cells is small they will recover and function normally. Extensive damage however will cause some of the cells to be killed outright. Others will only die later while attempting to divide. The time it takes before this happens depends on the cell's growth rate. It may take only hours but then again it may not happen for days or weeks or even years. Because of the nature of cancer cells, ionization has a greater effect on them than it has on normal cells. After destruction of the cancer cells by irradiation, the wound heals by reparative growth of surrounding normal tissue. It is imperative that the radiation dosage (i.e. the amount of ionization) that is delivered to the growth does not exceed the tolerance of the surrounding normal tissue.

[1] The process of removing electrons from or adding electrons to neutral atoms thereby creating atoms with unbalanced electrical charges.

If this is the case, healing will not take place and the result will be a permanent necrosis. The aim of the radiation oncologist is to inflict the maximum damage on cancerous cells while retaining the reparative powers of the surrounding normal tissue [51, p. 87].

2.2.3 Radiosensitivity of tissue

Different types of cells and tissue reacts differently to a specified dose of radiation. Rapidly dividing cells will be seriously damaged by a dose which will have no obvious effect on cells with a slow rate of division. This resistance or vulnerability is referred to as sensitivity of tissue or growth and is of great importance in radiotherapy. Radiotherapy is possible only because most cancers are more radiosensitive than their surrounding tissue. The cancer cells can thus be lethally damaged by a dose of radiation which will weaken but not kill the surrounding normal tissue. If a cancerous growth has the same radiosensitivity as its surrounding tissue, radiotherapy will fail because a cancercidal dose would at the same time prohibit healing [51, p. 87].

2.2.4 Time and dose factors

In planning radiation treatment, not only what amount of dose needs to be delivered to the tumour needs to be decided, but also how this dose should be distributed over time. It was initially thought that a single large dose would be optimal for cancers in general. Negative side effects such as poor cosmetic results and necrosis however soon led to the use of smaller repeated doses over a longer period of time. This technique, which came to be known as protracted fractionation, is better tolerated by tissue and takes advantage of the difference in radiosensitivity between cancerous and normal tissues. The effectiveness of this technique is graphically represented in Figure 2.1.

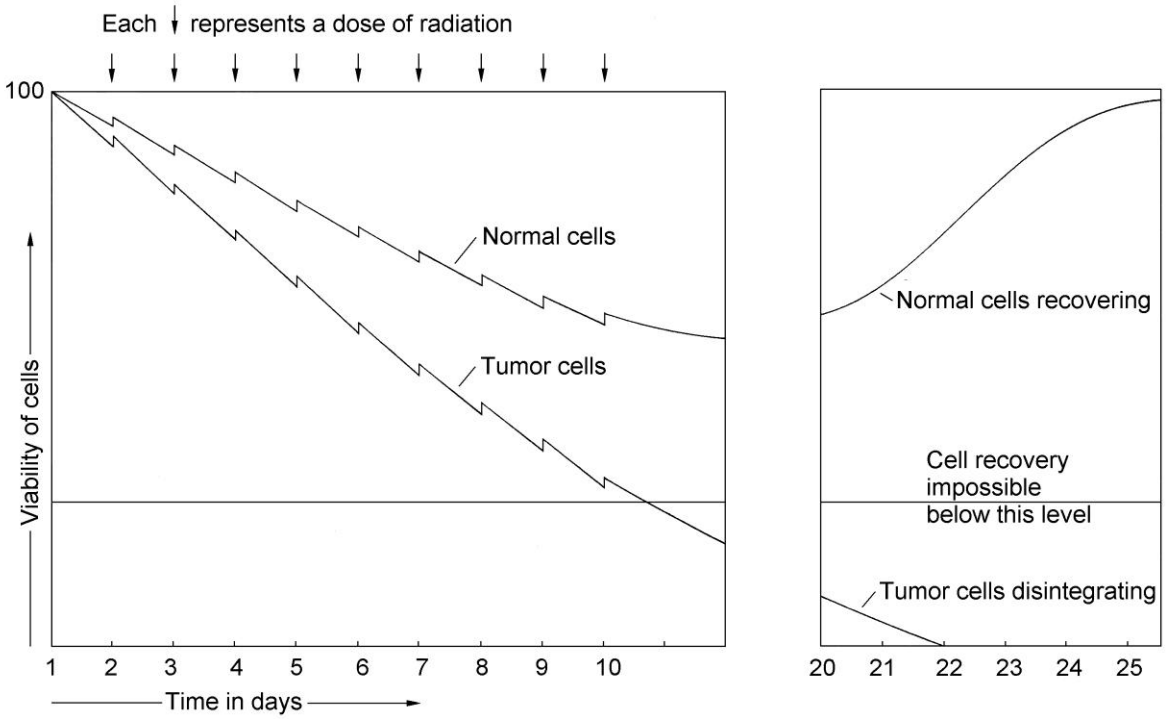

Figure 2.1 Schematic representation of a successful course of radiation treatment [51, p.80]

The cell viability gap between the cancer cells and the normal cells widens because the cancer cells suffer progressive damage as the treatment course proceeds. Eventually all tumour cells are irreversibly damaged while the normal cells still have the ability to recover [51, p. 79].

2.3 Radiotherapy treatment options

Today, there are various radiotherapy treatment options available for patients with malignant disease. These include the following:

- External beam therapy: Radiotherapy that is applied from outside the body by X-ray, gamma ray, electron or neutron beams.
- Intracavitary radiotherapy: Radioactive sources that are introduced into body cavities.

- Interstitial radiotherapy: Radioactive sources that are implanted into tissue.
- Nuclear medicine: Radioactive fluids that are introduced into the body via a vein or into a cavity.

The treatment that will be applied depends on the body site and type of cancer that affects the patient [51, p. 73]. For the purpose of this study only external beam radiotherapy, in particular X-ray and electron radiation will be described in detail.

2.3.1 Production of low energy X-rays

Low energy X-rays are produced by means of a special X-ray tube as shown in Figure 2.2. The tube consists of a cathode (negative electrode) and an anode (positive electrode), both sealed in an evacuated glass envelope. The cathode is a coiled tungsten filament while the anode consists of a small piece of tungsten (i.e. the target) mounted on a thick copper rod. If the tungsten filament is heated to a high temperature by passing an electrical current through it, electrons will be emitted from its surface. When a high voltage is applied between the anode and cathode, the electrons emitted from the filament will be accelerated towards the anode. Because the tube is evacuated to a high vacuum, the electrons do not collide with gas molecules between the cathode and anode and in this way acquire very high velocities. When the electrons are suddenly stopped in the tungsten target, X-rays are emitted [22, p. 37]. The X-rays pass through a beryllium window and emerges through a thin glass window in the tube envelope.

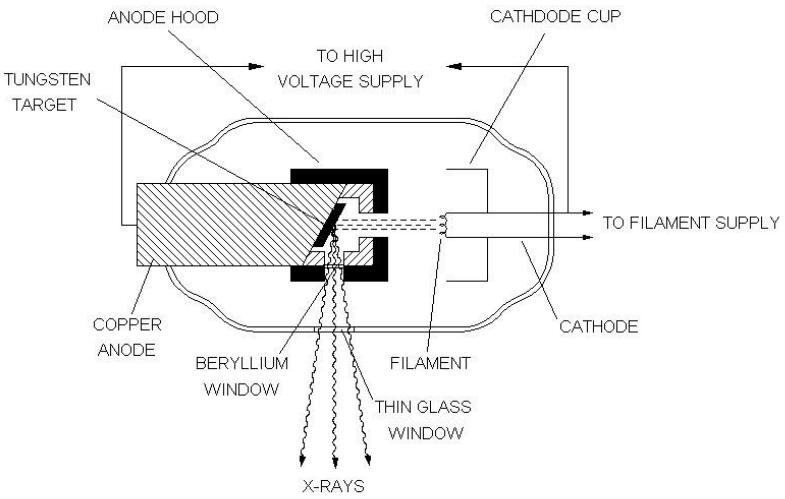

Figure 2.2 Schematic diagram of a therapy X-ray tube [23, p. 29]

A large part of the energy carried by the electrons appears as heat in the anode which needs to be removed. This is achieved by conduction of heat from the target to the copper rod onto which it is mounted. The copper rod extends to the outside of the tube where it is cooled by oil. Secondary electrons are produced from the target when it is being bombarded by electrons from the cathode.

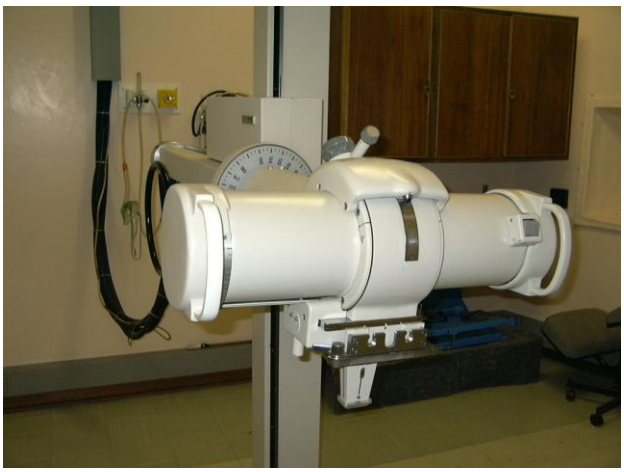

Figure 2.3 A Philips Medical Systems™ RT 250 kilovolt unit

To prevent these stray electrons from hitting other non-target components in the tube, the anode needs to be hooded by a tungsten covered copper shield. The copper in the shield absorbs the stray electrons while the tungsten absorbs the unwanted X-rays produced in the copper. The cathode filament is mounted in a focussing cup, the purpose of which is to focus the emitted electrons onto the target in the smallest possible area. This area known as the focal spot needs to be kept small in order to produce a sharply defined radiation field [23, p. 28]. X-ray tubes used for diagnostic work operate in the 80 kV range while those used for radiotherapy purposes can produce X-rays in the so called orthovoltage range of 100–250 kV. These low energy X-ray machines used in radiotherapy are also referred to as kilovolt units, an example of which is shown in Figure 2.3. A selection of applicators is available for these machines to collimate the radiation beam to different treatment field sizes. Additional field shaping is possible by shielding the area surrounding the tumour with lead sheet placed directly on the patient's skin. Kilovolt units can be used to treat most superficial cancerous lesions, especially skin cancers. These machines are however now replaced with linear electron accelerators in most cancer departments that are able to provide a variety of treatment options [23, p. 38].

2.3.2 Production of high energy X-rays and electrons

High energy X-ray and electron beams as produced by a linear electron accelerator can be used to treat both superficial and deep-seated tumours. The principles of operation of a linear electron accelerator (shortened to linac) are explained with reference to Figures 2.4 and 2.5. Negative polarity pulses are applied simultaneously to the cathode of a magnetron and an electron gun as shown in the diagram. The magnetron generates pulses of radio frequency (RF) waves at a nominal frequency of 2856 MHz. This RF power is fed through a rectangular

waveguide and is launched into the linear accelerator waveguide by a mode transformer. At the same instant, a pulse of electrons from the electron gun is injected into the accelerator waveguide, entering it with a velocity of about 0.4 times the velocity of light. The phase

velocity of the RF wave at the accelerator input is reduced to this electron velocity, so that some electrons are captured by each wave and accelerated by it [40, p. 8-5]. The accelerator waveguide consists of a cylindrical copper structure with copper irises inserted along its length at defined intervals to form a series of cavities. Each iris has a circular aperture through which the electrons injected by the electron gun can pass [18, p. 24]. The RF travelling waves have an axial component of electric field from which the electrons gain energy. The wave velocity and the amount of energy transferred to the electrons are governed principally by the accelerating guide radius and the iris apertures. Electrons injected into the accelerator waveguide increase in energy from 38 kV to 52 kV (depending on the machine's mode of operation) to their final energy of 4 MeV to 25 MeV. In the first part of the accelerator waveguide the electrons captured by the RF travelling waves are formed into electron bunches near the peaks of the waves.

Figure 2.5 An Elekta™ SL 25 linear electron accelerator

These electron bunches are rapidly accelerated to near the velocity of light. In the rest of the accelerator waveguide the electron velocity remains approximately constant at this level. In order to overcome defocusing effects on the electron beam during acceleration, a static axial

magnetic field is applied to the accelerator by means of a series of focus coils placed at intervals along its length. Compensation for deviation of the electron beam from the axis is provided by two sets of centring coils sited near each end of the accelerator [40, p. 12-4]. The travelling waves propagated down the accelerator waveguide transfer some power to the electron beam and some to the waveguide walls. Surplus RF power at the accelerator output is extracted by a mode transformer and absorbed by a RF load. High power machines employ feedback to recirculate unused output RF power to the waveguide input. Recirculated RF power is combined with the magnetron input power through a directional coupler to give an increased power flux into the accelerator. The correct phasing of the feedback RF for power recombination is set by a high-power phase-shifter in the feedback waveguide loop. The rectangular waveguide between the magnetron and the accelerator waveguide is pressurized with dielectric gas to prevent RF breakdown at the power levels used. Two ion pumps connected to the input and output ends of the accelerator waveguide maintain a high vacuum within the waveguide to facilitate electron acceleration [18, p. 48]. The rectangular and accelerator waveguides are separated by two RF windows situated in the input and output rectangular waveguide feeds.

On emerging from the accelerator waveguide the high-energy electrons pass into a flight tube which is connected to the waveguide via a bellows section. The flight tube passes through an achromatic triple-magnet beam bending assembly. Under the influence of the magnetic fields, the electron beam is deflected through various angles until it finally emerges at the target assembly area at the flight tube exit. The bellows section allows the entire flight tube and target assembly to be moved by a motorized drive so that either a target (X-ray mode) or an electron window (electron mode) is presented to the electron beam. In the X-ray mode the electrons are stopped by a high density metal target (e.g. tungsten). Some of the electron energy is converted into a symmetrical X-ray beam with the maximum intensity of radiation

directed forward in the same direction as the incident electrons. In the electron mode the beam passes centrally through a thin metal foil window. Beyond the target assembly the X-ray or electron beam passes into the radiation head. By the action of flattening filters in the radiation head, the X-ray beam becomes even or commonly referred to as "flat" in the treatment plane. The electron beam is scattered by a dual-foil filter arrangement to provide a uniform treatment beam [40, p. 12-1]. A beam-limiting device (i.e. the collimator) and adjustable diaphragms are used to define the X-ray field sizes. The four diaphragms can be moved independent of each other making possible asymmetric arrangements about the beam axis to provide offset as well as symmetrical treatment fields. Electron applicators can be attached to the radiation head to assist in the definition of the electron irradiation fields. Two ionization-chambers are mounted below the flattening and scattering filters in the radiation head. The ionization-chambers form part of a two-channel dosimetry system that monitors the radiation beam. The ionization-chamber assembly also monitors the radiation field flatness by providing data signals to the beam control system [40, p. 12-2]. Mounted in the radiation head is a light source that projects a light field that corresponds exactly with the radiation field. This field light also projects a cross wire that represents the centre of rotation of the radiation head. The field light is used during patient set-ups to show the treatment field's centre and borders. Linacs are able to produce X-rays in the so called megavoltage range of 4-20 MV while electrons are available from 4-25 MeV.

2.3.2.1 Linear electron accelerator design features

The layout of a modern linac is explained with reference to Figure 2.6. The waveguide assemblies, magnetron, etc. as described in the previous section are mounted on a large rotatable drum that is referred to as the gantry.

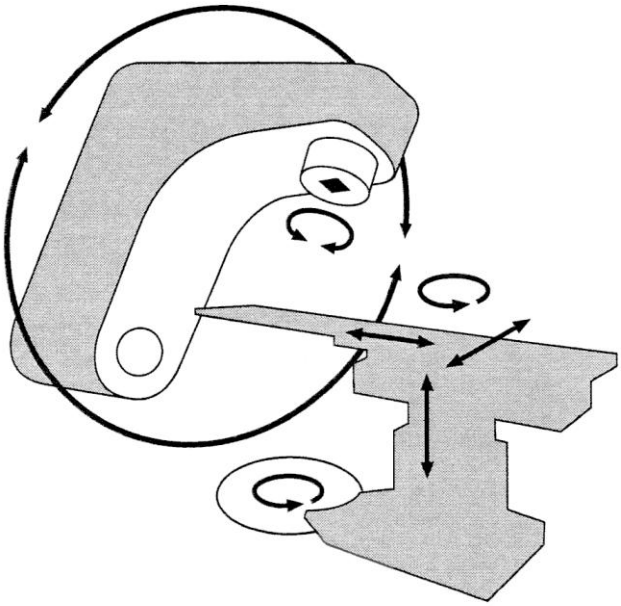

Figure 2.6 Linear accelerator gantry and table movements [19, p. 91]

Protruding from the front of the gantry is an arm containing the accelerator waveguide. The radiation head is attached to the outer end of this arm. It is possible to rotate the gantry through 360° so that treatment fields may be directed at the patient from any angle. It is also possible to rotate the radiation head through 360°. The axis of rotation of the radiation head is also the central axis of the radiation beam. If the axis of rotation of both the gantry and radiation head is extended they will intersect at a point in space known as the isocentre. The distance from the isocentre to the X-ray target in the radiation head is exactly 1 m. This distance is referred to as the source-to-axis distance (SAD). The treatment table rotates on a turntable mounted in the floor of the treatment room. The axis of rotation of the turntable also crosses the machine's isocentre [19, p. 16]. If the isocentre is placed at the centre of a tumour, irrespective of the machine's angle, the radiation will always be directed at the tumour.

2.4 Radiation measurements and dosage for X-irradiation

In radiotherapy the amount and distribution of radiation dosage is crucial to the success or failure of treatment. As described in section 2.2.2, the very purpose of radiotherapy is to do maximum damage to the volume containing the cancerous tissues without inflicting excessive damage on the healthy tissue surrounding it. Radiation dose and distribution is an exact science that requires the expertise of a physicist, who is considered an essential member of a radiotherapy department. Dose distribution and the amount of radiation required for treatment pertaining to X-irradiation will be discussed next:

2.4.1 Radiation dose distribution

The dose distribution from an external radiation beam within a medium can be described by two methods namely: Central axis depth-dose distribution and isodose distribution.

2.4.1.1 Central axis depth-dose distribution

When a beam of ionizing radiation penetrates a patient, the absorbed dose varies with depth within the tissue. Of particular importance in dose calculation is to establish the depth-dose variation along the central axis of the beam. For this purpose dose measurements are made at different depths in a water phantom (i.e. a water bath) with a device that measures ionization known as an ionization chamber. Water is used for these measurements since it closely approximates the radiation absorption and scattering properties of muscle and other soft

tissues. The variation in depth-dose along the central axis of the beam may be characterized by the percentage depth-dose. This concept is explained with reference to Figure 2.7.

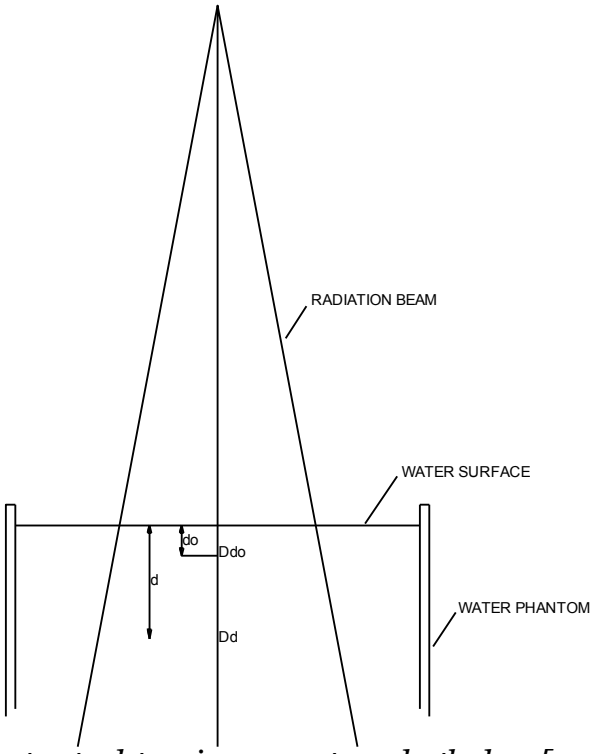

Figure 2.7 Water phantom setup to determine percentage depth-dose [23, p. 162]

Percentage depth-dose may be defined as "the quotient, expressed as a percentage, of the absorbed dose D(d) at any depth (d) to the absorbed dose D(do) at a fixed reference depth (do), along the central axis of the beam" [23, p. 161]. Percentage depth-dose P(d) is thus:

$$P(d) = \frac{D(d)}{D(do)} \times 100\% \qquad (2.1)$$

For orthovoltage (up to 400 kV) and lower-energy X-rays, the reference depth is usually taken as the water surface (do = 0). For higher radiation energies, the reference depth is taken as the position of the peak absorbed dose (do = dm). This peak absorbed dose is called maximum dose or simply D_{max}.

$$D_{\max} = \frac{D(d)}{P(d)} \times 100\% \qquad (2.2)$$

Central axis depth-dose distribution depends on various factors including beam energy, field size and source-to-surface distance. These factors will be discussed next:

a) Beam energy

The percentage depth-dose (at depths greater than maximum dose) increases with beam energy. Radiation beams with higher-energy have greater penetrating power and thus deliver a higher percentage depth-dose. This effect is graphically illustrated in Figure 2.8.

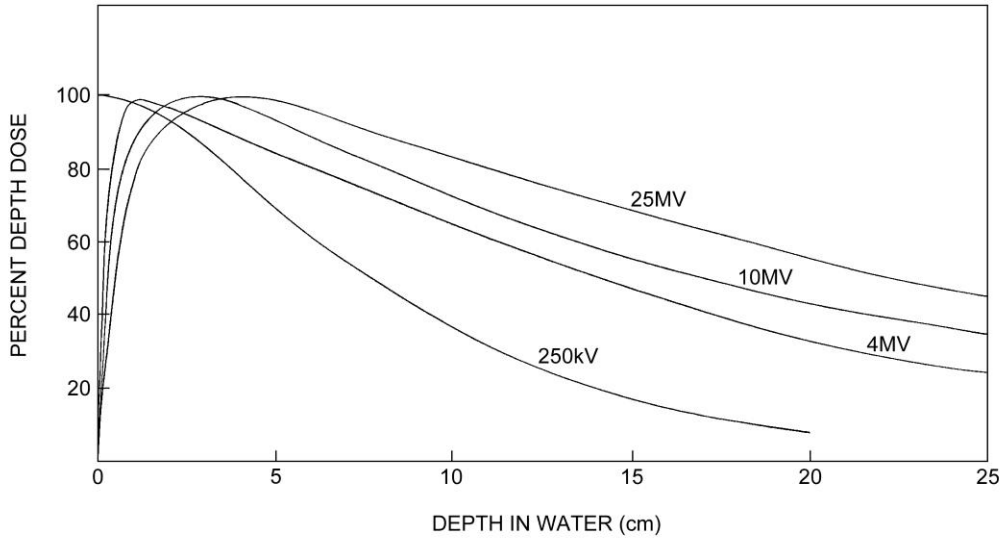

Figure 2.8 Central axis depth-dose distribution for different energy photon beams [23, p. 163]

The percentage depth-dose decreases with depth beyond the depth of maximum dose as can be seen in Figure 2.8 [23, p. 163]. There is however a build up of dose before the depth of maximum dose which becomes more pronounced as the energy is increased. For orthovoltage

the dose builds up to a maximum on or very close to the surface while for higher-energy beams the point of maximum dose lies deeper. The region between the surface and point of maximum dose on the graphs is referred to as the dose build-up region. For higher-energy beams such as produced by linacs, the surface dose is much lower than the maximum dose. This offers a great advantage over the lower energy beams where maximum dose occurs at the skin surface. A much higher dose can thus be delivered to a deep-seated tumour with a high-energy X-ray (photon) beam without exceeding the tolerance of the skin. This advantage of high-energy beams is clinically known as the skin-sparing effect [23, p. 162].

b) Field size

Radiation field size may either be specified geometrically or dosimetrically. The geometric field size is defined as "the projection, on a plane perpendicular to the beam axis, of the distal end of the collimator as seen from the front centre of the source" [23, p. 164]. The dosimetric or physical field size is defined as "the distance intercepted by a given isodose curve[2] (usually 50% isodose) on a plane perpendicular to the beam axis at a stated distance from the source" [23, p. 164]. In this research, unless stated otherwise, field size refers to geometric field size. It will also be defined at a predetermined distance such as source-to-skin distance (SSD) or source-to-axis distance (SAD). The SAD is the distance from the source to the isocenter on a linac.

---

[2] see section 2.4.2
For a very small radiation field, the depth-dose at a point along the central axis of the beam is effectively the result of primary radiation. The contribution of scattered radiation to the depth-dose can be considered as insignificant. If however, the field size is increased the contribution of scattered radiation to the absorbed dose will also increase. The increase in

percentage depth-dose as a result of increase in field size depends on beam energy. With higher-energy beams that scatter more predominantly in the forward direction, the effect of field size on percentage depth-dose will be less pronounced than for lower energy beams [23, p. 164].

c) Source-to-surface distance

The dose rate emitted by a point source of radiation varies inversely as a square of the distance from the source. This statement is motivated with reference to Figure 2.9.

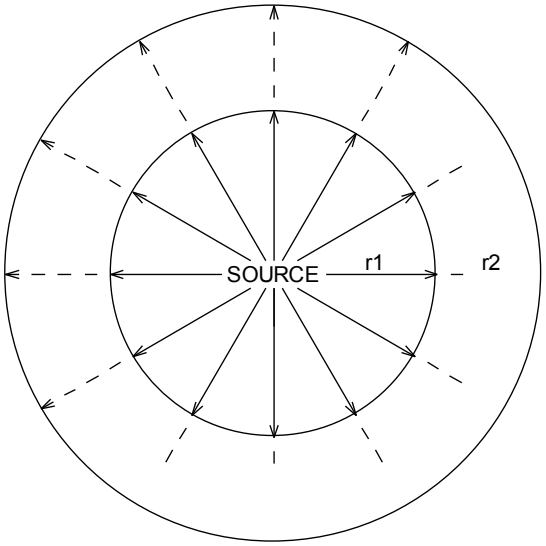

Figure 2.9 Radiation from a radioactive point source

For explanation purposes a few assumptions need to be made:

- Assume that the radiation originates from a point source.

- Assume that the radiation is isotropic; there will thus be the same amount of radiation in all directions from the source. The amount of radiation that penetrates any point on the surface of an imaginary sphere surrounding the source will be the same independent of the radius of the sphere. This is when the radiation is measured in a vacuum where there is no attenuation.
- Assume that the total amount of energy emitted by the source per second (W) stays constant.

Radiation intensity (I) can be defined as the energy that passes per unit time through a unit surface. From this follows:

Radiation intensity at a distance r_1: $$I_1 \bullet \frac{W}{4\pi r_1^2} \quad (2.3)$$

Radiation intensity at a distance r_2: $$I_2 \bullet \frac{W}{4\pi r_2^2} \quad (2.4)$$

Equation (2.4) / Equation (2.3): $$\frac{I_2}{I_1} \bullet \frac{r_1^2}{r_2^2} \quad (2.5)$$

Substitute $r_1 = 1$ in Equation (2.5): $$I_2 \bullet I_1 \times \frac{1}{r_2^2} \quad (2.6)$$

Percentage depth-dose increases with SSD because of the effect of the inverse square law. Although the actual dose rate at a specific point decreases with an increase in distance from the source, the percentage depth-dose, which is a relative dose with respect to a reference point, increases with SSD. This statement is illustrated with reference to Figure 2.10.

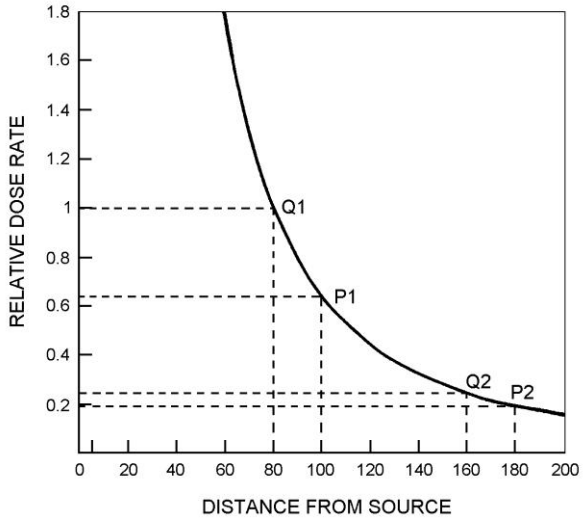

Figure 2.10 Relative dose rate as inverse square law function of distance from a source

In the diagram the relative dose rate from a point source of radiation is plotted as a function of distance from the source following the inverse square law. The plot shows that the drop in dose rate per unit interval between two points (P and Q) is much greater at smaller distances from the source than it is at large distances.

From Figure 2.10 follows that: $\frac{P_2}{Q_2} \text{ AA } \frac{P_1}{Q_1}$ (2.7)

This means that the percentage depth-dose, which represents depth-dose relative to a reference point, decreases more rapidly closer to the source than further away from it. SSD is a very important parameter in clinical radiation therapy. Because percentage depth-dose determines how much dose can be delivered at a certain depth relative to the surface dose or D_{max}, the SSD needs to be as large as possible. In practice however, since dose rate decreases with distance, the SSD is set at a distance which provides a compromise between dose rate and percentage depth-dose [23, p. 166].

2.4.1.2 Isodose distribution

Depth-dose distribution along the central axis of a radiation beam as described in section 2.4.1.1 is important for dose calculations. It is however insufficient to characterize a radiation beam that produces a dose distribution in a three-dimensional volume such as a human body. Variation in absorbed dose in a volume can be depicted by isodose curves which are lines passing through points of equal dose. These isodose curves are plotted at equal increments of absorbed dose and expressed as a percentage of the dose at a reference point. A series of isodose curves for a beam of radiation is referred to as an isodose chart. Standard isodose charts are drawn for each field size and radiation energy, examples of which are shown in Figure 2.11 [23, p. 204].

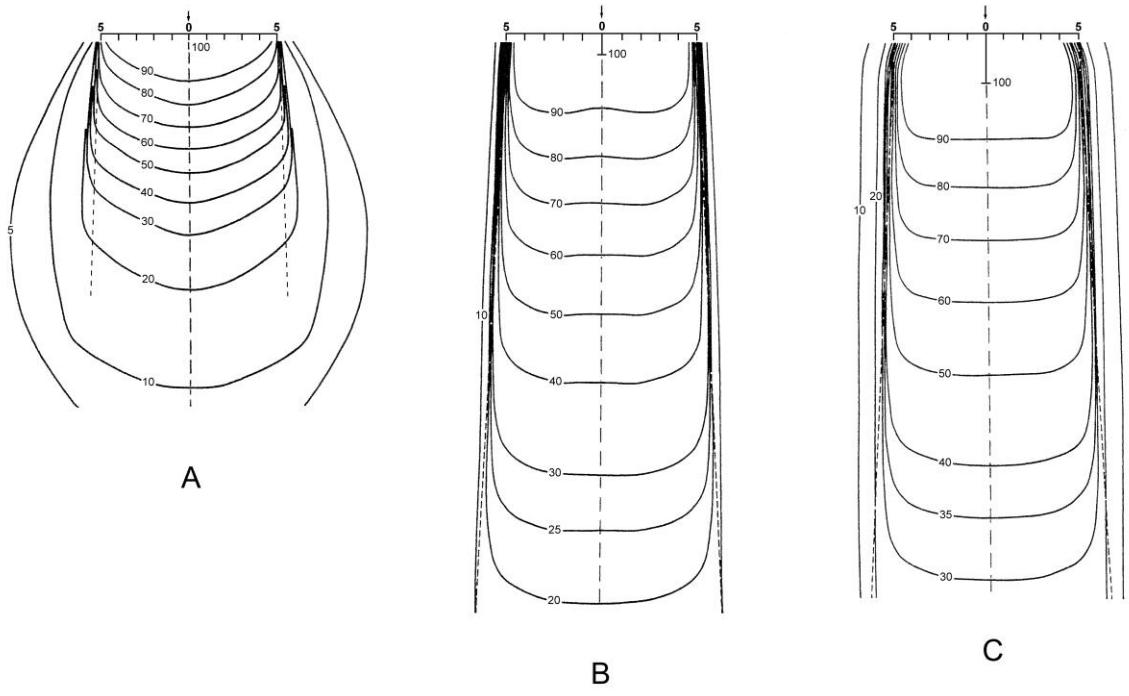

Figure 2.11 Comparison between isodose charts for (A) 200kV, (B) 4MV and (C) 10MV X-rays at 10 x 10 cm² field size [23, p. 204]

These standard isodose charts are used by radiotherapy personnel in planning a patient's treatment. Another way of depicting the dose variation across the treatment field is to plot isodose curves in a plane perpendicular to the central axis of the beam as shown in Figure 2.12.

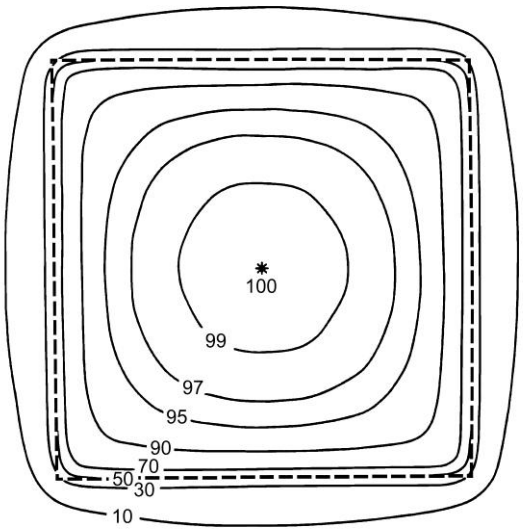

Figure 2.12 Cross-sectional isodose distribution in a plane perpendicular to the central axis of the treatment beam [23, p. 201]

In this depiction the isodose values are normalized to 100% at the centre of the field [23, p. 201]. Some of the parameters that effect isodose curves are beam energy, source size, skin-to-source-distance (SSD), source-to-diaphragm distance (SDD), beam collimation and field size. These parameters will be discussed next:

a) Beam energy

The central axis depth-dose distribution depends on beam energy as was explained in section 2.4.1.1a. The depth of a given isodose curve increases with an increase in beam

energy. This is because higher-energy beams, that have greater penetrative ability, produce a higher percentage depth-dose at a given depth. Beam energy also has an effect on the shape of isodose curves near the borders of the treatment field. Greater lateral scatter associated with lower-energy beams causes the isodose curves outside the field to bulge out as shown in Figure 2.11 A. The absorbed dose in the medium outside the primary beam is thus greater for low-energy beams than those for higher energies. Physical penumbra[3] also depends on beam energy. The isodose curves outside the primary beam (e.g. 10% and 5%) are greatly distended in the case of the orthovoltage beam as is shown in Figure 2.11 A. This scattered dose to tissue outside the treatment region is one of the disadvantages of orthovoltage radiation. The scatter outside the field for megavolt beams is minimized as a result of predominantly forward scattering [23, p. 203].

b) Source size, SSD and SDD

Source size, SSD and SDD affect the shape of isodose curves at the treatment field's edges through influencing the width of the geometric penumbra. SSD also affects the percentage depth-dose and therefore the depth of the isodose curves as was explained in section 2.4.1.1c). It is possible to distinguish between physical and geometrical penumbra. The physical penumbra can be defined as the lateral distance between two specified isodose curves (usually 20% and 80%) at a specified depth. The geometrical penumbra is explained with reference to Figure 2.13.

[3] The penumbra is the region at the edge of the radiation beam over which dose rate changes rapidly as a function of distance from the beam axis [23, p. 53].

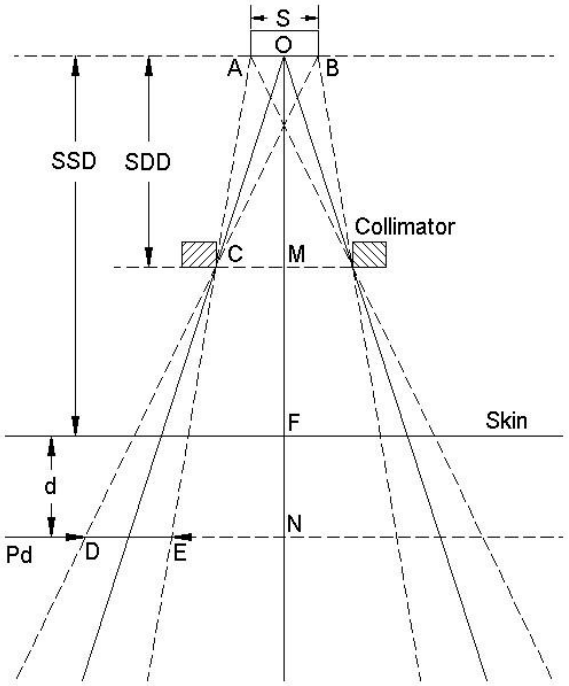

Figure 2.13 Diagram for calculating geometric penumbra [23, p. 54]

The geometric width of the penumbra (P_d) at any depth (d) from the surface of a patient can be determined by considering similar triangles ABC and DEC. From geometry, we have:

$$\frac{DE}{AB} = \frac{CE}{CA} = \frac{CD}{CB} = \frac{MN}{OM} = \frac{OF - FN}{OM} \qquad (2.8)$$

If AB = s, the source diameter, OM = SDD, the source-to-diaphragm distance, OF = SSD, the source-to-surface distance, then from the previous equation, the penumbra (DE) at depth d is given by:

$$P_d = \frac{s(SSD - d)}{SDD} \qquad (2.9)$$

The penumbra at the surface can be calculated by substituting d = 0 in Equation 2.9.

As Equation 2.9 indicates, the penumbra width increases with increase in source diameter, SSD and depth but decreases with an increase in SDD. The dose variation across the field border is a complex function of geometric penumbra, lateral scatter and collimation. Therefore, the field sharpness at depth is not simply determined by the source or focal spot size [23, p. 203].

c) Collimation

The term collimation not only refers to the collimator blocks that give shape and size to the beam but also the flattening filter and other absorbers or scatterers in the beam between the source and the patient. Amongst these, the flattening filter has the greatest influence in determining the shape of isodose curves. This is especially the case with megavoltage X-ray beams where the isodose curves will have a conical shape without this filter. The beam will thus show increased X-ray intensity along its central axis and a rapid reduction transversely. Since the function of the flattening filter is to make the beam intensity distribution uniform across the field, the filter is made thickest in its middle and tapers off towards the edges.

d) Field size

Field size is one of the most important parameters in treatment planning. For the tumour to be adequately covered dosimetrically, an appropriate field size needs to be determined. This decision on field size should always be made dosimetrically rather than geometrically. An isodose curve (e.g. 90%) that encloses the treatment volume should thus be used as a guide in choosing a field size rather than the geometric dimensions of the field. Care should be taken in using field sizes smaller than 6 cm since a large part of the field falls in the penumbra region. Depending on the source size, collimation and design of the flattening filter, the

isodose curves for small fields tend to be bell-shaped. Treatment planning with isodose curves should thus be considered mandatory for small field sizes [23, p. 205].

2.4.2 Radiation dose

Just as the distribution of dose within the patient is important, so the amount of dose applied to the patient during treatment is of equal importance. The following section explains how radiation data are gathered, displayed and daily dose calculated.

2.4.2.1 Commissioning tests for linacs

Upon acquisition of a new linear electron accelerator, certain commissioning tests need to be undertaken on the machine before it may be used clinically. This includes the collection of beam data to provide sufficient information to accurately predict the outcome of all possible treatment procedures. Measurements also need to be done to compare the performance of the radiation beam with that specified by the manufacturer and national and international guidelines. The measurements that need to be done include radiation energy, beam symmetry and flatness and machine output.

a) Beam energy

The nominal energy of the radiation beam is equal to the energy of the electron beam incident on the target. The beam specification is further defined in terms of the penetrating power of the X-rays produced [19, p. 66].

b) Beam symmetry and flatness

To ensure that the dose delivered to the patient is constant across the radiation field, the profile of the beam should be flat in the plane which is parallel to the incident plane of the radiation field. The flatness of the beam is measured at right angles to the central axis, across the width and length of the field and across the diagonals for different field sizes.

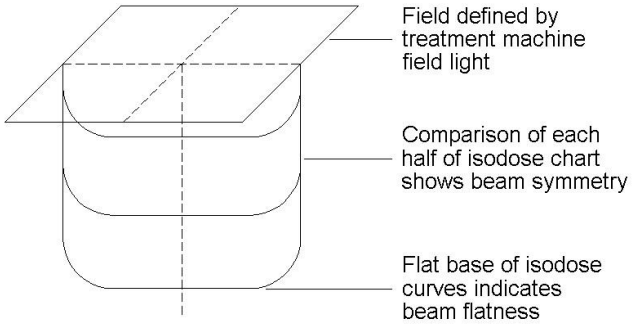

Figure 2.14 Diagram for showing beam flatness and symmetry [19, p. 66]

Symmetry is the overall balance between the two halves of a radiation beam during treatment delivery as shown in Figure 2.14. The beam symmetry is constantly monitored by the built-in ionization chambers in the linacs radiation head [19, p. 66]. The tolerance for beam flatness and symmetry is 5% for large fields and 3% for fields < 10 x 10 cm².

c) Machine output

The amount of radiation delivered by the treatment machine in a given time under treatment conditions is known as the output of the machine. The dose received by tissue is known as absorbed dose and gives an indication of the energy deposited in the body tissue from the radiation. The unit of absorbed dose is the gray (Gy) which is equivalent to an energy transfer of one joule per kilogram. The output is measured in monitor units (MU) per gray. This

output measurement is standardised for a 10 x 10 cm^2 field size, where 100 monitor units delivers a dose of 1 Gy at the dose maximum point. With a decrease in field size, there will be less scatter in the irradiated medium and therefore it is necessary to give more monitor units to deliver 1 Gy. The reverse applies with an increase in field size. The output will also decrease with increasing treatment distance.

2.4.2.2 Presentation of dosimetry data

Variation in the measured machine data with changing field sizes is presented using a system of equivalent squares. This system is used to ease the presentation of the data and for dose calculation. The equivalent square of a given treatment field is the equivalent irradiated area to that if the treatment field were square. The equivalent square of any given field will produce equivalent scatter conditions to the given field. Thus, before dose calculation can be performed, it is necessary to find the equivalent square of the prescribed treatment field. Equivalent square data are available in look-up table format from where any rectangular field can be easily converted to an equivalent square field.

2.4.2.3 Dose calculation

A planning computer is required for complex treatment plans where multiple radiation beams are required to obtain the desired clinical results. It is however possible to calculate simple single beam treatments using central axis depth-dose data and machine output data.

a) Central axis depth-dose data

Central axis depth-dose data are necessary to find the percentage depth-dose delivered to the target volume under treatment conditions. These data are available in look-up table format and shows changes in central axis depth-dose with changing equivalent square and depth for each field-to-source distance (FSD) in common clinical use.

b) Machine output data

Machine output data are necessary to calculate the monitor units needed to deliver the required dose under treatment conditions. Machine output varies with the equivalent square of the treatment field to be irradiated and the FSD at which the treatment is to be delivered. Output can be described by monitor units per gray.

$$Monitor\ units = Given\ dose \times MU/Gy \qquad (2.10)$$

Machine output data are presented in look-up table format where output over a range of equivalent squares is given at a fixed FSD.

2.4.2.4 Method for calculation dose for a single beam treatment

For dose calculation, the percentage depth-dose delivered to the target volume as well as the monitor units required to deliver the specified dose must be determined. The dose and beam energy of the radiation to be received by the tumour, the number of treatments as well as the radiation field size to be used are specified by a radiation oncologist. Since percentage depth-dose is affected by depth in tissue, beam energy and field size as described in section 2.4 it is necessary to determine the percentage depth-dose delivered under treatment conditions [19, p. 74]. This can be done using the following steps:

1. By making use of the equivalent square look-up tables, the equivalent square of the prescribed field size is found.
2. The depth of the tumour in relation to the skin can be determined from a lateral X-ray film of the body.
3. Using the depth-dose data provided for the prescribed beam energy, the percentage depth-dose delivered at the tumour depth can be found from the percentage depth-dose look-up tables.

The monitor units required to deliver the prescribed dose to the tumour can be determined by following the subsequent steps:

1. Determine the total dose for the treatment by making use of the following equation:

$$Total\ given\ dose\ (Gy) = \frac{Prescribed\ treatment\ dose\ (Gy)}{Percentage\ depth\ dose} \times 100 \qquad (2.11)$$

2. The total dose for the treatment must be divided by the number of treatments to give the daily dose.
3. Using the equivalent square, find the output for the treatment field from the output look-up table.
4. Combine the output and the daily given dose by multiplying the daily dose with the output to give linac monitor units
5. The calculated monitor units are applied daily to deliver the required tumour dose.

2.5 Radiation measurements and dosage for electron radiation

Radiation dose distribution as described in sections 2.4.1 and 2.4.2 is explained with reference to X-ray irradiation. The dose distribution in a medium by an electron beam does however differ significantly from that of X-rays. Electron beams have certain unique features that make it the modality of choice for some treatments as will be explained next.

2.5.1 Central axis depth-dose distribution

The major advantage of electron beam irradiation lies in the shape of the percentage depth-dose curve as shown in Figure 2.15 [23, p. 310].

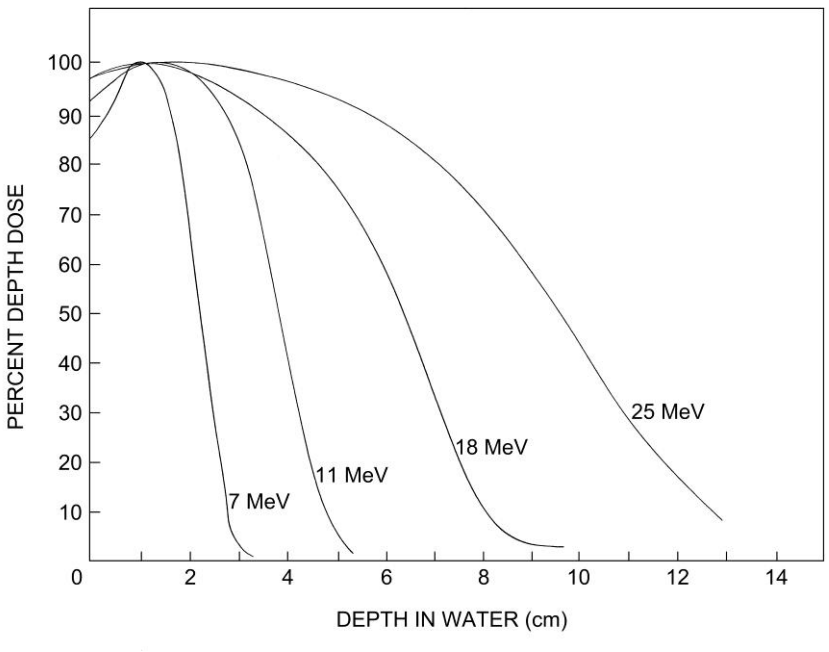

Figure 2.15 Comparison between central axis percentage depth-dose curves for different energy electron beams [23, p. 310]

The curves demonstrate a plateau of relatively even dose followed by a sharp dose fall-off beyond the 80% depth-dose. In terms of patient treatment, this means a homogeneous dose

can be delivered by a single beam to a defined depth of tissue with little dose received beyond that depth [19, p. 40]. The principal clinical applications for electron irradiation are:

- treatment of skin cancer
- chest wall irradiation for breast cancer
- administering boost dose to nodes
- treatment of head and neck cancers.

The most useful treatment depth, or therapeutic range, of electrons is represented by the depth of the 90% depth-dose. Because the dose decreases abruptly beyond this dose level, the electron energy must be chosen carefully.

2.5.2 Isodose curves

When an electron beam penetrates a medium, the electrons do not scatter primarily in a forward direction as is shown in Figure 2.16 [23, p. 311]. The electron beam expands rapidly below the surface, thus at depth a significant dose is deposited outside the defined field on the surface. Individual spread of the isodose curves varies depending on the isodose level, energy, field size and the accelerators collimation system.

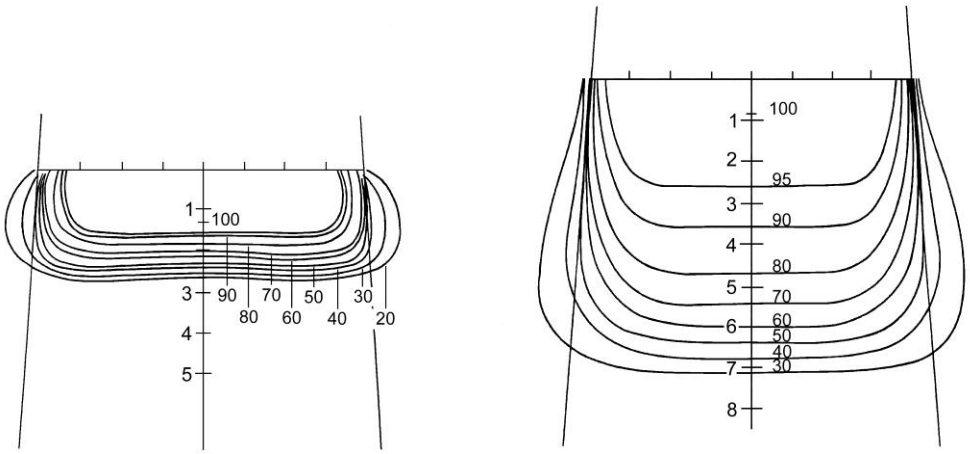

A B

Figure 2.16 Comparison between isodose curves for (A) 7 MeV and (B) 18 MeV electron beams [23, p. 311]

All the isodose curves show some expansion in the lower energy beam as shown in Figure 2.16 while only the isodose levels lower than 50% bulge out in the higher energy beam. The higher isodose levels (70% to 95%) also show some lateral constriction for both energies. This effect becomes more pronounced with a decrease in field size [23, p. 309].

2.5.3 Defining the electron beam

The electron field size is defined by a combination of the accelerator's adjustable diaphragms and the electron applicators that attach to the radiation head. The electron applicators are required to collimate the beam between the machine and the patient. This is to achieve good field definition since electrons are readily scattered by air. It is usual for the face of the applicator to be brought into contact with the patient's skin during treatment. The treatment distance is thus defined by the length of the applicator. Electron applicators are available that can produce rectangular, square or circular field shapes over sizes that range from 6 x 6 cm^2

to 25 x 25 cm^2 [35, p. 137]. The required field size is further defined by an end-frame that fits into the treatment end of the applicator [23, p. 42]. These end-frames are usually produced by machining from 10 mm lead sheet or through a casting process making use of a low melt shielding alloy. This end-frame casting process is described in Chapter 5.

2.5.4 Beam data and dose calculation

The performance of the electron beams and other relevant data that is required for treatment is collected as part of the commissioning process of the linac. Depth-dose data for each applicator and electron energy is measured and represented in look-up table format. Machine output is represented likewise and includes the output for each end-frame of each electron applicator at each electron energy. End-frames that are custom-made should also be measured for output, especially if the treatment field is irregular in shape making the scatter conditions for the field unpredictable. A radiation oncologist decides on an electron energy that will best deliver a homogeneous dose to the tumour. A treatment depth is also chosen; this may be the skin surface and/or a defined depth beneath it. Bolus (i.e. a tissue equivalent medium such as dental wax) of varying thickness may be applied to the treatment field to modify the skin dose and the dose at depth. The required radiation dose is prescribed to the selected percentage depth-dose, and the skin dose calculated if considered relevant. The applied dose is calculated using Equation 2.11. The number of monitor units can finally be calculated using the output and the applied dose as described in section 2.4.2.4 [19, p. 45].

CHAPTER 3

SKIN CANCER AND TREATMENT THEREOF

3.1 Introduction

Skin cancer is the most common form of cancer found in humans with more than 800 000 cases diagnosed in the United States each year. One in every three new cancers is a skin cancer. It is estimated that 40 to 50% of fair-skinned people who live to be 65 years old will have at least one skin cancer [10, p. 658].

3.2 Anatomy of the skin

The skin consists of two major layers namely the epidermis and dermis as shown in Figures 3.1 and 3.2.

3.2.1 Epidermis

The most important function of the epidermis is to produce a highly complex mixture of proteins collectively termed keratin. The outermost layer of the epidermis is composed of completely keratinized cells that provide the skin with much of its protective properties [38, p. 479]. The basal layer rests on the basement membrane separating the epidermis from the dermis.

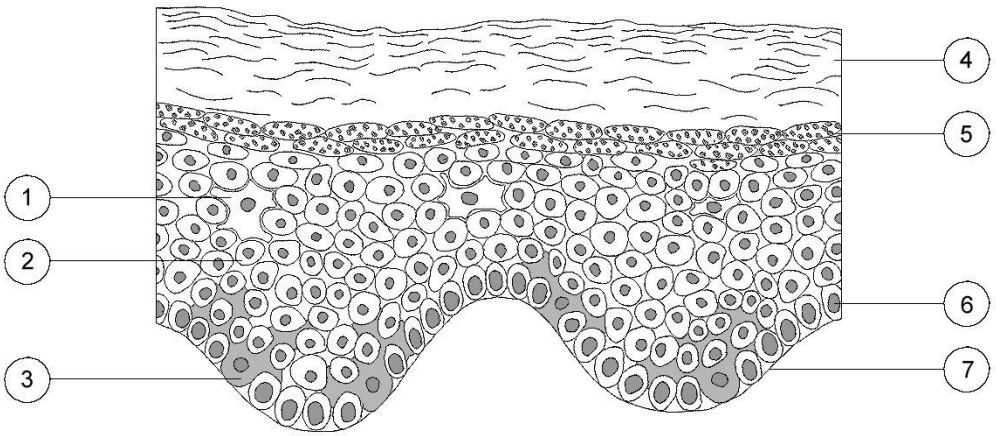

1. Langerhans' cells
2. Spinous or prickle cell layer
3. Melanocytes
4. 'Basket weave' keratin
5. Granular layer
6. Basal layer
7. Basement membrane

Figure 3.1 Schematic representation of normal epidermis [50, p. 674]

The cells in the basal layer divide and daughter cells progress through the epidermis to eventually die and contribute to the outer keratin layer. Melanocytes, located between the basal cells produce and donate pigment to surrounding epidermal cells [50, p. 674].

3.2.2 Dermis

The principal cells of the dermis are spindle-shaped fibroblasts. These fibroblasts secrete the characteristic dermal proteins collagen and elastin giving the skin much of its strength. Also located in the dermis are blood vessels, nerves, sweat glands, sebaceous glands, muscles and hair follicles [50, p. 675].

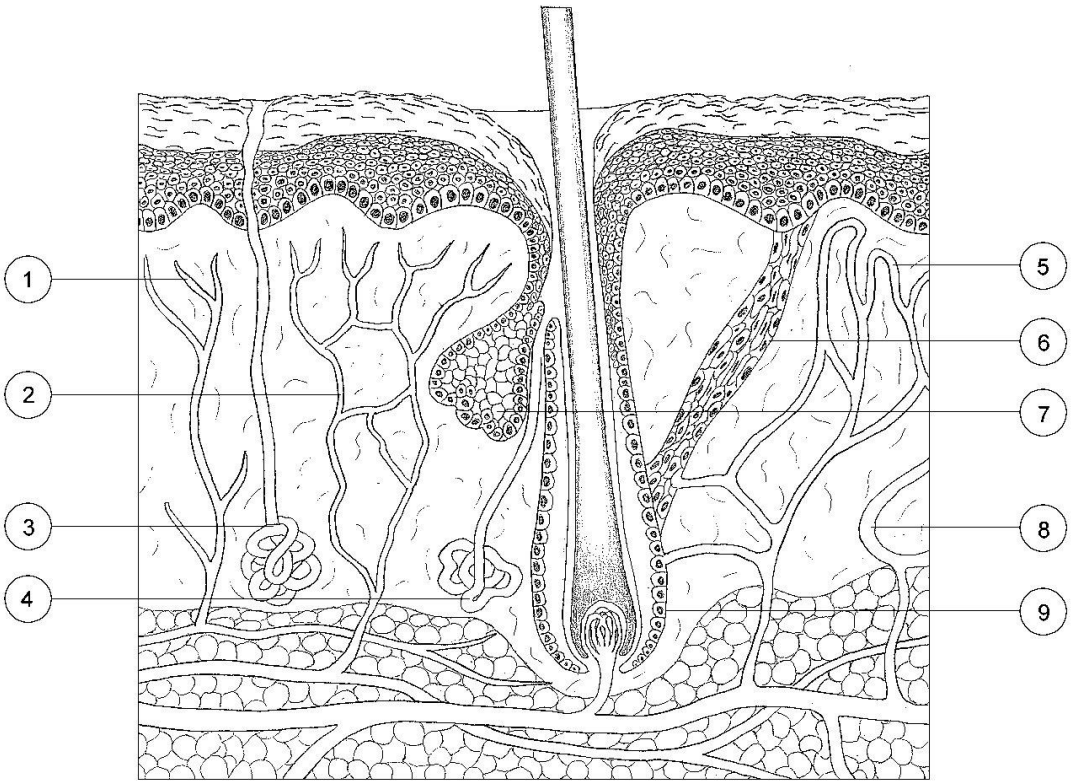

1. Lymphatics
2. Nerve
3. Eccrine sweat gland
4. Apocrine sweat gland
5. Superficial dermal vascular plexus
6. Arrector pilorium
7. Sebaceous gland
8. Deep dermal vascular plexus
9. Hair follicle

Figure 3.2 Schematic representation of normal skin [50, p. 674]

3.3 Carcinomas of the skin

Chronic sun exposure is the single most common cause of skin cancer as well as the most preventable. Fair skinned people living in countries with a high intensity of sunlight are most at risk. Because sun exposure is additive, skin cancer most often affect the elderly. Genetic relationship is also associated with increased incidence of skin cancer. Diagnostic radiologists

working without adequate protection or people repeatedly exposed to ionizing radiation during treatment of benign skin disorders are also at risk of contracting skin cancer. Long-term chronic ulceration seen in syphilis or burns or exposure to various chemicals such as arsenic trioxide, soot and tar can give rise to skin cancer [38, p. 480]. Examples of malignant lesions are the following:

- Basal cell carcinoma
- Intraepithelial carcinoma (Bowen's)
- Squamous cell carcinoma
- Keratoacanthoma (acute epithelial cancer)
- Melanoma
- Merkel cell carcinoma
- Adnexal tumours
- Connective tissue tumours
- Malignant lymphomas
- Mycosis fungoides
- Kaposi's sarcoma.

Basal cell carcinoma and squamous cell carcinoma are the most common making up approximately 95% of all malignant skin lesions while melanomas are considered to be most serious [38, p. 480].

3.3.1 Basal cell carcinoma

Basal cell carcinomas are the most common malignant tumours of the skin and are closely associated with chronic sunlight exposure. The tumours are believed to arise from the basal layer of the epidermis and from hair follicles. Most basal cell carcinomas occur on hair-bearing skin on the head and neck [38, p. 482]. Clinically it presents as ulcerated irregular lesions (hence their common name as rodent ulcers) with a raised pearly border, often with tiny blood vessels visible on the border [50, p. 686]. Sometimes proliferating basal cells remain contiguous with overlying epidermis and only invade superficially. They may however also invade deeply, as far as bone or even through bone, causing gross deformity or even death. Basal cell carcinomas rarely metastasize[1] and if diagnosed and treated at an early stage the prognoses is usually good [44, p. 253].

3.3.2 Squamous cell carcinoma

Squamous cell carcinoma is very common and is induced by chronic sunlight exposure or chemical carcinogens such as arsenic, soot or tar. They also occur in areas of chronic ulceration or scarring as well as areas of previous X-irradiation [50, p. 687]. Squamous cell carcinoma is a tumour of the keratinizing cells of the epidermis which have invaded beyond the dermal epidermal junction [38, p. 482]. They vary in their clinical presentation but the typical lesion is round to irregular in shape, plaque-like or even nodular and is overlaid with a warty keratotic scale.

[1] Spread of tumours to distant sites.

Metastasis to lymph nodes by the sun-induced carcinoma of skin occurs at a late stage in less than 0.5% of cases [44, p. 251]. Lesions arising from chronic ulceration or scarring are more aggressive with metastases occurring in about 10% of all cases [38, p. 482].

3.4 Treatment of basal cell and squamous cell carcinoma

There are many widely used methods to treat basal cell carcinoma (BCC) and squamous cell carcinoma (SCC). Factors to be considered in treatment selection include:

- Size and anatomic location of the lesion
- Involvement of adjacent cartilage or bone
- Depth of invasion
- Tumour grade
- Previous treatment
- Type of lesion
- Definition of its borders
- General medical condition of patient.

The most appropriate method of curing a specific skin cancer is the most effective, least toxic, most efficient and cosmetically elegant therapy [10, p. 662]. The treatment options are:

- Curettage and electrodessication
- Cryosurgery
- Chemotherapy
- Mohs micrographic surgery

- Laser therapy
- Radiation.

3.4.1 Curettage and electrodessication

With the patient under local anesthesia, the tumour is scooped out with a curette (sharp-tipped instrument) and electrodessicated. The procedure is repeated two or three times to ensure that all residual tumour is destroyed. Well defined superficial BCC and noninvasive SCC can usually be treated effectively with curettage and electrodessication [10, p. 662].

3.4.2 Cryosurgery

With this technique liquid nitrogen at -50°C is applied to the tumour surface freezing it in the process. The frozen tissue is then allowed to thaw for about two minutes. The frozen tumour cells lyse following their expansion by ice. This cycle is repeated two or three times. Cryosurgery is effective for treating superficial BCC and noninvasive SCC [21, p. 386].

3.4.3 Surgery

The standard treatment for both BCC and SCC is excision biopsy. In general the entire lesion, with an appropriate margin of apparently normal tissue, is excised. This is a more invasive and time consuming procedure than curettage and electrodessication [21, p. 385].

3.4.4 Mohs micrographic surgery

This technique was first described by Dr. Frederick Mohs in 1936. It involves the successive excision of thin horizontal layers of tissue with a 1–2 mm margin of normal appearing skin. Each layer is microscopically examined and the area that involves tumour is marked. The entire tumour is removed layer by layer with the marked area on the previous layer used as a guide for further excision. Mohs micrographic surgery has the highest cure rate of all treatment methods whilst sacrificing a minimum of unaffected skin. This treatment is recommended for all types of BCC and SCC. The disadvantages are that a great deal of expertise is required from the physician, the procedure is time-consuming and it requires more equipment than the other methods [10, p. 664].

3.4.5 Chemotherapy

The most widely used chemotherapeutic agent for the treatment of non-invasive epidermal tumours is 5% Fluorouracil (5 – FU). It is applied directly to the skin and works by blocking DNA synthesis, thereby preventing normal cell growth and ultimately causing cell death. While it is possible to control a tumour on the surface with 5 – FU it may continue to invade at the base. Recurrence rates are estimated to be 20 to 50%, so follow-up is important [10, p. 663].

3.4.6 Laser therapy

A carbon dioxide laser may be used for surgery where the laser is used as a cutting instrument, much like a scalpel. It is useful for removing superficial BCC and SCC in

locations that might be bloody or for patients who have a bleeding disorder or are taking anticoagulants [10, p. 665].

3.4.7 Radiation

Superficial radiation treatment of BCC and SCC has a reported cure rate of 89 to 95% over 5 years. The treatment is painless with very little risk to the patient. Radiotherapy is the preferred method for treating certain body sites such as the nose where cosmetic results of surgery are often disappointing [21, p. 387]. Radiation treatment of lesions on the trunk and extremities are less advantageous since the radiation may cause possible side effects at the site of radiation. This includes changes in the skin pigment and the formation of telangiectasias[2]. These side effects are mild initially, but become more marked in time, even to the extent that radionecrotic ulcers occasionally develop. There is also a small possibility of radiation treatment eventually causing new cancers at the radiation site. For these reasons, radiotherapy is usually recommended for patients older than 50 years of age [10, p. 663]. Different radiation sources are available for the treatment of skin cancer. Low energy X-rays as produced by kilovolt units are still in use in some cancer departments although electron treatments from linear accelerators are much more popular nowadays. Electrons do not penetrate as deeply as X-rays thereby offering the advantage of sparing underlying healthy structures. Bolus material (a tissue equivalent medium) of an appropriate thickness needs to be placed on the patient's skin during electron treatments above 18 MeV to ensure maximum dose to the skin surface. The radiation field size must include at least a 1 cm border of normal tissue for small lesions while 2 cm is recommended for larger lesions.

[2] Small obvious blood vessels.

Lead masks (as described in Chapter 5) are used to give shape to the treatment area and to protect the surrounding normal tissue. A standard square or rectangular electron applicator is chosen to fit over the opening in the mask as closely as possible. The applicator is fitted to the accelerator head and the gantry and head are rotated to bring the applicator perpendicularly into contact with the mask on the patient. The recommended radiation dose for skin cancers is dependant on the following factors:

- Histological type
- Size and depth of lesion
- Size of treatment field
- Dose fractionation
- Overall time of delivery.

Daily treatment fractions for most BCC may range from 200-500 cGy with total tumour doses of 3000-5000 cGy in 6-20 fractions. For most SCC 5000-6000 cGy in 6-30 fractions over a period of 10-35 elapsed days is recommended. BCC larger than 5 cm or thicker than 0.5 cm should be treated with doses similar to SCC [38, p. 484].

3.5 Melanoma

Melanoma is a malignant tumour of the skin arising in the epidermis. The cell of origin is the melanocyte which is present in the basal layer at the junction of the epidermis and dermis. It starts multiplying and invades upwards through the epidermis to the surface and downwards into the underlying dermis. Melanoma accounts for about 3% of all cancers and about 0.5% of all cancer deaths [44, p. 256]. It occurs most frequently in white adults where the lower leg in females and the trunk and back of males are commonly affected. It is rare in dark skinned

races and if it does occur it only does so on the palms of hands or the soles of feet. Sunlight exposure seems to be the main factor associated with the development of malignant melanoma. Instead of BCC or SCC which are associated with chronic sun exposure, melanoma appears to be initiated by episodic acute exposure to burning [50, p. 695].

3.5.1 Variants of malignant melanoma

The main variants of invasive malignant melanoma are:

- Lentigo maligna melanoma
- Superficial spreading melanoma
- Nodular melanoma
- Acral lentiginous melanoma.

3.5.1.1 Lentigo maligna melanoma (Hutchinson's melanotic freckle)

This is a flat pigmented lesion usually occurring on the sun-damaged skin of the elderly. It consists of a linear proliferation of atypical melanocytes within the epidermis. This may persist for years before becoming invasive [44, p. 256].

3.5.1.2 Superficial spreading melanoma

This type of melanoma accounts for 60 to 70% of cases and is characterized by nests of atypical melanocytes which grow horizontally within the epidermis with invasion into the dermis. Individual melanocytes migrate upwards through the epidermis [44, p. 257].

3.5.1.3 Nodular melanoma

Nodular melanoma does not have a significant radial growth phase and invasion takes place at an early stage. This melanoma makes up about 30% of all cases [44, p. 258].

3.5.1.4 Acral lentiginous melanoma

This is the most common form of malignant melanoma in dark skinned races. It shows a radial growth phase similar to that of Lentigo maligna but invasion takes place in an earlier stage.

3.5.2 Clinical course of melanoma

The prognosis of invasive melanoma depends predominantly on the depth of the lesion and the presence or absence of surface ulceration. The cure rate for completely excised non-ulcerated melanoma with thickness below 1 mm can be as high as 100% [50, p. 694]. The prognosis worsens with increased thickness. The chances of patients surviving 5 years after contracting malignant melanoma with lesions deeper than 4 mm or more is down to 40% [44, p. 256]. All malignant melanoma finally lead to metastatic spread as soon as they come into contact with superficial dermal vessels. The tumour spreads to all parts of the body with a predilection for the brain, skin and gastrointestinal tract [50, p. 694].

3.5.3 Treatment of Melanoma

3.5.3.1 Surgery

Surgery is considered to be the only curative treatment for all but the most advanced stages of the disease. Lesions with little or no invasion are surgically excised with a safe border of skin around it. Removal of a larger radius of surrounding skin is needed with excision of thicker lesions. Regional lymph nodes should also be removed with thicker lesions as a precautionary measure since they may be tumour-bearing [38, p. 490].

3.5.3.2 Chemotherapy

One method of treating regional or distant spread of melanoma is through the administration of chemotherapy. Single-drug chemotherapy is however effective in no more than 20% of patients with the disease in advanced form. Drug combinations can cause 50% shrinkage of all tumour masses for at least four weeks in 40 to 60% of cases according to recent reports. The duration of response is still fairly short and the percentage of complete remissions is low but the increased percentage of response is encouraging [10, p. 574].

3.5.3.3 Immunotherapy

This technique involves stimulating the patient's immune system with biological response modifiers to reject the tumour. Moderate doses of interferon-alpha has resulted in about a 20% response rate while a new biological substance called Interleukin – 2 (IL – 2) has had responses in 25% of patients. Remarkable degrees of shrinkage of lesions have for example been observed in the liver. Active specific immunotherapy (melanoma vaccines) has also shown considerable promise in treating advanced melanoma. The most successful of the melanoma vaccines resulted in about 20% of patients having had partial or complete remissions [10, p. 574].

3.5.3.4 Radiation

Malignant melanoma cells show apparent resistance to radiation with the result that high individual doses are required to enhance cell kill. Radiotherapy can be used to treat isolated large lesions if surgical excision is deemed too radical or it can be used to help relieve pain. Brain metastases are treated by somewhat lower radiation doses. Stereotactic radiotherapy (focused radiation) is now replacing neurosurgery in some centers for treatment of small brain metastases [10, p. 574].

CHAPTER 4

BREAST CANCER AND TREATMENT THEREOF

4.1 Introduction

Breast cancer accounts for 20% of all cancers in the United Kingdom and is the most common cause of death among women in the 35 to 55 year age group. Recent reports show there to be 39500 new cases each year in the UK. Internationally, the highest incidence rates are found in North America, North–West Europe and Australia with much lower rates in Asia and parts of Africa. It is estimated, in the higher risk areas, that any individual woman has a one in nine chance of developing the disease in her lifetime [50, p. 479].

4.2 Types of breast cancer

Virtually all breast cancers arise from the epithelial cells lining the lactiferous ducts and acini that are contained in the lobules as shown in Figure 4.1. These types of cancers are generally divided into: noninvasive or in situ cancers and invasive cancers [32, p. 17]. The many lobules in the breast produce milk while the ducts carry it to the nipple. Cancers originating in the ducts and lobules are referred to as ductal and lobular cancers respectively.

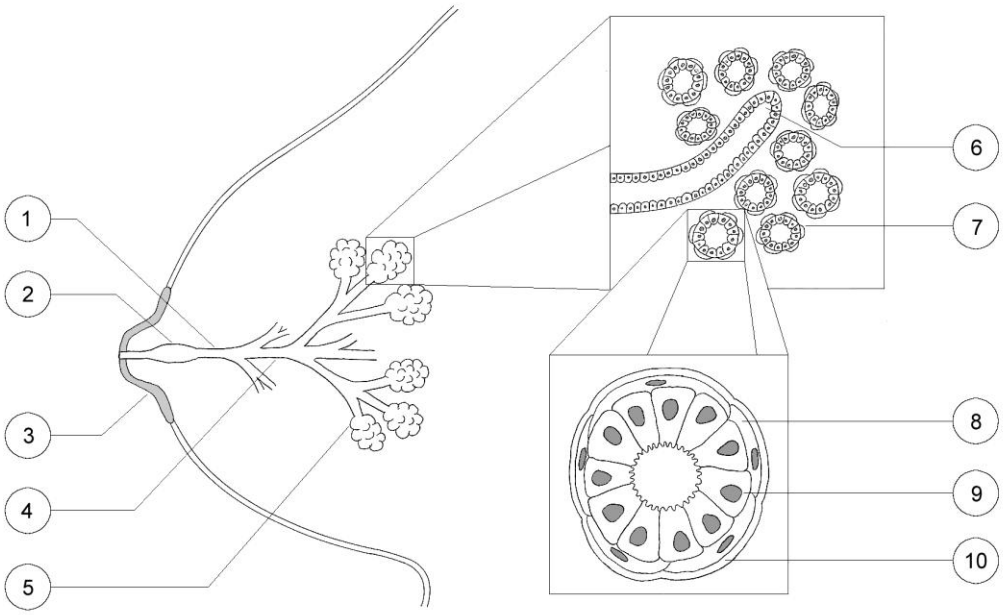

1. Lactiferous duct
2. Lactiferous sinus
3. Nipple
4. Duct (drainage system)
5. Lobules containing acini
6. Intralobular duct
7. Acini
8. Myoepithelial cells
9. Epithelial cells
10. Basement membrane

Figure 4.1 Structure of the adult female breast, showing the major components [50, p. 478]

4.2.1 Non–invasive carcinomas

The term 'non–invasive' means that the malignant cells are confined within the lining of the ducts or lobules. There is thus no evidence of penetration of the tumour cells through the basement membranes of these structures into the surrounding fibrous tissue [50, p. 479]. There are two types of non–invasive breast carcinoma: ductal carcinoma in situ and lobular carcinoma in situ.

4.2.1.1 Ductal carcinoma in situ (DCIS)

DCIS accounts for about 5% of breast carcinomas and can occur in both pre- and post menopausal women, usually in the 40 to 60 year age group. The disease is usually confined to one quadrant of the breast although a larger area could be involved with large lesions. Occurrence of the disease in both breasts is uncommon [50, p. 482]. DCIS has the ability over a long period to become invasive if left untreated making it necessary for the tumour to be completely removed [10, p. 357].

4.2.1.2 Lobular carcinoma in situ (LCIS)

LCIS is usually diagnosed in pre-menopausal women. It affects more than one quadrant of the breast in up to 90% of cases and is found in both breasts in 25% of cases. About 25 to 30% of patients with LCIS will go on to develop invasive carcinoma within 20 years if the condition is left untreated. This may occur in either or both breasts and may be of the ductal or lobular type [21, p. 515].

4.2.2 Invasive breast carcinoma

An 'invasive' breast tumour is one whose cells have broken through the basement membrane around the breast structure in which they have arisen and spread into surrounding tissue [50, p. 483]. The types of invasive carcinoma and their relative incidence are:

- Infiltrating ductal (75%)
- Infiltrating lobular (10%)
- Mucinous (3%)
- Medullary (3%)

- Tubular (2%)
- Others (7%).

4.2.2.1 Invasive ductal carcinoma

Invasive ductal carcinoma makes up the majority of infiltrating breast carcinomas. It can occur in both pre- and post-menopausal women and usually forms at one focus in a single breast [50, p. 484].

4.2.2.2 Invasive lobular carcinoma

While lobular carcinoma in situ is usually diagnosed in pre-menopausal women, the infiltrating lesion can also occur in post-menopausal women. Invasive lobular carcinoma can be multifocal not only in the same breast, but also in the opposite one [50, p. 485].

4.3 Spread of breast carcinoma

Behavior of breast carcinoma is particularly unpredictable. It is not unusual to encounter patients with widespread bone disease but without any evidence of soft tissue disease while others develop relentless local recurrence without distant metastasis [47, p. 253]. It also exhibits marked variation in the time span between presentation of the primary carcinoma and the appearance of recurrent / metastatic disease. In some patients breast carcinoma never recur while in others reappearance of the disease may be within two to five years.

It is however also possible for the disease to recur as much as 20 years after the original excision [50, p. 488]. Breast carcinoma can infiltrate locally through direct spread or metastasize to more distant sites via lymphatics and the bloodstream as shown in Figure 4.2.

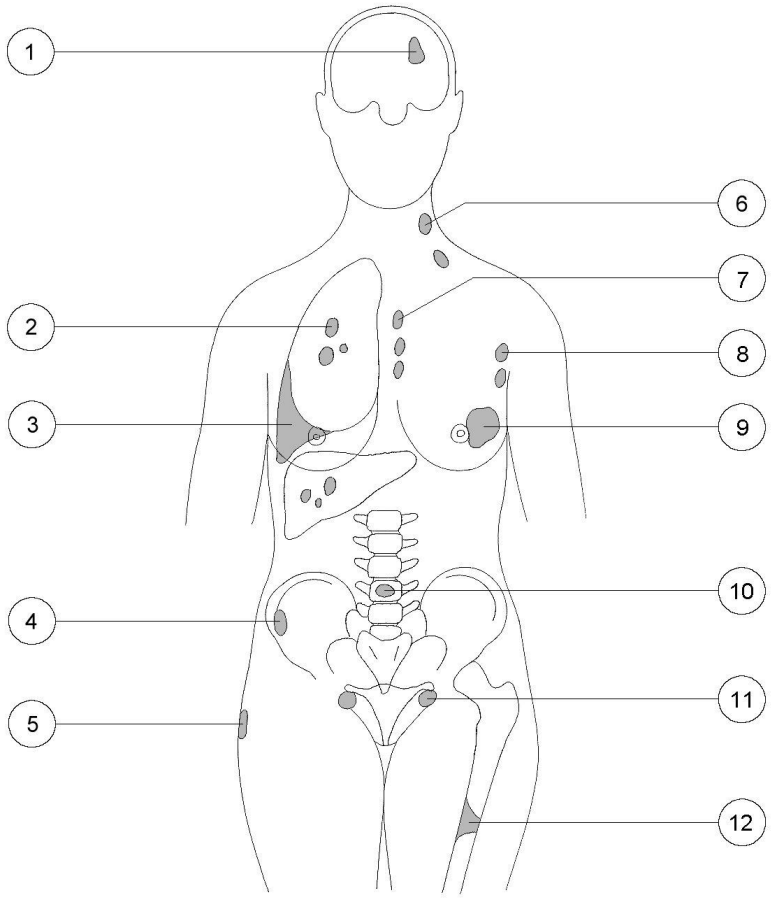

1. Brain
2. Lung
3. Pleural effusion
4. Bone marrow
5. Skin
6. Supra clavicular lymph nodes
7. Internal mammary nodes
8. Axillary lymph nodes
9. Chest wall
10. Bone (especially axial skeleton)
11. Ovary
12. Pathological fracture

Figure 4.2 Local, nodal and distant spread in breast cancer [47, p. 252]

4.3.1 Direct spread

Local infiltration may occur either to the underlying muscles and chest wall or to overlying skin [47, p. 252].

4.3.2 Lymphatics

Sites of metastasis via lymphatics are axillary, supraclavicular, internal mammary or tracheobronchial regional lymph nodes. The axillary nodes provide the major drainage of the breast tissue. Histological analysis of these nodes presents the single most important prognostic factor for breast cancer [29, p. 233]. Finding tumour deposits in the supraclavicular lymph node group is a particular adverse clinical sign since this indicates advanced local infiltration [21, p. 515].

4.3.3 Blood stream

Blood-borne metastasis of breast carcinoma involves the lungs, bone (especially the axial skeleton), liver, skin and central nervous system (both brain and spinal cord). Intra-abdominal and pelvic metastases are also common [47, p. 253].

4.4 Risk factors associated with breast cancer

Despite great effort and enormous expenditure, the main factor that causes breast cancer still eludes researchers. Several risk factors are however well established [12, p. 1].

- Family history of breast cancer in first degree relatives (e.g. mother, sister, daughter). The risk is about six times greater if a mother or sister had breast cancer before menopause and up to 10 times greater if the cancer involved both breasts.
- Women who carry a first full-term pregnancy over the age of 30 years are three times more likely to develop breast cancer than those who do so under 20 years.
- Early onset of menstruation and late onset of menopause increases risk.
- Obesity, with postmenopausal women at higher risk.

4.5 Staging of breast cancer

When a woman is diagnosed with breast cancer, it is of the greatest importance to determine the advancement of the disease both locally and distantly through metastatic spread. To this end a process termed staging is undertaken. With the TNM classification system, as shown in Table 4.1, staging is done according to the primary tumour size (T), involvement of the axillary nodes next to the affected breast (N) and if metastasis is present or not (M). The clinical stages range from I to IV [10, p. 363].

Table 4.1 TNM (Tumour Node Metastasis) classification for breast cancer

Stage I	T1	N0 /N1a	M0
Stage II	T0	N1b	M0
	T1	N0,1a, 1b	M0
	T2	N0, 1a, 1b	M0
Stage III	T1	N2	M0
	T2	N2	M0
	T3	N0 /1 /2	M0
Stage IV	T4	Any N /M	
	Any T N3	Any M	
	Any T /M	M1	

T1 Tumour < 2 cm
   a. Without fixation to underlying structures
   b. Fixed to underlying structures
T2 Tumour between 2 and 5 cm – a and b
T3 Tumour > 5 cm but < 10 cm or < 5 cm with infiltration, ulceration or fixation
T4 Tumour of any size fixed to chest wall or skin
   a. Chest wall
   b. Oedema, ulceration of the skin of the breast or satellite skin nodules
   c. a and b
   d. Inflammatory

N0 Node-negative
N1 Mobile nodes
   a. Clinically uninvolved
   b. Clinically involved
N2 Nodes involved and fixed
N3 Supraclavicular or infraclavicular nodes or arm oedema

M0 No distant metastases
M1 Metastases present

Staging determines the treatment to be offered to the breast cancer patient especially if several treatment techniques are available as will be discussed next.

4.6 Treatment of breast cancer

Significant advances have been made in the treatment of breast cancer in recent years. A multidisciplinary treatment approach is now standard with a combination of surgery, radiotherapy and chemotherapy.

4.6.1 Surgery

The primary method for the treatment of invasive breast cancer, which is apparently confined to the breast, is surgical removal of the tumour. Very small tumours can be excised by a procedure termed a lumpectomy while most early breast cancers can be treated with a segmental resection [10, p. 364]. Larger tumours require a quadrantectomy. With this procedure the quadrant of the breast centered on the cancer is removed [21, p. 521]. If the tumour has spread throughout the breast a mastectomy needs to be performed. In advanced situations where the cancer is attached to underlying muscle, a Halsted radical mastectomy which removes the entire breast with the affected muscle is performed [47, p. 257]. Lymph nodes in the axilla (armpit) are generally removed as part of the surgical procedures. This is done to determine the extent of the cancer. Cancer present in these nodes indicates a significant risk of metastases outside the breast requiring additional therapy [10, p. 365].

4.6.2 Chemotherapy

Although chemotherapy was introduced much more recently, it has rapidly become one of the most important treatment methods for breast cancer. Different drug combinations are often prescribed as an adjuvant therapy for patients after surgery. This is in an attempt to prevent or minimize the growth of microscopic deposits of tumour cells that might grow into recurrent tumours [10, p. 372]. A variety of drug combinations are also widely used in the treatment of metastatic and locally advanced breast cancer. Since cure is usually not possible in these situations the main aim of therapy is relief of disease related symptoms which may last for months and often years [21, p. 529]. Another type of treatment that can be prescribed on an adjuvant basis or as treatment of metastatic disease is hormonal therapy. The hormonal balance was once manipulated through removal of the ovaries or adrenal glands and sometimes the pituitary gland. The same effects can now be achieved through the use of

various drugs. With hormonal therapy there is a 30% likelihood of women responding to treatment while chemotherapy has a response rate of double this figure. Hormonal induced responses are however much less toxic to the patient and tend to be more durable [47, p. 265].

4.6.3 Radiotherapy

There are various recommended radiotherapy techniques for the treatment of both breast-conserving and post mastectomy breast cancer patients. Some of the most successful techniques will be discussed next.

4.6.3.1 Radiation therapy techniques for the breast-conserving patient

Following removal of the primary breast tumour by surgery, local recurrence of the disease in the chest wall, regional lymph nodes or residual breast occurs with a frequency of 7 to 30% [47, p. 257]. This is due to microscopic cancer cells remaining in the surrounding tissue or lymph nodes after surgery. To overcome this problem in the past, the Halsted radical mastectomy procedure was performed as standard. This procedure has a low recurrence rate of around 4% but often has negative psychological implications for the patient [47, p. 259]. The preferred treatment for early breast cancer nowadays is a lumpectomy or segmental resection followed by radiation treatment to the breast and internal mammary, axillary and supraclavicular lymph nodes if involved. Results from these procedures have shown to be equivalent to the radical mastectomy in terms of patient survival [10, p. 371].

a) Opposing tangential fields to the chest wall and breast

A widely used method for the treatment of the intact breast is by irradiation with two opposing photon fields applied tangentially to the chest wall with no more than 2 to 3 cm of the lung included. Figure 4.3A shows an anterior view of treatment fields commonly applied to breast cancer patients while Figure 4.3B shows a transverse slice of the body with tangential photon fields applied.

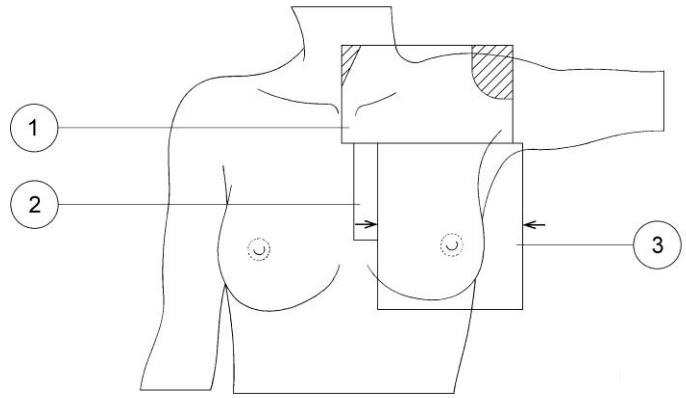

A

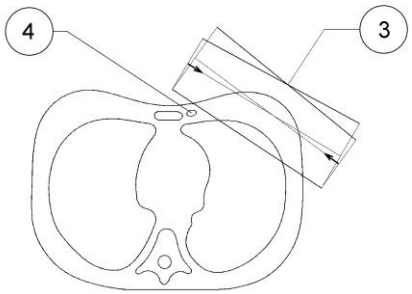

B

1. Supraclavicular field
2. Internal mammary field
3. Tangential fields
4. Internal mammary node

Figure 4.3A Anterior view of treatment fields commonly applied to breast cancer patients [19, p. 176]

Figure 4.3B Transverse slice of the body with tangential photon fields applied [38, p. 913]

The gantry angle is adjusted to achieve alignment of the anterior edges of the tangential fields to prevent divergence into the lung. The patient is positioned supine on the linear accelerator table with the thorax supported by a rigid wedge. The angle of the support wedge is chosen so that the patient's sternum lies parallel to the treatment table. This is done to simplify the tangential field setup [19, p. 177]. The patients arm on the treatment side is supported at 90° to the body and the head is turned sharply to the contra lateral side. The entire breast needs to

receive a total dose of 4500-5000 cGy of radiation in five to six weeks at 180-200 cGy per day with five fractions in a week [38, p. 904].

b) Internal mammary lymph node treatment

If the internal mammary nodes require irradiation they may be included in the tangential treatment beams by moving the field border 3 to 5 cm across the patient's anterior midline. It should however be ascertained that an excessive amount of lung or heart tissue will not be included in the tangential beams as shown in Figure 4.4A. If this is the case, a separate photon or electron field may be applied adjacent to the tangential field's edge as shown in Figure 4.4B. The recommended total dose to the internal mammary field is 4500-5000 cGy at 180-200 cGy per day. Electron radiation in the order of 13 MeV is preferred for a portion of the treatment to spare underlying lung, mediastinum and spinal cord. The usual proportion is 1440 cGy with 4-6 MV photons and 3060 cGy with electrons at 180 cGy per day [38, p. 912]. Also shown in Figure 4.4B is a potential dosimetric "cold" area (indicated in blue) between the internal mammary and tangential fields with large chested women.

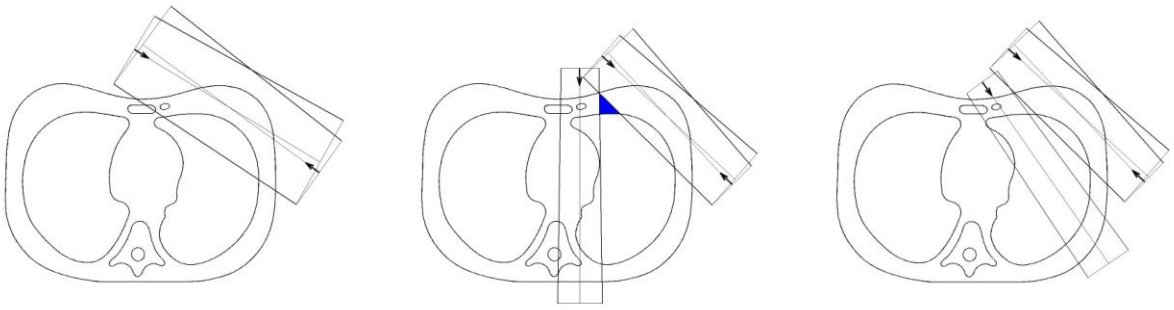

A B C

Figure 4.4A, B and C Transverse slices showing different radiation techniques to include internal mammary nodes in the treatment of breast cancer [38, p. 913]

To overcome this problem, Woudstra and van der Werf describe a technique using an oblique incidence of the internal mammary field as shown in Figure 4.4C. By matching the orientation of the adjacent tangential fields a more homogeneous distribution at the field junction will result [38, p. 911].

c) Supraclavicular lymph node treatment and field matching problems

The recommended total dose to the supraclavicular lymph nodes is 4600 cGy at 200 cGy per day in five fractions per week [38, p. 913]. Field matching problems often occur between the supraclavicular treatment field and the opposing tangential fields. Because of the divergence of the tangential beams into the supraclavicular field and the supraclavicular beam into the tangential field a dosimetric "hot spot" (indicated in red) will exist just beneath the skin surface where the fields meet as shown in Figure 4.5A and B. This increase in dose may result in severe match line fibrosis or even rib fracture [38, p. 910].

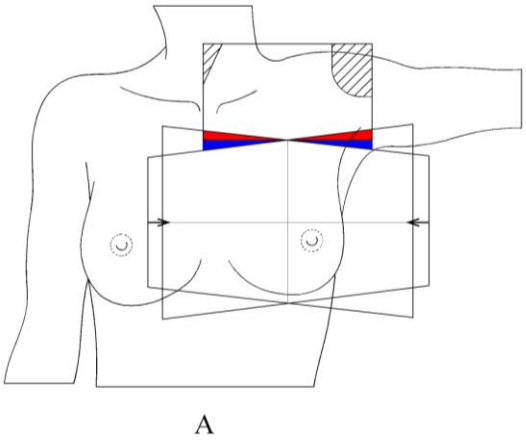

A

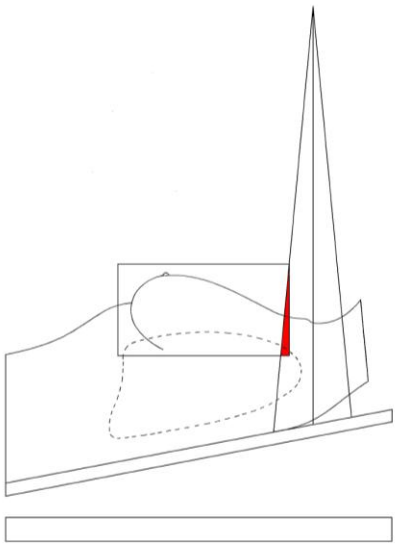

B

Figure 4.5A Anterior view showing field matching problems with tangential and supraclavicular radiation treatment fields [19, p. 180]

Figure 4.5B Lateral view showing field matching problems with tangential and supraclavicular radiation treatment fields [19, p. 180]

Careless field matching may also result in a dosimetric "cold spot" (indicated in blue in Figure 4.5A) with possible recurrence of the disease in that area. Various methods of matching the treatment fields are in use, each with their own limitations and difficulties which will be discussed next.

i) Table and gantry rotation

Treatment table rotation can be applied as a means of matching the supraclavicular field to the tangential field as shown in Figure 4.6A. By rotating the table alternately to the divergent superior borders of the tangential fields, they can be arranged to line up perfectly with the inferior border of the supraclavicular field.

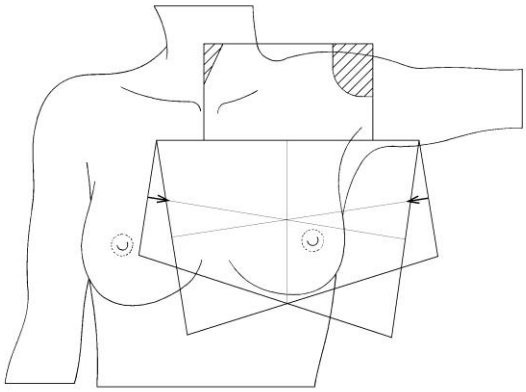

A

Figure 4.6A Anterior view showing field matching through table and gantry rotation [19, p. 182]

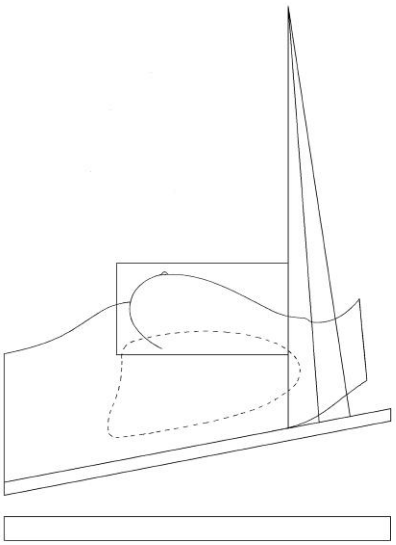

B

Figure 4.6B Lateral view showing field matching through table and gantry rotation [19, p. 180]

To match the supraclavicular field to the tangential fields, the treatment table can be rotated through 90° and the gantry angled to take up the divergence of the anterior beam as shown in Figure 4.6B. In addition to this, the anterior beam should be angled 15° laterally to spare the spinal cord [19, p. 182].

ii) Asymmetry

If the linear accelerator that is used for treatment is equipped with asymmetric diaphragms (meaning that the diaphragms are able to move independently of each other), matching of treatment fields can be simplified.

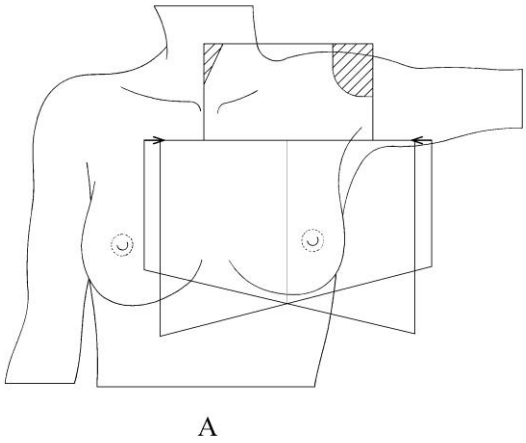

A

Figure 4.7A Anterior view showing field matching through asymmetric diaphragms [19, p. 181]

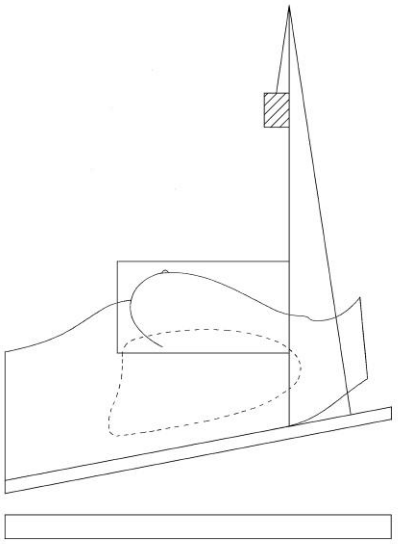

B

Figure 4.7B Lateral view showing field matching through asymmetric diaphragms [19, p. 181]

Half blocking the superior borders of the tangential and inferior border of the supraclavicular beams with the asymmetric diaphragms ensures no divergence of the beams into each other as shown in Figure 4.7A & B. Again the anterior beam should be angled 15° laterally to spare the spinal cord [19, p. 181].

d) Axillary lymph node treatment

If the axillary lymph nodes are at risk the supraclavicular field may be extended both inferiorly and laterally to include the axillary nodes. Once treatment to the supraclavicular field is competed, the dose to the axilla can be supplemented by a posterior axillary field. The patient is positioned prone on the treatment table without a wedge support and the field is administered anteriorly to correspond with the supraclavicular field [29, p. 238]. The total

dose recommended for the axillary lymph nodes is 4600-5000 cGy at 200 cGy per day [38, p. 914].

4.6.3.2 Post mastectomy radiotherapy techniques

Radiation treatment is prescribed after a mastectomy procedure if the tumour was very large, if it invaded the chest wall muscles or if many lymph nodes were involved. In these cases it is assumed that there are undetectable tumour cells present in the chest wall or lymph nodes that can be eradicated through radiation. Radiation fields are in most cases applied to the skin flaps on the chest wall and the regional lymph nodes of the same side [51, p. 118].

a) Electron treatment to the chest wall

The post mastectomy patient can be treated with the same irradiation techniques as that which will be used for a patient who had breast-conserving surgery. However since a mastectomy procedure simplifies the body contours in the chest area the opportunity arises to use electron treatment fields instead of tangential photon fields. Electron beams have the advantage of rapid dose fall-off after achieving maximum dose, making it ideally suitable for irradiation of the chest wall where underlying lung tissue needs to be spared. If the patient has a fairly flat chest wall contour, a single electron field can be used for treatment as shown in Figure 4.8A. For patients with a fairly curved chest wall, a second treatment field with 35° lateral tilt can be added that abuts the first field as shown in Figure 4.8B. The match line needs to be moved laterally on a weekly basis to avoid dose buildup [29, p. 236].

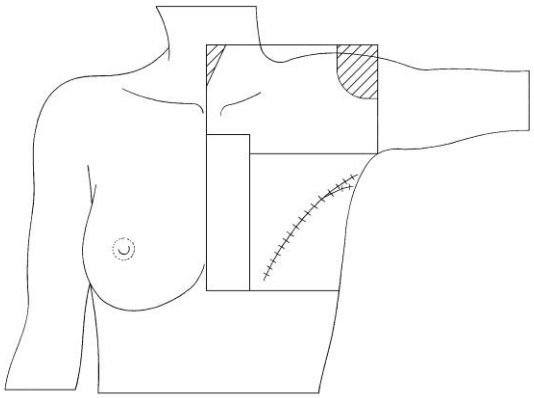

A

Figure 4.8A Anterior view showing two electron fields setup [29, p. 237]

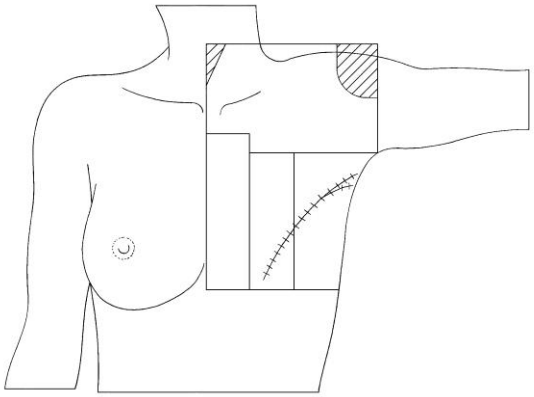

B

Figure 4.8B Anterior view showing three electron fields setup [29, p. 237]

If the mastectomy scar extends beyond the mentioned electron fields, an additional field may be added to cover this area. Bolus may be added to the chest wall during electron treatments to minimize lung dose and to increase skin surface dose. The recommended total dose for electron treatment of the chest wall is 5000 cGy over a period of five weeks [29, p. 236]. Internal mammary, supraclavicular and axillary lymph nodes are treated in the same way as was described for the breast-conserving treatment techniques.

b) Opposing tangential fields to the chest wall

If the skin flaps left after the mastectomy procedure are very thick or electron treatment is not available opposing tangential photon beams can also be used for the treatment of post mastectomy patients. To ensure adequate skin dose, bolus can be added to the entire photon treatment field for one third of the treatments and to only the scar for an additional third of treatments [38, p. 959]. A disadvantage of using bolus is the formation of telangiectasias and resultant poor cosmetics [19, p. 176]. The radiation dose to the chest wall is the same as that will be applied to the treatment of the intact breast.

c) Isocentric rotational electron beam irradiation

An electron irradiation technique developed at the Division of Radiation Oncology, University of Utah involves rotating the gantry in a semi arc around the patient's thorax while irradiating the chest wall in a continuous field [31, p. 1287]. This technique can be used for post mastectomy patients that will be difficult to treat with conventional photon or fixed electron beam irradiation. Long mastectomy scars, tumours extending across the midline or onto the posterior thorax and variation in target volume depth are common problems that make treatment with conventional techniques technically difficult [6, p. 1969]. The patient is positioned supine on the treatment table with the isocenter at a depth within the patient so as to maintain a uniform SSD throughout the arc. Figure 4.9 shows the setup for rotational electron beam irradiation schematically. Two shielding blocks that are screw mounted onto an acrylic tray with the central part of the tray removed are placed in the linear accelerator's shadow tray. These blocks are adjustable to be opened or closed symmetrically about a central point producing a rectangular or trapezoid shape. The purpose of the shielding blocks is to serve as a secondary collimator to account for changes in the radius of the thorax from the superior to the inferior field borders [28, p. 988]. It is also necessary to sharply define the edges of the treatment field on the patient. For this purpose a radiation shield needs to be produced that conforms to the individual patient's thorax. This can be done by pouring molten Lipowitz metal into a mould that was produced from an impression taken of the treatment area on the patient. The Lipowitz metal cast is lined with foam and is placed on the patient's thorax during treatment [28, p. 989]. All patients who are to be treated by rotational electron beam irradiation needs to be scanned on a computerized tomography (CT) scanner. This is done to determine the chest wall thickness as well as depth of internal mammary nodes that can be included in the treatment field if required. Bolus may be added to the chest wall in

places where it is thin to produce a more uniform chest wall thickness. The radiation dose to variable depths within the treatment volume is controlled by varying the electron energy and dose rate through the arc. Different radiation energies, are for example, required over the internal mammary nodes and the chest wall [37, p. 2150].

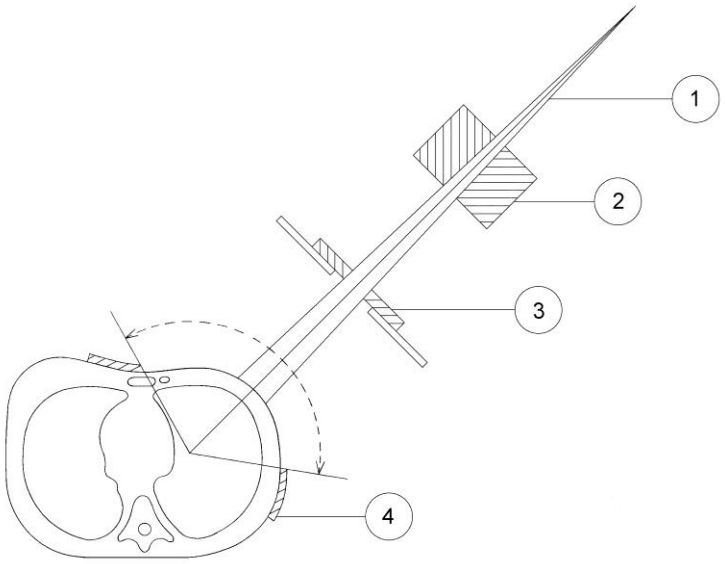

1. Electron beam
2. Diaphragms
3. Shielding blocks
4. Cerobend cast

Figure 4.9 Isocentric rotational electron beam irradiation [28, p. 988]

Disadvantages of this technique are that the fabrication of the Lipowitz metal shielding cast and CT treatment planning are time and labour intensive. Advantages of the technique are better dose uniformity and reduction in dose to underlying lung when compared to standard treatment techniques [28, p. 995].

4.6.3.3 Boost to the tumour site

Breast cancer that recurs after a combination of surgery and irradiation occurs in 65–80% of cases around the primary tumour site [38, p. 908]. This statistic provides strong motivation for

a radiation boost to the scar for both conservation surgery and post mastectomy patients to have a greater probability of tumour control. The preferred boost technique is by applying an electron field with a 2-3 cm margin around the tumour bed. An electron energy is selected that will cover the target volume depth without delivering substantial dose to the underlying lung [49, p. 259]. Several methods are in use to delineate the treatment borders as will be explained in Chapter 5.

CHAPTER 5

TRADITIONAL RADIATION FIELD SHAPING TECHNIQUES

5.1 Introduction

Both linacs and kilovolt units make use of applicators to collimate the radiation beams produced by the units to required treatment field sizes as described in sections 2.3.1 and 2.5.3. Square, rectangular and round applicators of different field sizes are available to both types of treatment units. One of these standard field shapes is chosen to fit the shape of the cancer affected area on the patient as closely as possible as shown in Figure 5.1A.

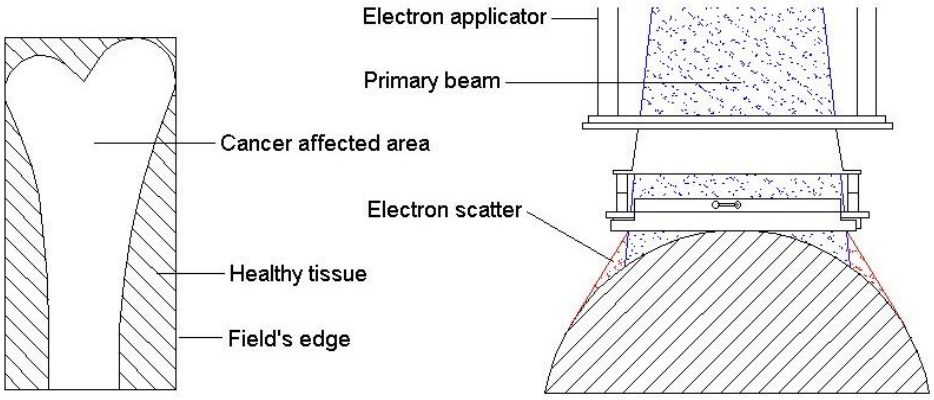

Figure 5.1A Rectangular treatment field applied to cancer affected area

Figure 5.1B Electron applicator setup showing stand-off

Since the cancer affected areas are irregular in shape, there will always be an area of healthy tissue between the edge of the cancer affected area and the edge of the standard field shape.

This healthy tissue will be inadvertently irradiated along with the cancer during treatment. This is undesirable since the cancer wound heals through reparative growth of the surrounding healthy tissue after treatment as described in section 2.2.2. The problem will be made worse if the cancer affected area is large and located across a curved area of the patient's body. During treatment, the radiation unit's applicator is brought into contact with the patient's skin as shown in Figure 5.1B. Considering that the treatment end of the applicator is flat, there can be a considerable stand-off between the patient's skin and the applicator at the field's edges. A stand-off will result in radiation scatter beyond the field's edges resulting in a larger area being irradiated than intended.

5.2 Existing radiation field shaping techniques

Different field shaping techniques where developed to overcome the problems mentioned in section 5.1. These techniques will be discussed next together with their respective disadvantages.

5.2.1 Lead masks

Lead masks are commonly used to shield healthy tissue surrounding malignant skin tumours during treatment with low energy X-rays or electrons [24. p. 883]. These masks are used with small treatment fields that are applied across a relatively even treatment area. For large treatment fields applied across a curved area, the wax casting field shaping technique as described in section 5.2.2 is preferred. The fabrication of a lead mask is explained with reference to Figure 5.2A-R. To begin with a radiation oncologist identifies and marks the cancer affected area on the patient's skin by means of a water based marker. If the cancer affected area is located in the facial area, as is often the case, thin plastic film is cut to size

and is placed over the patient's eyes (Figure 5.2A). Strips of wet plaster bandage are laid down on the patient's skin up to two or three layers (Figure 5.2B). The plastic film prevents the plaster from sticking to the eyelids and eyebrows. When the plaster bandage impression has set, it is removed from the patient's skin (Figure 5.2C). The water based markings are dissolved by the wet plaster bandages and are thus transferred to the impression. These transferred markings are redrawn on the impression. The open ends of the impression are blocked with additional plaster bandages (Figure 5.2D). Liquid soap is painted onto the plaster bandage impression to serve as separation medium (Figure 5.2E). Yellow-stone™ plaster is mixed to a liquid consistency and is poured into the impression (Figure 5.2F). Again the markings are transferred this time to the stone plaster model.

A

B

C

D

E

F

G

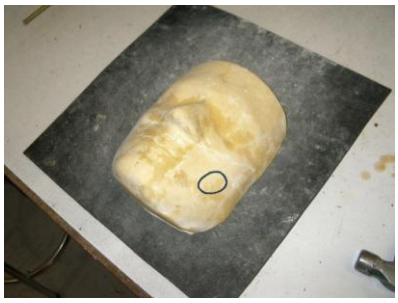

H

I

J

K

L

M

N

O

P

Q

R

Figures 5.2A-R Fabrication of a lead mask

When the stone plaster has set, the plaster bandages are removed (figures 5.2G and 5.2H). Lead sheet with thickness according to the intensity of the radiation to be applied during treatment (2–6 mm) is roughly cut according to the size of the required mask [16, p. 336]. The lead sheet is placed onto the model and is formed according to the shape of the model by means of a special hammer (Figure 5.2I). Excessive lead sheet is trimmed away with tin snips (Figure 5.2J). Often the shape of the model requires the mask to be partially split to be able to take on the shape of the model (Figure 5.2K). This split line needs to be soldered once shaping is completed (Figure 5.2L). To prevent the joint line from hurting the patient it needs to be trimmed on the inside of the mask (Figure 5.2M). For higher radiation energies, extra pieces of lead sheet need to be cut to shape and soldered on to the mask in the position of the patient's eyes. This is to assure that no radiation will pass through to these radiation sensitive areas. To transfer the position of the tumour from the model to the mask, a thin sheet of dental wax is lightly heated and is pressed onto the marked area on the model (Figure 5.2N). The wax is cut according to the shape of the marked area on the model by means of a heated instrument (Figure 5.2O). The mask is heated slightly and is pressed firmly onto the model, in so doing transferring the wax to the mask (Figure 5.2P). A hole is cut in the mask according to this marker with a jig saw (Figure 5.2Q). Finally the mask is dipped in molten dental wax in order to prevent the patient's skin from coming into contact with the lead mask. The mask is placed onto the patient's skin during treatment thereby limiting the radiation to only the cancer affected area (Figure 5.2R).

Disadvantages of the Lead mask technique are:

- The Yellow-stone™ plaster has to be left at least overnight to harden sufficiently to prevent it from breaking up while forming the lead sheet on it. A technologist can thus only start fabricating the mask a day after the plaster bandage impression was taken.
- The technique of forming the lead sheet on the model requires a great deal of skill, effort and time especially if the lead sheet needs to be thicker than 2 mm.
- Most radiotherapy departments are unable to recycle the lead from used masks since special equipment is required to melt the lead and role it into sheets of the required thickness. Lead is thus only used to shield around small treatment fields since it is uneconomical to use the material for large fields where wax castings are preferred.
- The procedure of taking a plaster bandage impression of a patient, especially in the facial area, is often traumatic and uncomfortable for the patient.

5.2.2 Wax castings

Wax castings are used for field shaping purposes with large electron treatment field sizes that are applied across a curved area of a patient's body. A typical example of this is the treatment of the scar left after a radical mastectomy procedure was performed on a breast cancer patient as described in section 4.6.3.3. An electron boost of 4–10 MeV is applied to ensure that no cancerous cells remain in that area that may result in further cancerous growth [29, p. 236]. The traditional method of shielding the healthy tissue surrounding the scar is by means of a wax casting, the fabrication process of which is explained with reference to Figure 5.3A-U. A radiation oncologist identifies and marks the borders of the scar tissue on the patient's skin with a water based marker. Two or three layers of wet plaster bandages are laid down across the marked area on the patient while allowing for a sufficient border around the area. When the plaster bandage impression has set it is removed from the patient (Figure 5.3A). The

markings that were transferred from the patient's skin to the inside of the impression are redrawn with the marker. The open ends of the impression are blocked with additional plaster bandages (Figure 5.3B). Plaster of Paris is mixed to a medium thick paste and the impression is filled with it (Figure 5.3C). After the plaster has set the plaster bandages are removed and the markings redrawn on the model (Figure 5.3D).

A

B

C

D

E

F

G

H

I

J

K

L

M

N

O

P

Q

R

S

T

U

Figures 5.3A-U Fabrication of a wax casting

A rectangular Perspex™ frame with a size according to the radiation field size to be applied during treatment is placed on the model (Figure 5.3E). The gap between the flat underside of the frame and the curvature of model is filled in with plaster bandages (Figure 5.3F). Papier mâché is used to fill the space between the frame and the edge of the scar tissue on the model (figures 5.3G and 5.3H). Liquid soap is painted over the area of scar tissue on the model to serve as separating medium (Figure 5.3I). Plaster of Paris is again mixed to a medium thick paste and the cavity formed by the papier mâché is filled with it (figures 5.3J and 5.3K). When the plaster has set it is taken out of the frame along with the papier mâché (figure 5.3L and 5.3M). The plaster as formed by the papier mâché is sawn on a band saw according to the shape of the markings that were transferred from the model (Figure 5.3N). The sawn piece of plaster is replaced inside the Perspex™ frame according to the position of the scar tissue and molten dental wax is poured into the cavity between the frame and the plaster (figures 5.3O and 5.3P). The wax has to be poured in consecutive layers with a cooling period in between to prevent cavities forming inside the casting while the wax cools (Figure 5.3Q). With the casting process complete, the plaster and frame are removed from the wax casting (Figure 5.3R). The wax needs to be at least 5 cm thick to shield a 4-6 MeV electron beam. For higher radiation energies additional shielding is required. For this purpose Wood's alloy is melted and cast in a frame according to the size of the wax casting. The thickness of the alloy casting is dependent on the intensity of the radiation to be applied during treatment. The shape of the cavity in the wax casting is drawn on the alloy casting and is sawn on a band saw (Figure 5.3S). A heated instrument is used to solder the joint line once sawing is completed (Figure 5.3T). Masking tape is used to tape the alloy casting to the wax casting (Figure 5.3U). The finished wax and alloy casting is placed on the patient during treatment thereby limiting the radiation to the scar tissue.

Disadvantages of the wax field shaping technique are:

- A wax casting is typically produced over a period of three days making this field shaping technique time consuming. The technologist has to wait for the plaster to set during each step of the process as well as for each layer of the wax to cool during casting.
- A plaster bandage impression has to be taken of the area with the scar tissue that may be traumatic and uncomfortable to the patient.
- Great care should be taken in trimming the plaster casting as formed by the papier mâché on the band saw (Figure 5.3N). This casting may be as thick as 11 cm and may easily slip while sawn with the possibility of serious personal injury to the technologist producing the wax casting.

5.2.3 Shaped end-frames

An electron field shaping technique often used in oncology departments is to fabricate Wood's alloy shaped end-frames (also referred to as endplates) [17, p. 792], [39, p. 882], [46, p. 561]. Wood's alloy, named after American metallurgist B. Wood is a eutectic alloy that becomes a liquid at a temperature of approximately 70 °C. The alloy is made up of bismuth, lead, tin and cadmium with the following percentages by weight: 50% Bi, 26.7% Pb, 13.3% Sn and 10% Cd [43]. The alloy is also known as Cerrobend™, Bend alloy™, pewtalloy or Lipowitz metal [48]. Instead of conforming to the contours of the treatment area on the patient such as with lead masks or wax castings, shaped end-frames fit into the electron applicators in place of the standard square or rectangular end-frames. The fabrication process of a shaped end-frames is explained with reference to Figure 5.4A-F. The shape of the area to be treated on the patient is usually determined on the oncology department's treatment planning system. A printout of the treatment plan is sent to the department's workshop where

the treatment area is cut from the plan with scissors (Figure 5.4A). This piece of paper is glued to a block of polystyrene that is slightly thicker than what the end-frame needs to be. The shape of the treatment area is cut from the polystyrene on a hot wire cutter using the paper as guide (Figure 5.4B).

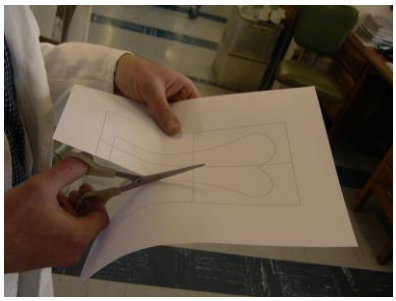

A

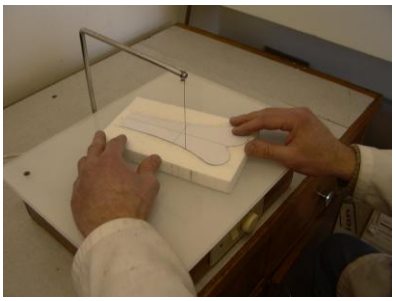

B

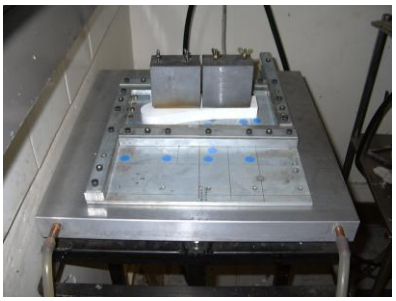

C

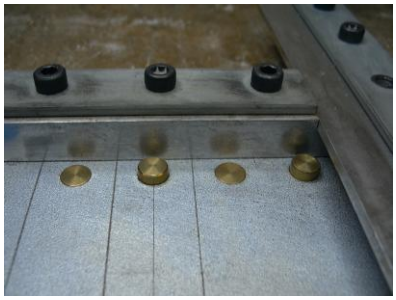

D

E

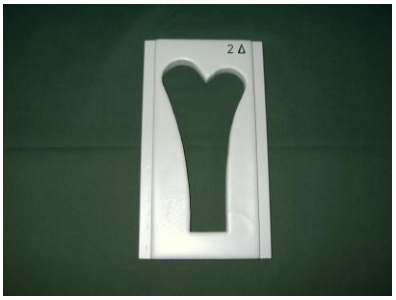

F

Figures 5.4A-F Fabrication of a shaped end-frame

The cut piece of polystyrene is centred on a special jig and is weighed down by means of lead blocks to prevent it from floating while casting the end-frame (Figure 5.4C). The jig is adjustable to accommodate all the different sizes of electron applicators that are available in the oncology department. There are four holes partially drilled through the base plate of the jig into which either removable inserts to blank off the holes or pegs can be inserted (Figure 5.4D). While casting the end-frame corresponding holes will be formed in the insert by the pegs. When the end-frame is fitted into the electron applicator the holes in the insert

line up with four micro switches in the applicator. This is registered by the accelerator as a binary code. Each end-frame can thus be individually coded to verify that the correct end-frame will be used for a specific patient. The base plate is also equipped with two additional repositionable pegs that form locating holes in the end-frames. These locating holes are used to centre the end-frame in the applicator. The jig is placed on an aluminum block that has internal waterways. The block is connected to a hot water supply and is heated to a temperature above the melting point of the Wood's alloy. Molten Wood's alloy is poured into the cavity between the frame of the jig and the polystyrene up to the top level of the frame (Figure 5.4E). Cold water is passed through the aluminum block allowing the end-frame to cool rapidly. It is preferable to cool the end-frame rapidly since slow cooling often causes air cavities forming inside the Wood's alloy. When the end-frame has completely cooled it is removed from the jig and is spray painted to finish it off (Figure 5.4F).

Disadvantage of shaped end-frames are:

While this is a quick and easy way to create a radiation field shaping shield, it makes no provision for any curvature of the treatment area. Electrons will scatter past the edges of the shielded area with a stand-off allowing a larger area to be irradiated than intended.

CHAPTER 6

THERMAL-SPRAY PROCESSES

6.1 Introduction

To overcome some of the disadvantages of the traditional low energy radiation field shaping techniques described in Chapter 5, the author investigated the possibility of using a thermal-spray process as an alternative means of producing radiation field shaping shields. A literature study was undertaken to determine if any one of the existing thermal-spray processes could be used as is or modified to fulfil this new role intended for it.

6.2 What is thermal-spraying?

Thermal-spraying is a generic term to describe a collection of processes involving acceleration of at least partially melted metallic or non–metallic particles to impact a surface thereby forming a coating. The first thermal-spray process was developed by Schoop in the late 19th century. He discovered that the passage of zinc particles through a flame resulted in adhesion of the particles onto a surface [20]. This experiment initiated a series of process improvements leading to a wide range of coating methods. Today any material that can be plastically formed can be deposited onto a surface (i.e. the substrate) by thermal-spraying [3]. Functions, applications and recommended coating materials for different thermal-spray processes are shown in Table 6.1.

Table 6.1 Functions, applications and coating materials for thermal-spraying [14]

Function	Application	Coating material
Adhesive Wear	Bearings, piston rings, hydraulic press sleeves	Chrome Oxide, Babbit, Carbon Steel
Abrasive Wear	Guide bars, pump seals, concrete mixer screws	Tungsten Carbide, Alumina /Titania, Steel
Surface Fatigue Wear	Dead centers, cam followers, fan blades (jet engines), wear rings (land based turbines)	Tungsten Carbide, Copper /Nickel /Indium Alloy, Chrome Carbide
Erosion	Slurry pumps, exhaust fans, dust collectors	Tungsten Carbide, Stellite
Heat Resistance	Burner cans /baskets (gas turbines), exhaust ducts	Partially Stabilized Zirconia
Oxidation Resistance	Exhaust mufflers, heat treating fixtures, exhaust valve stems	Aluminum, Nickel / Chrome Alloy, Hastelloy
Corrosion Resistance	Pump parts, storage tanks, food handling equipment	Stainless Steel, Aluminum, Inconel, Hastelloy
Electrical Conductivity	Electrical contacts, ground connectors	Copper
Electrical Resistance	Insulation for heater tubes, soldering tips	Alumina
Restoration of dimensions	Printing rolls, undersize bearings	Carbon Steel, Stainless Steel

The raw coating material that is fed into the spray source may either be in wire, rod, powder or liquid form depending on the process. Solid materials are melted and atomized, powder particles are heated to semi-molten or molten state and liquids atomized before being propelled towards the substrate. The heat source may be either electrical or chemical (combustion) while the particles or droplets are accelerated by either compressed air or as a result of the combustion process [14]. The high thermo-kinetic energy imparted to the particles or droplets during the thermal-spraying process causes them to deform upon impact with the substrate. A coating forms by layering individual flattened particles, also known as

lamellae or "splats", on top of one another. The lamellae form around prior surface features, cool and solidify [20]. Bonding of the coating to the substrate depends on both the material being deposited and the process used for deposition. If the materials are compatible, a chemical bond may form between the coating and base material. More commonly this is not the case making it necessary for the base surface to be roughened by a process such as grit blasting to provide a basis for a mechanical bond. The bonding strength between the structural elements within the coating determines the coating strength. This is referred to as cohesive strength while the bonding strength of the coating to the substrate is termed adhesive strength [20]. Defects found in thermal-spray coatings are pores or micro cracks in brittle materials while oxides and porosity characterize metal sprayed layers. Imperfections in coatings arise from unmelted particles, isolated large particles, low velocity impact, metal oxidation and cold induced fragmentation of splats [2].

6.3 Thermal-spray processes

The most widely utilized thermal-spray processes are: Flame spray, Arc spray, Plasma spray, High velocity oxy-fuel spray and Molten material spray. A comparison between the different processes in terms of form of coating material, spray temperature and the velocity at which the particles or droplets are accelerated is shown in Table 6.2. Each of these processes is now discussed, in turn.

Table 6.2 Comparison between different thermal-spray processes [2]

Process	**Coating Material**	**Temperature °C**	**Velocity m/s**
Flame Spray	Metal	3000	40-100

Arc Spray	Metal	3000-6000	50-150
Plasma Spray	Metal, Ceramics, Thermo-plastics	5000-25000	80-300
HVOF Spray	Metal, Ceramics	3000	400-800
Molten material Spray	Metal, Thermo-plastics	400-3000	50-150

6.3.1 Flame spray process

With this process oxygen and acetylene are burnt in a special nozzle as shown in Figure 6.1.

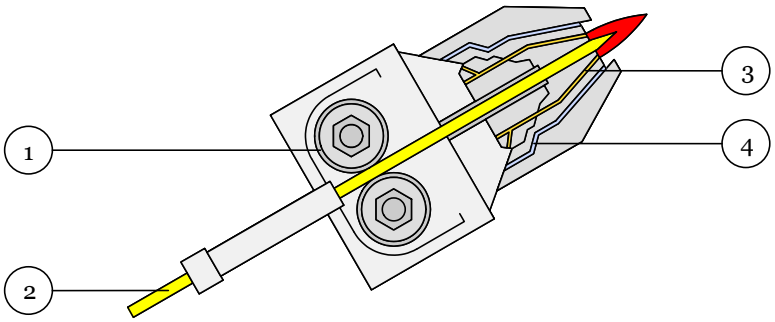

1. Wire feed rollers
2. Wire
3. Compressed air
4. Oxygen and acetylene

Figure 6.1 Flame spray gun [34]

The coating material, in wire form, is fed through the centre of the nozzle into the flame where it is melted. The molten material is atomized by a cone of compressed air around the flame and is propelled towards the substrate [34].

6.3.2 Arc spray process

In the arc spray process, two wires made of the coating material are fed simultaneously through a gun at an angle so as to meet as they exit from the gun. The wires are electrically charged, one positive and one negative as shown in Figure 6.2.

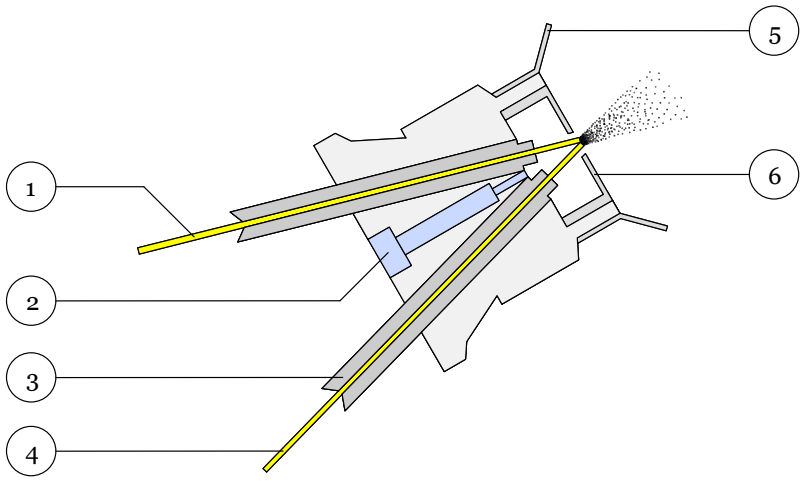

1. Positive wire
2. Compressed air
3. Contact tube
4. Negative wire
5. Shroud
6. Nozzle

Figure 6.2 Arc spray gun [34]

When the wires come into contact with each other an electric arc (ionized path) is formed melting the material. Compressed air is injected just behind the arc, atomizing the metal and propelling it towards the substrate. Advantages of the arc spray process are high adhesive strength of the deposits while the use of compressed air and electricity alone produce more economic coatings [14], [34].

6.3.3 Plasma spray process

A plasma is created by an electric arc forming in an inert gas atmosphere between the cathode and anode within a plasma spray gun as shown in Figure 6.3. The expanding inert gas passing through the gun is formed into a high velocity plasma jet by the gun's nozzle.

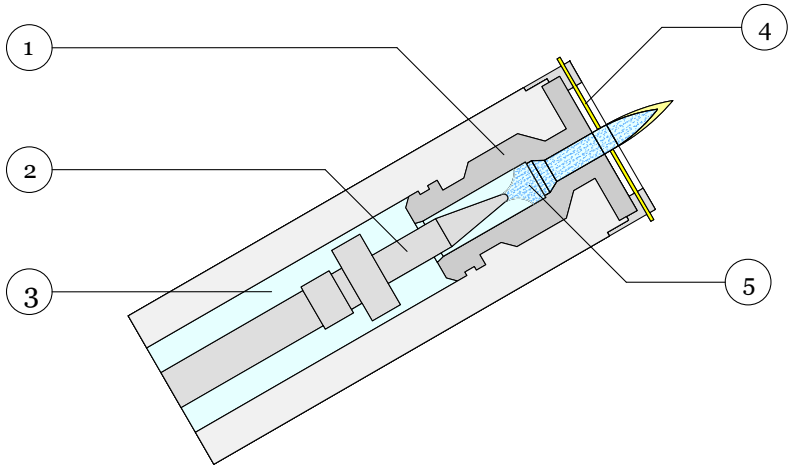

1. Nozzle (Anode)
2. Cathode
3. Inert gas
4. Coating material
5. Plasma

Figure 6.3 Plasma spray gun [34]

Coating material in powder form is injected into this jet where it is melted and accelerated towards the coating surface [34]. This process is termed atmospheric plasma spraying (APS). To avoid oxidization of the heated particles traveling to the coating surface, spraying can be carried out in an inert gas atmosphere at reduced pressure. This is known as vacuum plasma spraying (VPS) or low pressure plasma spraying (LPPS) [5, p. 205]. Deformation of the

coating surface is limited with plasma spraying since the heat source in the form of a plasma is localized at the gun [34].

6.3.4 High Velocity Oxy-Fuel (HVOF) spray process

Hydrogen and oxygen are fed under regulated pressure into a combustion chamber where they burn to produce a hot, high pressure gas stream as shown in Figure 6.4.

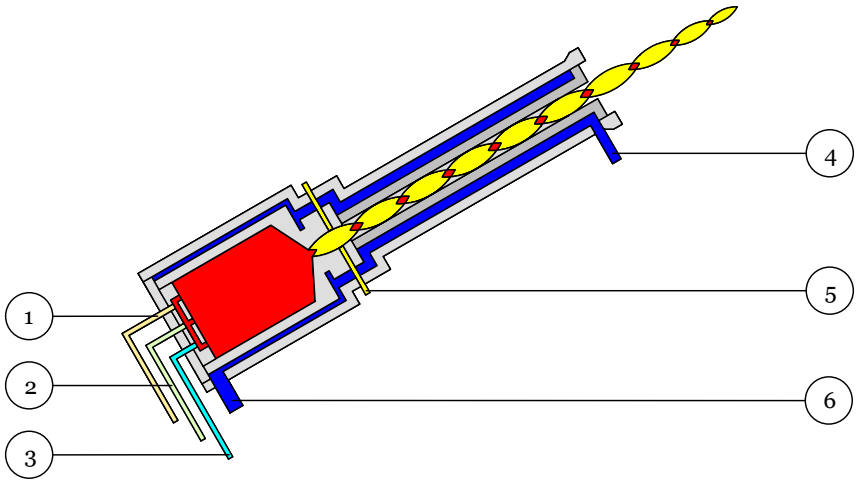

1. Fuel
2. Oxygen
3. Hydrogen
4. Cooling water in
5. Coating material
6. Cooling water out

Figure 6.4 HVOF spray gun [34]

This gas stream is expanded through a Laval type nozzle increasing the gas velocity and decreasing the pressure to slightly above atmospheric. At this reduced pressure the coating material in powder form can easily be injected into the gas stream. The gas stream heats and accelerates the powder particles to a high velocity within the nozzle so that they impact the substrate with tremendous energy. Oxidation and decomposition of sprayed coatings are

minimal with this process since the particles are not subjected to very high temperatures and traveling time from the gun to the substrate is short [34].

6.3.5 Molten material spray

Molten material spray refers to pre-melted feedstock material that is fed to the thermal-spray gun in molten rather than solid or powder form as is the case with the spray processes already mentioned. A number of different types of apparatus are available, as discussed below.

6.3.5.1 Force fed spraying apparatus

In his 1943 patent, Brennan describes an invention for spraying pure pre-melted aluminum. The spraying apparatus comprises a cylindrical pressure chamber with a removable lid that is secured by a number of bolts as shown in Figure 6.5. An electrically heated crucible is supported on rails within the pressure chamber. Aluminum billets are placed inside the crucible and melted with the pressure chamber's lid bolted shut. Gas is forced into the pressure chamber thereby applying pressure onto the surface of the molten aluminum inside the crucible. An inert gas such as nitrogen is utilized for pressurization to prevent oxidization of the molten aluminum.

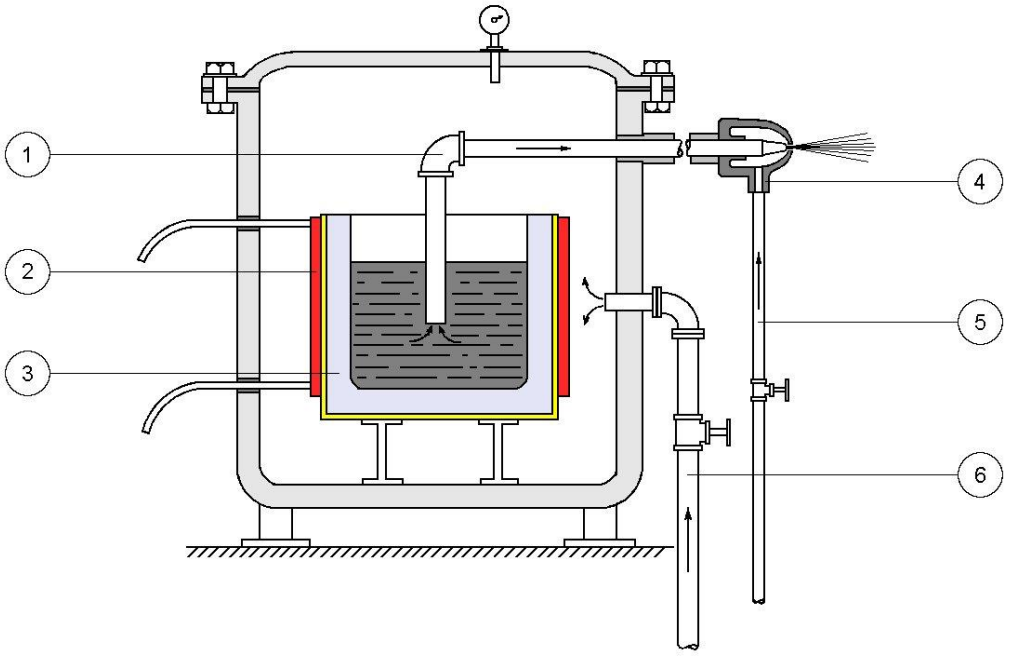

1. Pick-up tube
2. Heating elements
3. Crucible
4. Nozzle
5. Compressed air
6. Compressed inert gas

Figure 6.5 Force fed spraying apparatus [8]

The molten aluminum is forced out of the pressure chamber to a spray nozzle through an insulated conduit. Compressed air is supplied to the spray nozzle to atomize the liquid aluminum and to accelerate the metal droplets onto the coating surface [8].

6.3.5.2 Portable spraying apparatus

In 1973 Payne patented a portable thermal-spraying apparatus. The apparatus is equipped with an insulated container with a heating element installed at the bottom as shown in Figure 6.6.

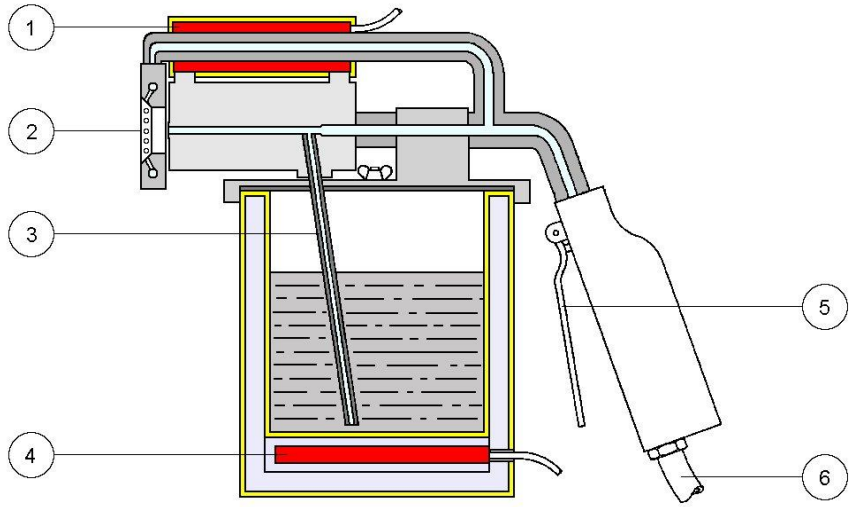

1. Heating element
2. Nozzle
3. Pick-up tube
4. Heating element
5. Trigger
6. Compressed air supply

Figure 6.6 Portable spraying apparatus [36]

A spray head with a pick-up tube that is connected to venturi inside the head is mounted on top of the container. Fusible metal or metal alloy billets are placed inside the container and are melted by the heater. Heated air is supplied under pressure to the spray gun. A second electric heater is installed in the spray head. This heater super heats a portion of the air from the air supply to a temperature at or above the melting point of the metal. The pre-heated air from the air supply flows at high velocity through the venturi inside the spray head. This causes the molten metal to be siphoned from the container through the pick-up tube and transported to

the spray nozzle. The air from the nozzle atomizes the liquid metal and together with the air flowing through the venturi accelerates the droplets. The super heated air from the nozzle ensures that the droplets remain in a liquid state while traveling to the coating surface [36].

6.3.5.3 Gravity fed spraying apparatus

Baiker (1954) describes a thermal-spray apparatus in his patent for spraying thermo-plastic materials such as synthetic resin, bitumen or shellac. The spraying apparatus consists of an insulated container, a double walled flexible hose and a spray gun as shown in Figure 6.7.

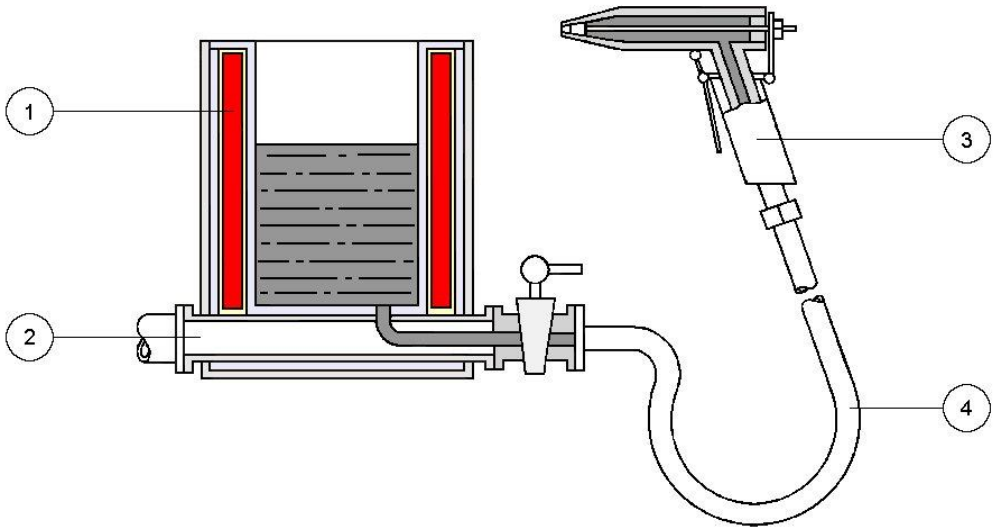

1. Heating elements
2. Heated compressed air
3. Spray gun
4. Flexible hose

Figure 6.7 Gravity fed spraying apparatus [4]

Heating elements are installed in the walls of the container to melt the thermo-plastic material. The molten material flows under gravity through the flexible hose to the spray gun. To prevent the material from cooling and solidifying in the gun and hose, pre-heated compressed

air is forced between the inner and outer walls of the hose and out of the gun's nozzle. Besides heating the hose and gun the air also atomizes the thermo-plastic material in the spray gun's nozzle and accelerates the droplets onto the coating surface [4].

CHAPTER 7

DEVELOPMENT OF NEW THERMAL-SPRAY EQUIPMENT

7.1 Introduction

This chapter describes the patented thermal-spray equipment (see Addendum D), that was designed and fabricated for the research project. The author decided on the following criteria regarding the thermal-spray equipment and the feedstock material used for producing radiation field shaping shields. The criteria were set to be in the best interest of the operator that will be producing the shields as well as the patient during treatment.

- The spray of shielding material should be contained to prevent the material from spreading in the radiotherapy departments mould room where the radiation field shaping shields will be produced.
- The equipment used for producing the radiation field shaping shields should be both user and environmentally friendly not to expose the operator or environment to hazardous metal dust or gasses.
- It should be possible to fabricate the thermal-spray equipment with locally available tools and machinery from affordable components to make the project financially viable.
- The material used for producing radiation field shaping shields should be recyclable in order to make the technique cost effective.
- It should be possible to produce a radiation field shaping shield within a reasonable time frame using the thermal-spray equipment.

- The shielding material used in the process should be of high enough density to effectively block low energy radiation without the shield becoming too heavy for the patient to bear.

7.2 Shielding material

The material chosen for producing radiation field shaping shields by thermal-spraying was Wood's alloy. This is the same material as described in section 5.2.3 for casting shaped end-frames. Wood's alloy is used in modern radiotherapy departments where the alloy is commonly used to shield radiosensitive areas during high energy X-irradiation. It is cast in 9 cm blocks according to the shape of the area to be shielded and is positioned in the radiation field during treatment for that application. Because of the alloy's low melting point of 70ºC it was decided to pre-melt the alloy and feed it to the thermal-spray gun in liquid rather than solid or powder form. A high flow rate of the alloy through the gun is possible with this technique resulting in a rapid build-up of the alloy on the substrate during spraying.

7.3 Thermal-spray cabinet: Mechanical design and fabrication

Since none of the existing thermal-spray techniques and equipment described in Chapter 6 meets all of the criteria set in section 7.1, it was decided to design new thermal-spray equipment tailor-made to produce radiation field shaping shielding masks. In this design the alloy is sprayed in an enclosed cabinet as shown in Figure 7.1. The spray cabinet is of steel construction with a framed Perspex™ lid hinged at the back of the cabinet.

Figure 7.1 Thermal-spray cabinet

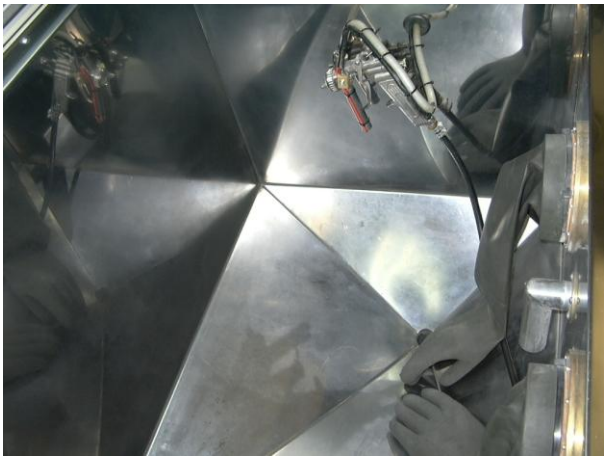

Figure 7.2 Inside spray chamber

Over-center catches are used to lock the lid shut before spraying. Access to the inner workings of the apparatus is possible through two hinged doors at the front of the cabinet.The top half of the cabinet is a double walled construction with the inner wall made of stainless steel. This inner container (referred to as the spray chamber) has a sloped bottom with a drain hole at the lowest point and has two rubber gloves attached to its front wall as shown in Figure 7.2. The operator has access to the spray gun and model to be sprayed through these gloves. The spray gun is similar to that used for paint spray purposes but was modified by attaching a 12 V heating element to the frame of the gun as shown in Figure 7.3. The gun is connected to a melting pot as shown in Figure 7.4 attached to the outside of the cabinet by means of a tube to feed the molten Wood's alloy to the gun. The feed tube consists of an inner and outer silicone tube with a nickel-chrome resistance wire coiled around the inner tube.

Figure 7.3 Spray gun

Figure 7.4 Melting pot

An electrical current of 24 V is applied to the resistance wire to provide heat to the Wood's alloy flowing through the inner tube. This is to prevent the alloy from cooling and setting while passing through the tube. The melting pot is a double walled construction with two 12 V heating elements installed in the inner container. The outer wall is insulated from the inner container to prevent heat transfer to the outer surface of the pot that might lead to injury to the operator. Compressed air from an outside source is supplied to the spray gun via a pressure regulator / water trap to ensure a constant flow of clean air.

7.3.1 Model support stands

To support the models in the spray chamber while spraying two stands and a support frame were constructed. The first stand as shown in Figure 7.5 is equipped with a turntable that is supported by a lockable universal joint and is intended for small models. The second stand is intended for larger models and is a square tubing construction mounted on a ball bearing as shown in Figure 7.6.

Figure 7.5 Stand for small models

Figure 7.6 Stand for large models

Both stands were made to slide on the square tubing support frame. The stands and frame are positionable inside the spray chamber to suit the operator.

7.3.2 Cleaning system of spray chamber

A result of spraying Wood's alloy inside the spray cabinet is that over sprayed alloy and dust accumulate on the inner walls and bottom of the spray chamber. In order to clean the spray chamber a small boiler was constructed as shown in Figure 7.7 with the inside of it's lid shown in Figure 7.8. The boiler is equipped with a 3 kW heating element that is able to heat the 20 liters of water it holds to boiling point in 45 minutes. The working principal of the cleaning cycle is explained with reference to Figure 7.9. Hot water is pumped from the boiler to the spray chamber by means of a small circulating pump. The hot water is sprayed onto the accumulated alloy on the walls and floor of the chamber by the operator. A removable flexible hose that connects to a socket in the inner left side wall of the spray chamber is used for this purpose. The alloy melts and flows with the water back to the boiler where the alloy is caught in a trap.

Figure 7.7 Boiler

Figure 7.8 Boiler lid

The boiler can be removed from the spray cabinet by disconnecting the couplings to the spray chamber outlet and the circulating pump as well as the heating element's plug. After opening the four over-centre catches that keep the boiler's lid shut, the alloy trap can be removed in order to recover the Wood's alloy.

7.3.3 Air filtration system

Compressed air is forced into the spray chamber via the spray gun during the spraying process resulting in a higher air pressure inside the chamber than outside. This excess air needs to be filtered to remove the Wood's alloy dust that forms as a result of spraying before it exits the spray cabinet. Inhalation of this dust will be very detrimental to the operator's health considering the lead and cadmium content of the alloy.

To overcome this problem an air filtration system was devised as explained with reference to Figure 7.9. A vacuum cleaner with a high efficiency particulate (HEPA) filter is connected to the boiler inside the spray cabinet as shown in Figure 7.10.

Figure 7.10 Inside of spray cabinet

HEPA filters are able to remove at least 99,97% of airborne particles with a diameter of 0,3 micrometers (μm). Particles of this size are considered to be the most penetrating and are consequently the most difficult to filter. Larger or smaller particles are removed with even higher efficiency by a HEPA filter [13]. The boiler is connected to the outlet of the spray chamber, the same way as it would be for the cleaning cycle. Vacuum is drawn on the boiler by means of the vacuum cleaner resulting in air flowing from the spray chamber through the boiler to the vacuum cleaner. Since the inlet into the boiler is below the water surface inside the boiler the airflow will cause the water to bubble trapping airborne alloy dust in the process. Any dust passing through the boiler will subsequently be caught by the vacuum cleaner's air filter. Air from the vacuum cleaner's outlet pipe is split allowing part of the air to

be recirculated back to the inlet of the spray chamber via a control valve. The surplus air is vented outside the building. By adjusting the control valve the vacuum inside the spray chamber can be increased or decreased as required. The spray chamber is constantly ventilated by air passing through the chamber from the inlet to the outlet while the air filtration system is in operation. This flow of air effectively removes any airborne alloy dust particles resulting from spraying from the air inside the chamber. The possibility of the operator inhaling any of the dust upon opening the spray cabinet's lid to take out the model after spraying is thus minimized.

7.3.4 Interlock system

In order to prevent the operator from operating the spray gun with the spray cabinet's lid open or without the air filtration system switched on some interlocks were installed as safety precautions. The air line to the spray gun is equipped with a solenoid valve and the cabinet's lid with a switch. The lid's switch is positioned such that it rests on the Perspex™ window of the lid. When vacuum is drawn on the spray chamber with the lid closed, the window flexes slightly inwards thereby operating the switch and switching on the solenoid valve. Should the lid be opened while spraying or the airflow of the filtration system interrupted in any way, the vacuum in the spray chamber will fall away switching off the solenoid valve, thereby terminate spraying. A water level switch is also mounted inside the boiler. When the water level falls below a specified depth, it will not be possible to switch on the heating element. It will also not be possible to switch on the vacuum cleaner without sufficient water in the boiler. Too low a water level inside the boiler will not allow the air to bubble sufficiently through the water rendering the air filtration system ineffective. Without vacuum the lid switch will not be activated and as a result neither will the solenoid valve open, making spraying impossible.

7.4 Thermal-spray cabinet: Electronic design and fabrication

All electrical features of the thermal-spray cabinet are controlled by a PIC18F452 microcontroller running at a clock speed of 40 MHz. The microcontroller, a liquid crystal display (LCD), push buttons and circuitry are all mounted in a control box that is attached to the left-hand side of the cabinet. The control box is shown in Figure 7.11 with its inner workings in Figure 7.12 while Figure 7.13 shows the complete layout of the thermal-spray cabinet's circuitry schematically.

Figure 7.11 Cabinet control box

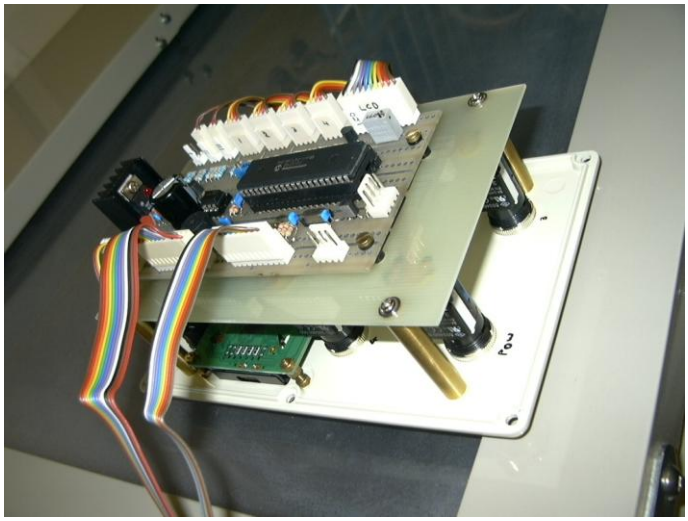

Figure 7.12 Inner workings of control box

The microcontroller switches the vacuum cleaner, water heating element, circulating pump and solenoid valve on or off as required through solid state relays. The status of the vacuum and water level switches provide the microcontroller with input in determining switching for these components.

7.4.1 Spray gun, feed tube and melting pot heating

Also controlled by the microcontroller through solid state relays are the temperatures of the heating elements in the spray gun, alloy feed tube and melting pot. The 12 V to the heating elements in the gun and pot and 24 V to the alloy feed tube are supplied by a transformer mounted in a separate compartment in the back of the spray cabinet as shown in Figure 7.14.

Figure 7.14 Solid state relays, transformers and circuitry

Also mounted in the compartment are the solid state relays, a 9 V transformer that supplies power to the microcontroller and a distribution board that connects the relays to the microcontroller. LM35 heat sensors mounted on the gun, pot and pipe sends analogue signals to the microcontroller. The microcontroller converts the analogue signals to digital signals through a built-in 10 Bit analogue to digital converter. This information allows the microcontroller to accurately regulate the temperatures of the gun, pot and pipe at the temperatures set by the operator.

7.4.2 Duty cycle of heating element

The duty cycle and thus the rate of heating of the elements in the gun and pot are adjustable through the microcontroller. Since it was not possible to mount the heat sensors directly onto the heating elements, they had to be mounted in the closest convenient position on the gun and pot. This distance between the elements and sensors causes the sensor readings to lag behind the temperature of the elements. This is because it takes time for the heat to conduct from the elements to the sensors. By the time the heat sensor reaches the temperature set by the operator and the microcontroller switches off the element, the element has over-run this set temperature by a number of degrees Celsius. This effect is dependant on the rate at which the elements are heated. The higher the rate of heating, the greater the temperature over-run. Heating the elements at a reduced duty cycle will allow more time for heat conduction to the sensors making more accurate temperature control possible through the microcontroller. An over-run in temperature may cause the Wood's alloy close to the elements to be heated to above its boiling point of 120 ℃ which is undesirable.

7.4.3 Airflow switch

Provision was made to boost the spray gun's temperature while spraying. Air flowing through the gun when the trigger is pulled causes the gun's nozzle to cool down rapidly to below the melting point of the Wood's alloy. This causes a blockage in the flow of the alloy making further spraying impossible. Spraying can only continue by stopping the air flow through releasing the trigger and waiting for the nozzle to heat up again. The reduced duty cycle at which the gun is normally operated is insufficient to keep the nozzle properly heated during

spraying. It is possible to heat the element at a higher duty cycle but this will cause an unacceptable temperature over-run as described in the previous section.

The problem was solved by having the microcontroller switch the gun's element to a higher duty cycle only while air is flowing through the gun. Mounting a switch behind the trigger on the gun's frame was considered a means of signaling airflow to the microcontroller. The gun's design did however not allow for a switch to be mounted in that position. As an alternative the author fabricated an airflow switch that is mounted in the air line between the gun and the solenoid valve. The airflow switch consists of a tube into which a cylindrical magnet fits loosely. A magnetic reed switch is mounted next to and close to the top of the tube. When the spray gun's trigger is pulled, air passes through the tube and forces the magnet upwards. This brings the magnet into close proximity with the reed switch activating it through its magnetic field. This is noted by the microcontroller with which the switch is connected. The microcontroller overrides the signal from the heat sensor mounted on the gun and switches on the element at an increased duty cycle (as specified by the operator) for as long as the trigger is held in. When the spray gun's trigger is released the airflow stops, the magnet falls back, the reed switch is deactivated and the microcontroller returns the gun's element to normal temperature control. The additional heat generated by switching on the element at a higher duty cycle during spraying is sufficient to compensate for heat loss due to the airflow through the gun. Spraying can thus be performed continually without blockages in the flow of Wood's alloy.

7.5 Thermal-spray cabinet: Software

The microcontroller performs its functions under the directions of a software program written in the programming language C. The functions of the program are presented in the form of a

flow chart shown in Figure 7.15. It consists of a sequence of representations of the control box with the LCD display, indicator lights and four push buttons shown. The program displays information pertaining to the thermal-spray apparatus and possible control options on the LCD screen. Two-colour light emitting diodes (LED's) mounted in the push buttons indicate to the operator which buttons are available to choose from under a given control option. The LED's in the buttons turn from green in standby mode to red if pressed to show that a specific function has been activated. Two indicator lights mounted above the LCD screen indicate to the operator whether the thermal-spray cabinet is in spraying or cleaning mode. Figure 7.16A shows the setup sequence for adjusting the gun, pot and pipe temperatures as well as for the water pump speed. The duty cycle setup sequence for the gun, pot, pipe and the temperature boost to the gun during spraying is shown in Figure 7.16B. The temperature and duty cycle menus are accessible by pressing the buttons on the control box indicated in the flow charts in combination.

Figure 7.15 Flowchart indicating spray cabinet control options

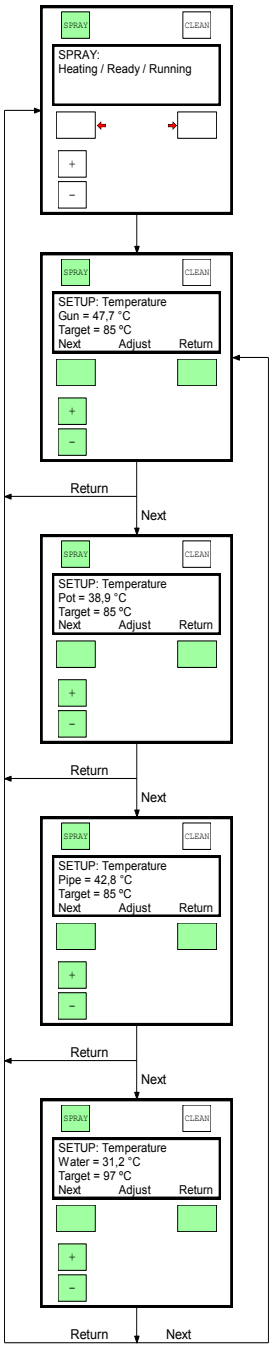

A

Figure 7.16A Flowchart indicating temperature setup

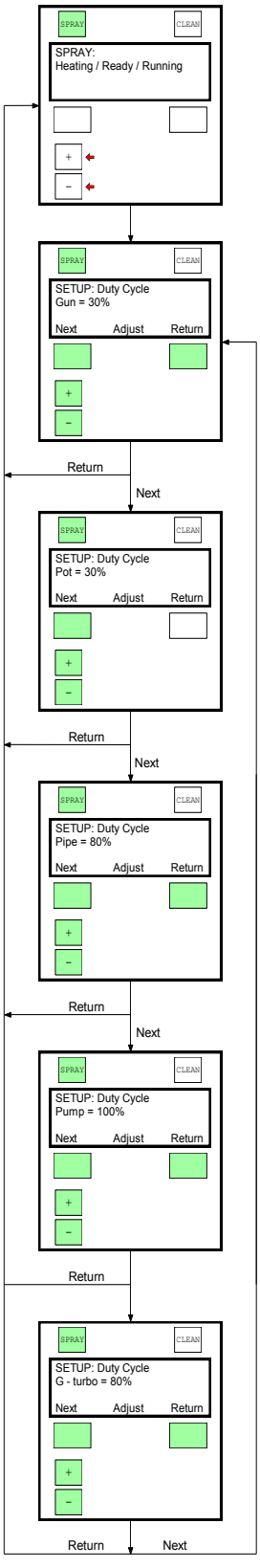

B

Figure 7.16B Flowchart indicating duty cycle setup

CHAPTER 8

THERMAL-SPRAY RADIATION FIELD SHAPING TECHNIQUE

8.1 Introduction

To overcome some of the disadvantages of the traditional radiation field shaping techniques described in Chapter 5, the author developed a new thermal-spray field shaping technique[1]. Different procedures to obtain the contours of the treatment area and methods to fabricate the model onto which the shielding alloy is sprayed to produce a field shaping mask were investigated. Figure 8.1 shows the thermal-spray field shaping technique with the different contour acquisition and model fabrication techniques graphically.

8.2 Treatment area contour acquisition techniques

In order to produce a thermal-sprayed field shaping mask that fits the patient properly, the topography of the treatment area on the patient needs to be determined accurately. The contours of the treatment area can be acquired either through direct contact with the patient's skin or through various non-contact techniques.

[1] also see published article regarding the subject in Addendum E

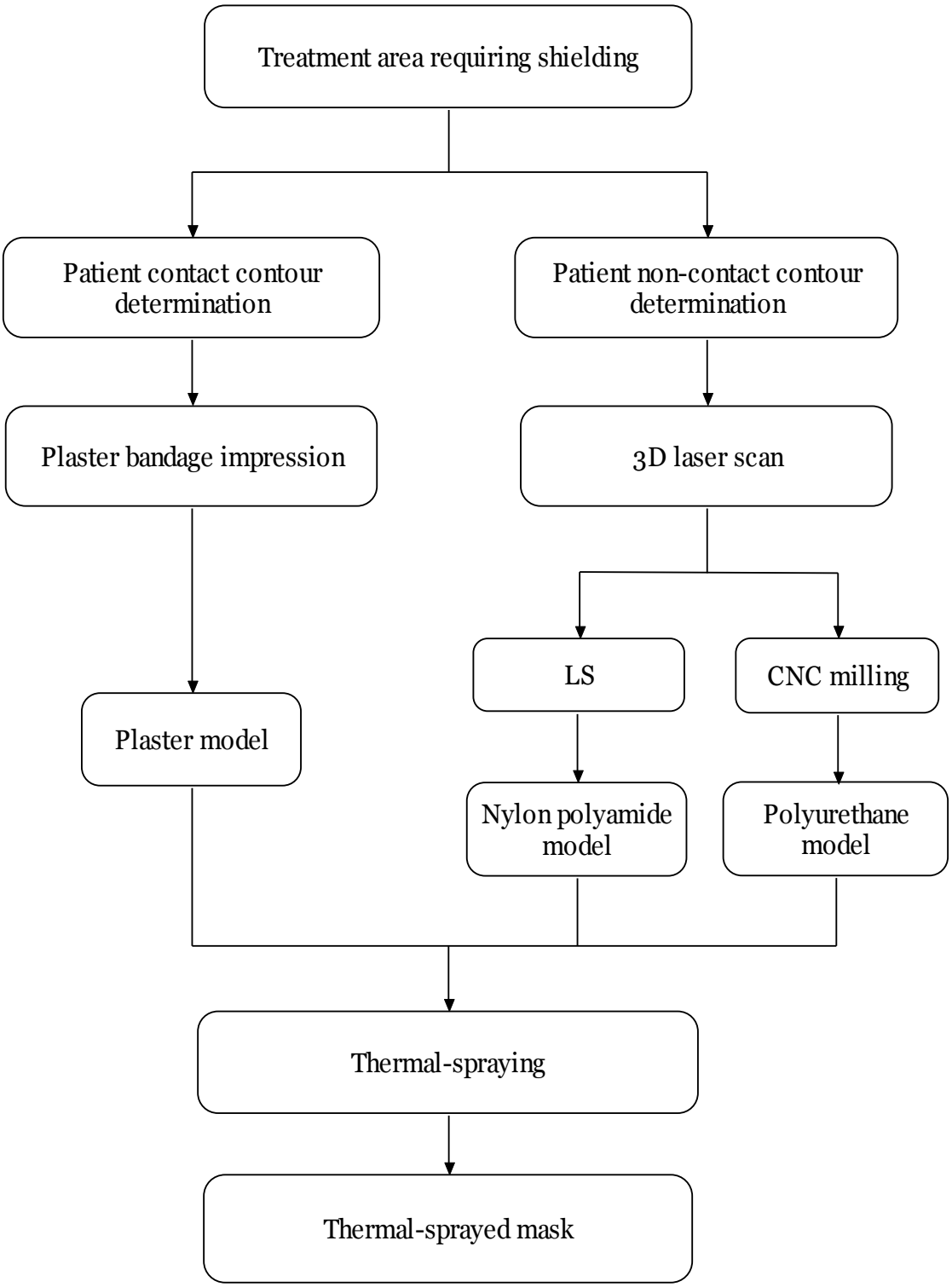

Figure 8.1 Flowchart of the thermal-spray field shaping technique

8.2.1 Patient-contact contour acquisition

The most basic technique to acquire the contours of the treatment area for producing a thermal-sprayed mask is by taking an impression of the area with plaster bandages. This is the same technique as is described in section 5.1 for producing a lead mask and section 5.2 for producing a wax casting. Taking a plaster bandage impression of the patient may be traumatic and uncomfortable to the patient as is also mentioned under the disadvantages of the traditional field shaping techniques. If tumor mass shrinkage occurs during the period of radiation treatment, the fit of a radiation field shaping mask will become unsatisfactory. This necessitates a second plaster bandage impression to be taken of the contour altered treatment area to produce a revised field shaping mask. If the skin that is sensitive from the radiation comes into contact with the wet plaster bandages, severe skin reaction may result [51, p. 91]. Open wounds, such as those commonly encountered with advanced skin cancer patients, pose another problem for taking plaster bandage impressions. Placing a thin plastic film over the wound makes taking the impression possible but may still be very uncomfortable for the patient.

8.2.2 Patient non-contact contour acquisition

Non-contact contour acquisition is understood to mean that no physical contact with the patient's skin is required to determine the treatment area's contours. Not touching the patient during contour acquisition presents some obvious advantages over the traditional plaster bandage technique as described in the previous section. Literature describes various non-contact contour acquisition techniques including:

- Iso-height light projection [27, p. 741]

- Moiré fringes [33, p. 513], [7, p. 20]
- Stereo imaging [15, p. 646]
- Computer tomography (CT) scanning [23, pp. 241–245], [45]
- 3D laser scanning

8.2.2.1 3D laser scanning

A 3D laser scanning technique that was first developed by the National Research Council of Canada in 1978 shows some advantages over the other mentioned techniques in terms of either speed or accuracy of contour acquisition [30]. This technique, also known as laser triangulation scanning, makes use of a low power laser emitter and a monochrome solid state video camera. The working principal of the scanner is explained with reference to Figure 8.2.

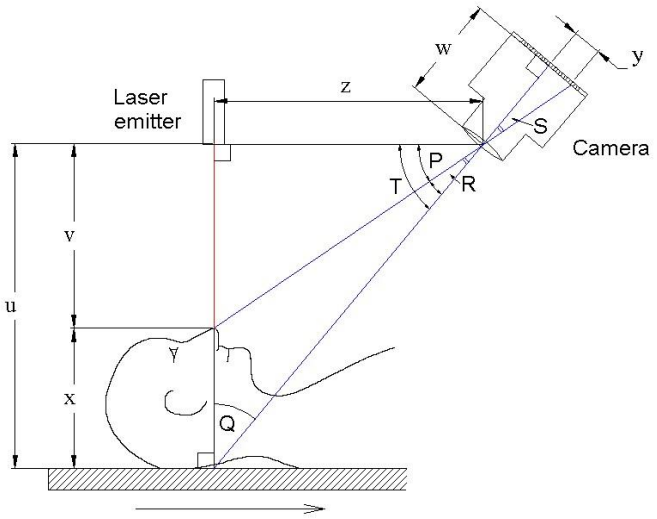

Figure 8.2 Schematic representation of a triangulation(3D) laser scanner

The laser emitter is mounted perpendicular to the working surface and the camera at a set angle (Q) with respect to the laser emitter. The laser emitter shines a laser dot on the object to

be scanned while the camera views the location of the dot on the object. Depending on how far away from the laser emitter the dot strikes the object, the dot appears at different places in the camera's field of view. The laser dot, laser emitter and the camera forms a triangle where the distance between the emitter and the camera is known (z) as well as the distance of the laser emitter from the working surface (u). The distance between the camera lens and the charged couple device (CCD) inside the camera is also known (w). The angle of the camera's view of the laser dot (S) can be determined through the location of the dot in the camera's field of view (y). With all the variables known, the displacement from the working surface to the object surface (x) can be determined through triangulation. A projected laser line instead of a single dot is used in most cases to speed up the contour acquisition process. The object to be scanned is moved across the laser line at a steady speed while the camera takes frames of the deformation of the line. The frames are taken at equal increments of linear motion of the object by making use of a frame-grabber equipped personal computer. By combining all the taken frames, the contours of the object can be accurately determined. In a radiotherapy application, the laser emitter and camera combination can be attached to the head of a linac or simulator[2]. Andrew and Aldrich [1, p. 426] describe such an installation on a simulator where longitudinal movement of the patient is made possible by making use of the simulator's motorized table. Contour acquisition can also be performed by rotating the linac or simulator's gantry with the patient at isocentre height [11]. A readout of table position or gantry angle is required from the machine involved to time the scanner's frame grabber for these two techniques.

[2] a diagnostic X-ray unit with dimensions similar to that of a linac that is used in planning patient setup

8.2.2.2 Konica Minolta™ laser scanner

Improving on the basic triangulation laser scanner is a laser scanner developed by Konica Minolta™ as shown in Figure 8.3. The VI-910 also makes use of a projected laser line and CCD camera but instead of having to move the object to be scanned across the laser line, the laser line is swept across the object by a mirror. Very accurate mirror rotation is made possible through a high precision galvanometer. The deformation of the laser line while sweeping across the object is captured by the scanner's CCD camera which rapidly takes frames at equal increments of mirror rotation. The surface contour of the object is derived from the image of the line in each frame through triangulation. Two scanning modes are available on the VI-910 scanner: Fine mode collects 307200 data points in as little as 2.5 seconds while Fast mode collects 76800 data points in an even faster 0.3 seconds.

Figure 8.3 Konica Minolta™ VI- 910 laser scanner

This quick scanning ability makes the scanner ideal for scanning areas on patients that are prone to movement. Examples of these are the torso where movement occurs because of breathing and areas on small children which are difficult to keep still during contour

acquisition. Scanning areas of approximately 10 cm^2 to 1 m^2 are possible with the VI-910 at distances of 0.6-2 m. The scanners come standard with their own Polygon Editing Tool (PET) software. The software converts the surface data to a lattice of vertices (connected points) to create a polygonal-mesh with all connecting information retained. In doing so geometric ambiguities are eliminated and detail capture improved. The software also allows the user to edit and convert the scanned data into any of several common data formats including: DXF, STL, Wavefront, Softimage, VRML 2.0 and MGF. These data formats are applicable to rapid prototyping (RP), reverse engineering (RE), computer aided design (CAD), computer aided machining (CAM) and 3D modeling technologies. Editing functions that the software provides include; filtering of irregular polygons and noise and perform smoothing. The scanner captures 24-bit colour images simultaneously with acquiring surface information using the same CCD. These colour images are produced through a rotating filter inside the scanner that separates the acquired laser light [26]. A colour image can be superimposed onto the surface information using the software supplied with the camera. This makes it possible to reproduce the borders of the treatment areas that were marked on the patient's skin in the surface information.

8.3 Techniques for producing models for thermal-spraying

Once the topography of the treatment area has been accurately determined, the contours of the area need to be reproduced in a suitable medium onto which the molten shielding material can be sprayed. This reproduction of the treatment area, or simply referred to as a model of the area, can be produced through various techniques and will be used to produce a field shaping mask. Three techniques for producing models for thermal-spraying will be discussed next. The first technique makes use of a patient contact contour acquisition technique (plaster

bandage impression) while the remaining two techniques use a non-contact technique (3D laser scanning).

8.3.1 Thermal-spray models through plaster bandage impressions

Plaster bandage impressions can be used to produce plaster models for thermal-spraying which is the same as would be done for the traditional lead masks and wax castings. A model for thermal-spraying can be produced from standard Plaster of Paris instead of Yellow stone plaster that is required for producing a lead mask. Plaster of Paris can be used since the model need not be as strong for thermal-spraying as it needs to be for forming a lead mask. The markings of the treatment area that were transferred from the patient to the model through the plaster bandage impression need to be scribed onto the model using a scriber. When the sprayed mask is removed from the model, the scribed markings will be visible inside the mask.

8.3.2 Thermal-spray models through laser sintering

Laser sintering (LS) is a rapid manufacturing technique that was developed and patented by Dr. Carl Deckard at the University of Texas at Austin in the mid-1980s [41]. The LS process is explained with reference to Figure 8.4.

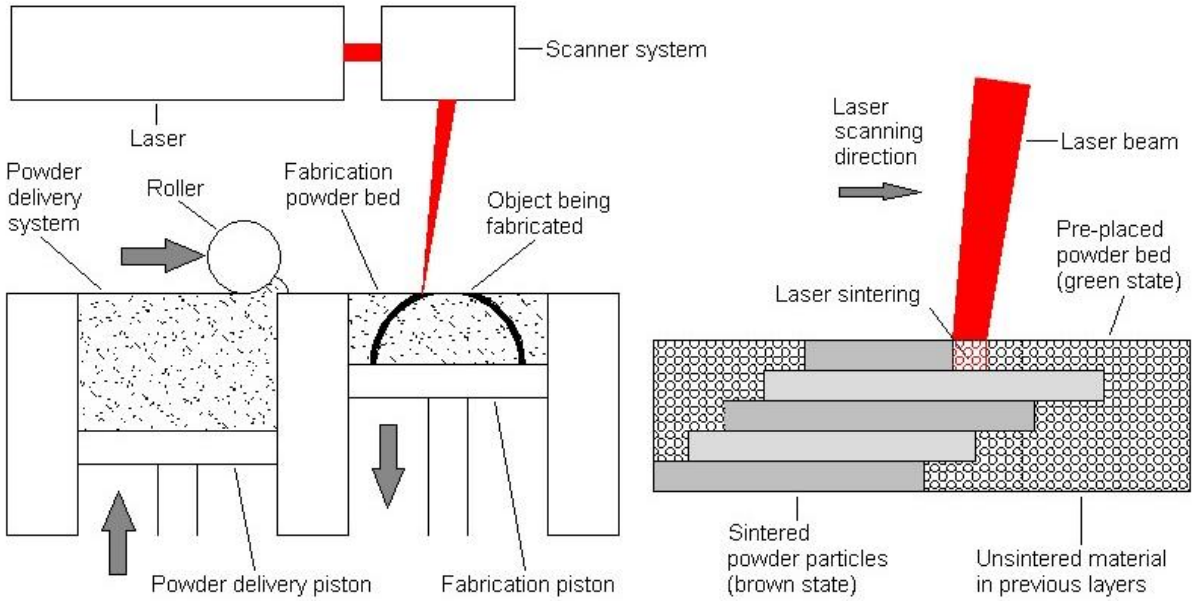

Figure 8.4 Schematic representation of the LS process [41]

To manufacture a part through LS, a computer generates cross-sections of the part from a 3D digital description of the part. Various software packages (for example Magics RP) are commercially available to perform this operation. The digital description of the part may be either a CAD file of the part or it may be a digital scan of an existing part. A laser beam from a high power laser is controlled to scan a cross-section of the part onto a bed of powdered material thereby selectively fusing the particles of the material. After a cross-section is scanned, the powder bed is lowered by one layer thickness. A new layer of material is laid down on top of the previous layer and scanning continues. Besides fusing the particles in a layer together during scanning, the particles are also fused to the scanned particles in the previous layer [41]. This process is repeated until the part is completed. A relatively wide range of powder materials are available to produce parts through LS. These include: nylon, polystyrene, steel, titanium and composites [52, p. 13]. Figure 8.5 shows an EOSINT™ P385 LS manufacturing system at the Central University of Technology Free State.

Figure 8.5 EOSINT™ P385 LS manufacturing system

If LS is to be used to produce models for thermal-spraying the treatment area on the patient needs to be digitized. A laser scanner such as the Konica Minolta™ VI- 910 described in section 8.2.2 will be ideal for this purpose. The model can be produced in nylon polyamide which is a material well suited to low temperature thermal-spraying. Since the VI- 910 scanner makes it possible to reproduce the treatment area's border markings in the surface data of the patient, the markings can also be reproduced on the LS model. A convenient means of reproducing the markings on the model is by creating a hole in the model according to the markings when the digital description of the model is prepared.

8.3.3 Thermal-spray models through CNC milling

A computer numerical controlled (CNC) milling machine can be used to reproduce the contours of the cancer affected area on the patient in a block of material that will be suitable for thermal-spraying. There are various 3-axis CNC milling machines commercially available

that will be able to perform this task. Figure 8.6 shows a Torchmate™ CNC cutting system from Applied Robotics Inc. that was used to investigate the feasibility of this model fabrication technique.

Figure 8.6 Torchmate™ CNC cutting system with router modification

The machine is normally used for CNC plasma cutting and was modified by replacing the plasma torch with a router. A 6 mm ball nosed cutter was used for milling the model in a block of polyurethane foam. In order to create a digital description of the treatment area, the relevant area on the patient needs to be digitized. A 3D laser scanner such as the Konica Minolta™ VI-910 is similarly to the LS application also ideally suited to this application. The scanned data either in STL or IGES format can be used to generate CNC codes according to which the CNC machine will be able to perform the milling operation. There are various CAD/CAM packages commercially available to generate the codes using STL files as input. The treatment area markings can be reproduced in the digital description of the model

allowing the CNC machine to mill a hole in the model to coincide with the treatment area on the patient.

8.4 Producing thermal-sprayed masks

The author's aim in developing the thermal-spray radiation field shaping technique was to replace all of the traditional field shaping techniques described in Chapter 5. Through this new technique it should be possible to shape any radiation field commonly used in the treatment of superficial cancerous lesions independent of the field size or skin surface contours.

8.4.1 Thermal-sprayed masks for small treatment fields

Thermal-sprayed masks can be produced to shield around small low energy X-ray or electron treatment fields. This task was traditionally performed by lead masks. The procedure for fabricating the thermal-sprayed masks is explained with reference to Figure 8.7A-F. The model (produced through any of the techniques described in section 8.3) is placed inside the spray chamber of the thermal-spray cabinet and layers of Wood's alloy are sprayed onto it (Figure 8.7A). When a sufficient build-up of alloy has formed on the model, the mask is removed and its thickness measured by means of a purpose made outside caliper (Figure 8.7B). The required mask thickness is determined by the intensity of the radiation to be applied during treatment as described in section 9.3. If the mask measures too thin, it is replaced onto the model and further layers of alloy are sprayed onto it.

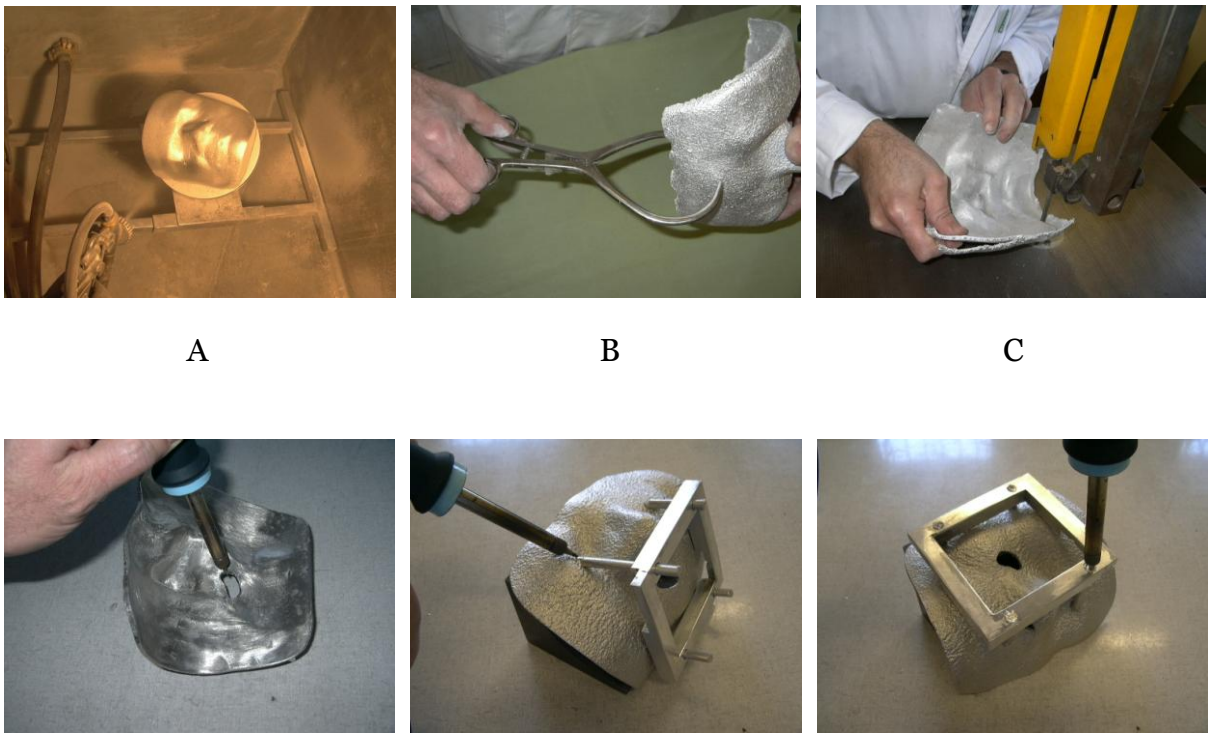

A B C

D E F

Figure 8.7A-F Fabricating a thermal-sprayed mask for a small electron treatment field

When the thickness measures correctly the mask's outer dimensions can be determined. This entails adding a border of sufficient width (to stop radiation scatter outside the primary beam) to the radiation field size that will be applied during treatment. A border width of 4 cm measured perpendicular to the central axis of the treatment beam was decided upon. This width was derived from the degree of scatter caused by a 4 MeV electron beam with a stand-off (see section 9.2.4.2) plus an additional margin added for safety. This border width is also sufficient for masks used with low energy X-ray treatment on a kilovolt unit. Low energy photons scatter less in air than electrons for the same field size and stand-off. Once the mask's outer dimensions have been determined it can be marked out on the surface of the mask. A band saw can be used to cut the mask to size (Figure 8.7C) where after all edges need to be made smooth using files and sanding paper. If the mask was produced from a plaster model, a hole needs to be made in the mask according to the area on the patient that requires radiation

treatment. Using a small soldering iron, this hole can be melted into the mask (Figure 8.7D) according to the markings of the treatment area that was transferred from the patient (see section 8.3.1) to the mask. Melting the portal should be done in a well ventilated area to prevent the operator from inhaling any fumes that may result from melting the alloy. If a LS or CNC milled model is used there will be a hole in the model according to the treatment markings that was produced through the specific model fabrication technique. This hole will be reproduced in the mask when the alloy is sprayed onto the model requiring the technologist only to make the edges of the hole smooth. A mask that was produced through thermal-spraying onto a traditional plaster model is shown in Figure 8.8. Figures 8.9 and 8.10 shows thermal-sprayed masks that were produced from LS and CNC milled models respectively. The LS model was created in nylon polyamide while the CNC milled model was machined from a block of polyurethane foam. All the masks shown are intended for shielding low energy X-rays in the 100-250 kV range.

Figure 8.8 Thermal-sprayed mask produced from traditional plaster model

Figure 8.9 Thermal-sprayed mask produced from LS model

Figure 8.10 Thermal-sprayed mask produced from CNC milled model

If the mask is to be used for electron beam field shaping, an aluminum frame with outer dimensions the same as the end of the electron applicator to be used during treatment needs to be attached to the sprayed mask. This has to be done for two reasons. Firstly, the mask's output factor for electrons needs to be determined as described in section 2.5.4. The aluminum frame with the mask can be attached to the electron applicator using two bulldog clamps. Ionization measurements can then be conveniently done under the mask as required. Secondly, the aluminum frame serves as a guide to position the applicator against the mask. By bringing the applicator into contact with the frame, the radiation beam will always be directed at the treatment area at the same angle from treatment to treatment. The frame is attached to the mask through Wood's alloy rods that are cast for this application. The rods are soldered to the mask using four holes drilled into the frame as a guide (Figure 8.7E). The rods are then cut to the required length and soldered to the frame. This is done by inserting the soldering iron's tip into each of the four holes in the frame respectively (Figure 8.7F). The Wood's alloy melts and fills the thread that was tapped into the holes thereby firmly fixing the rods to the frame. There is no need to attach aluminum frames to masks that will be used for shielding low energy X-rays. Instead of measuring the output factor for these masks, the output factor for the closest equivalent square to the treatment portal is used. Aluminum frames will also not be of much use in aligning the kilovolt unit's applicators with the treatment areas. All these applicators have dome shaped transparent plastic covers attached to their treatment ends. The applicators can thus not be brought flush into contact with the frames as is the case with electron applicators. To finish a thermal-sprayed mask, the inside is sprayed with a thin layer of clear lacquer paint. This is done to prevent the metal, especially the lead and cadmium that forms part of the alloy from being absorbed by the patient's skin when placed upon it.

8.4.2 Thermal-sprayed masks for large electron fields

When a large electron field is applied across an uneven area such as a boost to a radical mastectomy scar, the surrounding healthy tissue was traditionally shielded using a wax casting as described in section 5.2.2. Similar shielding results to the wax casting can be achieved with a sprayed mask. The procedure for producing a thermal-sprayed mask for a large electron treatment field is the same as that for producing a mask for a small treatment field. Instead of melting the treatment portal in the mask using a soldering iron (for masks produced from plaster models), it can be cut using the band saw that is used for trimming the mask's edges. Using a soldering iron may be too time consuming since the size of the portal may be considerable in this application. The soldering iron is however required to solder the entry cut into the treatment portal in the mask.

8.4.3 Thermal-sprayed masks for rotational electron fields

The procedure followed to produce a thermal-sprayed mask for a rotational electron field (see section 4.6.3.2c) is the same as for a large stationary electron field. It is not necessary to attach an aluminum frame to the mask with this treatment technique since the radiation is applied in an arc around the treatment area.

CHAPTER 9

EVALUATION OF THE THERMAL-SPRAY TECHNIQUE

9.1 Introduction

The thermal-spray technique as a means of producing radiation field shaping shields was evaluated by comparing masks produced through the technique to radiation field shaping shields produced through traditional techniques. The required thicknesses of the sprayed masks to effectively shield both electron and low energy X-rays at different radiation energies were also determined. Finally, sprayed sheets of Wood's alloy were inspected to determine if the thermal-spray process caused any defects within the sprayed layers. Any defects may adversely influence the shielding ability of masks.

9.2 Comparison between different field shaping techniques

An electron boost to a radical mastectomy operation[1] scar was chosen as an ideal setup for comparing the different field shaping techniques. These scars are usually long and extend across the side of the chest wall necessitating a large radiation field to be applied. The size of the field together with the curvature of the chest wall will in most cases cause a sizeable stand-off at the field's edges with resultant radiation scatter beyond the primary beam.

[1] see section 4.6.3.3

9.2.1 Perspex™ phantom and radiation field shaping shields

To simulate a patient's chest wall, the author manufactured a Perspex™ phantom as shown in Figure 9.1. The curvature of the phantom was based on the average curvature of 12 plaster models that were used for producing wax castings for actual patients.

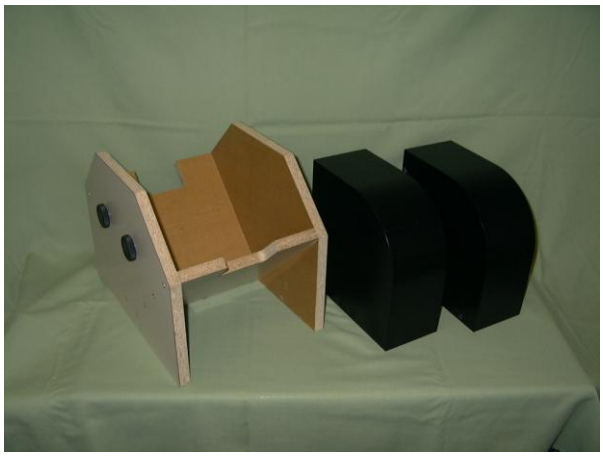

Figure 9.1 Perspex™ phantom with wooden box

Figure 9.2 Radiation field shaping shields produced for arbitrary field shape

The phantom was produced in two halves and was equipped with four locating pins that were used to accurately align the halves. The two halves of the phantom were placed in a custom made wooden box and clamped together using two clamping screws mounted on one side of the box. An arbitrary field shape was marked out on the surface of the phantom. The shape of this arbitrary field was based on field shapes that are often encountered with boosting post mastectomy scars. Radiation field shaping shields were produced to shield the area around the chosen field shape using the shaped end-frame, wax casting and thermal-sprayed mask techniques as described in Chapters 5 and 8. These radiation field shaping shields were made to fit onto the treatment end of a 20 x 10 cm² electron applicator since this is the field size most often used with this type of treatments. Figure 9.2 shows the various radiation field

shaping shields produced. The author also compared the effectiveness of the different field shaping techniques at the edge of the 20 x 10 cm² treatment field. This can be considered a worst case scenario for radiation scattering since the stand-off at the edges of the field is at its greatest and will cause the maximum scatter beyond the primary beam. A wax casting and a thermal-sprayed mask were produced to shield the area around the entire 20 x 10 cm² radiation field.

9.2.2 Field shaping comparison through radiographic film

Radiographic film was chosen as the means through which the different field shaping techniques were compared. This type of film is composed of a transparent film base (polyester resin or cellulose acetate) that is coated with an emulsion containing minute silver bromide crystals. Exposure to ionizing radiation or visible light causes chemical changes to take place within the exposed crystals to form what is known as a latent image. When the film is processed on an automatic film processor, it is passed through a bath of developer solution where the chemically changed exposed crystals are reduced to small grains of metallic silver. The film is then passed through a bath of fixing solution where the unaffected crystals are washed away leaving clear film in their place. The grains of metallic silver, upon which the fixer has no effect, causes the film to darken. The degree to which an area of film is darkened is dependant on the amount of silver that was deposited and consequently indicates the amount of radiation that was absorbed in that area [23, p. 151].

9.2.2.1 Films taken for the arbitrary electron field

Diagnostic Kodak™ X-OMAT V Film was used to determine how effectively the different field shaping techniques shape the radiation beam to the required treatment area. A film within its protective envelope was taped to the surface of the phantom and the 20 x 10 cm^2 electron applicator was attached to an Elekta™ SL25 linac's radiation head. A rectangular end-frame that fits the shape of the arbitrary test shape (in this case 18 x 6 cm^2) the closest was inserted in the treatment end of the applicator. The linac's table was raised for the treatment end of the applicator to touch the film on the phantom as shown in Figure 9.3A. A radiation energy of 4 MeV was selected on the linac and the film was exposed for 50 MU. This is the radiation dose recommended by the manufacturers of the film to produce good imaging results.

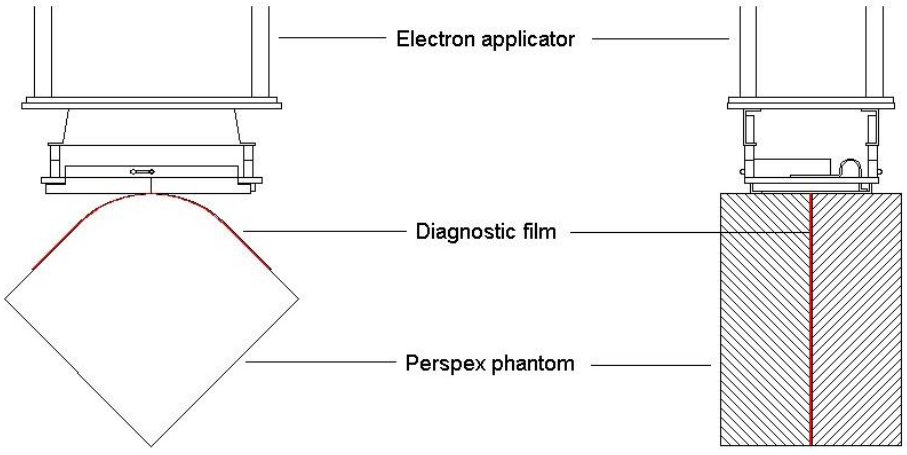

Figure 9.3A Linac setup for taking a film to determine surface dose distribution

Figure 9.3B Linac setup for taking a film to determine cross-sectional dose distribution

The shaped end-frame was inserted into the applicator, a new film was taped to the phantom and the film taking procedure was repeated. For the wax casting and sprayed mask, the 20 x 10 cm² end-frame was inserted in the applicator and films were taken with the casting and mask positioned on the phantom. The closest fitting end-frame to the arbitrary test shape was included in the lineup of field shaping techniques since some cancer departments do not do any field shaping at all and merely make use of a standard end-frame. Additional films were taken at 6, 8 and 10 MeV with all four radiation field shaping shields for each energy level. Radiation energies of 4–10 MeV were chosen to demonstrate the dose distribution for the various field shaping techniques since these are the energies most often used for patients receiving electron boosts.

9.2.2.2 Films taken for the 20 x 10 cm² electron field

Surface films were also taken for radiation energies of 4-10 MeV for the open field (20 x 10 cm² end-frame), wax casting and sprayed mask following the same procedure as for the arbitrary field shape. Figure 9.4 shows the setup for taking a surface film on the linac with the wax casting and Figure 9.5 with the sprayed mask. All the films taken for surface dose distribution for both the arbitrary and 20 x 10 cm² field where developed on a Dürr Medicine™ 430 film processor. Not only is it important to know how the different field shaping techniques compare in terms of surface dose, it is also important to know how they compare in terms of dose distribution within the phantom. To determine what the dose distributions within the phantom will be for the different techniques, the author traced the outline of the phantom onto the envelope of a sealed film with a pen. The film was then carefully cut along the traced lines using a pair of scissors in a darkroom under the appropriate lighting conditions so as not to expose the film.

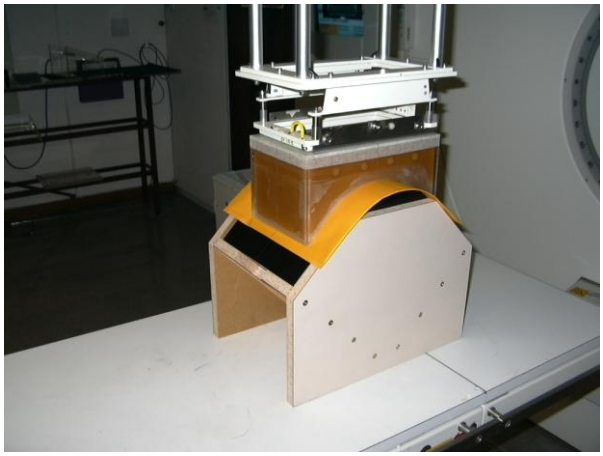

Figure 9.4 Linac setup to determine surface dose distribution for a wax casting

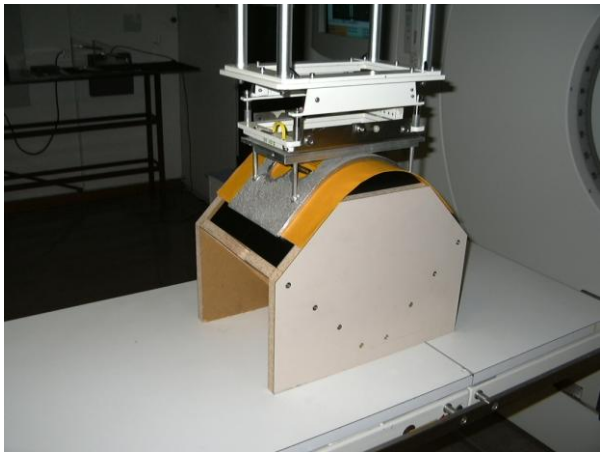

Figure 9.5 Linac setup to determine surface dose distribution for a thermal-sprayed mask

The cut piece of film was clamped between the two halves of the phantom using the clamping screws that were installed in the phantom's wooden box. Masking tape that was sprayed black was used to seal the joint line between the two halves of the phantom so as not to let any light in that might ruin the film. The phantom in its wooden box was placed on the linac's treatment table and the 20 x 10 cm^2 applicator was attached to the radiation head. A 20 x 10 cm^2 end-frame was inserted into the applicator, the table was raised to touch the applicator and the film was exposed for 50 MU at 4 MeV. Figure 9.3B shows the setup for taking a cross-sectional film on the linac. The film was taken out of the phantom in the darkroom and developed. Additional films were taken for 6, 8 and 10 MeV following the same procedure used with the 20 x 10 cm^2 end-frame. The film taking procedure was also repeated for the wax casting and sprayed mask for all the radiation energies.

9.2.2.3 Films taken for the rotational electron beam field

An investigation was undertaken to determine whether the thermal-spray technique can be used to produce field shaping masks for use with rotational electron beam therapy as described in section 4.6.3.2c. A field shaping mask was produced as described in Chapter 8 to shield the area around a 20 x 10 cm^2 area on the phantom as shown in Figure 9.6. The phantom was placed on the table of the linac and positioned such that the center of the phantom coincided with the linac's isocenter. A film was placed between the radiation field shaping shield and the phantom and a special applicator used with rotational therapy was attached to the linac's radiation head. The film was exposed at 6 MeV for 250 MU while the gantry was rotated through an arc of 160 degrees around the phantom as shown in Figure 9.7.

Figure 9.6 Radiation field shaping shield produced for rotational electron beam therapy

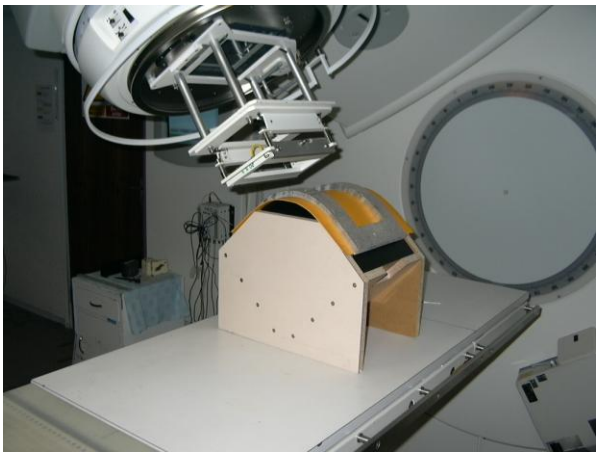

Figure 9.7 Setup to determine surface dose distribution for rotational electron beam therapy

Since the center of the phantom was placed at the linac's isocenter, the distance between the applicator and film was kept constant across the arc of rotation. Another surface film was

taken at 10 MeV following the same procedure as well as additional cross-sectional films of the phantom at both radiation energies.

9.2.3 Film-image conversion to isodensity curves

All the films taken for the arbitrary field shape, 20 x 10 cm^2 field and rotational electron beam field were scanned on a Vidar™ film scanner. This device consists of a light source and a light detector (photocell) that measures the light intensity transmitted through an area of film when placed between the light source and detector. The light intensity transmitted (i.e. optical density) thus indicates the degree of darkening of a given area of film. The scans were next converted to isodensity curves using Osiris™ Version 4 software on a personal computer. The Osiris™ software displays black as 100% and white as 0% with the degree of darkening awarded percentages in between the two extremes. Figure 9.8 shows a scan from the Vidar scanner of the arbitrary field shape as defined by a shaped end-frame at a radiation energy of 8 MeV while Figure 9.9 shows the same image converted to isodensity curves as an example. Isodensity curves can be defined as lines passing through points of equal density and are expressed as percentages of the density at a reference point. Since film density represents the darkening of the film in an area and the darkening of the film represents the amount of dose absorbed, isodensity curves can also be considered to connect points of equal absorbed dose. Isodensity charts of all the films that were taken to compare the different field shaping techniques are shown in Addendum A.

Figure 9.8 Example of a film scanned on a Vidar™ film scanner

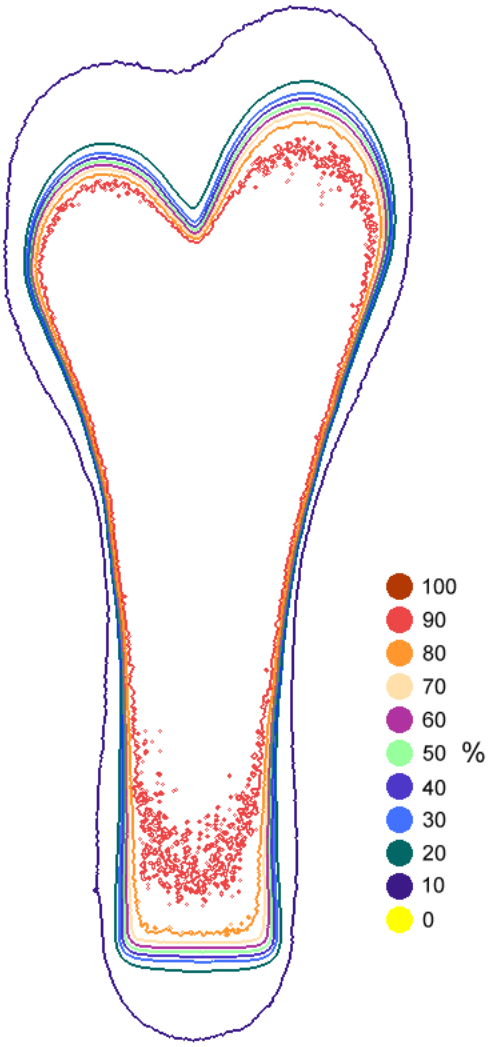

Figure 9.9 Scanned image converted to isodensity curves

The isodensity charts that show surface dose distribution are presented with the original field shapes (shown by the hatched areas) superimposed on the isodensity charts. With the cross-sectional films for the 20 x 10 cm^2 field, the field's edges are shown. The original field shapes and field edges are indicated to show to what extent the different field shaping techniques limit the radiation to the required treatment area.

9.2.4 Discussion on isodensity charts for different radiation shields

Isodensity curves produced through the technique described in the previous section are discussed with reference to Addendum A1 for the arbitrary electron field shape, Addendum A2 for the stationary 20 x 10 cm² field and Addendum A3 for the 20 x 10 cm² electron arc field.

9.2.4.1 Arbitrary electron field (Addendum A1)

The closest fitting rectangular end-frame to the marked treatment area proves to be a poor alternative to define the treatment area. No attempt is made to shape the radiation field according to the treatment area using this technique. A large amount of healthy tissue can thus potentially be irradiated depending on the shape of the cancer affected area inside the rectangle. The stand-off between the flat undersurface of the end-frame and the phantom's curved surface also causes a significant amount of electron scatter at the rectangular field's edges. This electron scatter causes an even larger area of surrounding healthy tissue to be irradiated as shown by the isodensity curves. If one considers that cancer wounds heal after regenerative growth of the surrounding healthy tissue after treatment, irradiation of this tissue is undesirable. The shaped end-frame provides field shaping but the technique does not make provision for a treatment area with irregular contours. The distension of the isodensity curves beyond the marked treatment area illustrates the effect of a stand-off on field shaping with the shaped end-frame. The isodensity curves for the wax casting and sprayed mask are largely contained within the boundaries of the marked treatment area. This indicates effective shielding for both these field shaping techniques. The advantage of conforming the radiation field shaping shield to the treatment areas contours is thus made clear.

9.2.4.2 20 x 10 cm² field (Addendum A2)

Surface films taken with the 20 x 10 cm^2 field shape show similar field shaping characteristics to the arbitrary field shape for the different field shaping techniques. The open field cross-sectional isodensity chart shows the extent of electron scatter through air at the field's edge. The scatter is at its worst at an electron energy of 4 MeV where the 20% isodensity curve measures 15 mm from the field's edges. The distension of the isodensity lines beyond the field's edge diminishes with increase in radiation energy. This is because higher energy electrons scatter more in the forward direction in air than low energy electrons do [23, p. 319]. The cross-sectional isodensity curves for the wax casting and sprayed mask shows that these field shaping techniques limit the radiation well to the radiation field's edges. Noteworthy is the 10% isodensity curve which shows significant distension for both the wax casting and sprayed mask. The distension is not because of partial radiation transmission through the radiation field shaping shields but because of electron scatter in the Perspex™ phantom within which the films were taken. All the isodose curves show some bulging outside the field's edges because of electron scatter with the effect becoming more prominent with an increase in radiation energy. The cross-section isodensity charts also show an increase in depth dose with an increase in radiation energy for each field shaping technique.

9.2.4.3 Rotational electron beam field (Addendum A3)

The thermal-sprayed mask defines the rotational electron beam field well with all the isodensity curves contained within the marked treatment area. The cross-sectional isodensity chart shows good dose uniformity across the arc of rotation. When compared with the cross-sectional dose distribution from the stationary electron fields which is less uniform, the advantages of rotational electron beam therapy becomes obvious.

9.3 Required thickness of thermal-sprayed masks

A prerequisite for producing thermal-sprayed masks is to determine what thickness the masks need to be to effectively shield the healthy tissue surrounding the treatment area. Measurements were made to determine what the thickness of sprayed Wood's alloy masks need to be to attenuate the open beam by 90% and 95% for both electrons and low energy X-irradiation.

9.3.1 Mask thickness for electron irradiation

The relative percentage dose reduction for different thicknesses of sprayed Wood's alloy for electrons having accelerator energies of 4, 6, 8, 10, 12, 15, 18 and 20 MeV were determined on an Elekta™ SL25 linac. Transmission ionization measurements were made for two field sizes namely 10 x 10 cm^2 and 20 x 20 cm^2.

9.3.1.1 Apparatus requirements and measurement procedure

In order to determine what amount of radiation is transmitted through a given thickness of sprayed Wood's alloy, thin sheets of the alloy had to be produced. For this purpose the author sprayed layers of Wood's alloy onto a sheet of plate glass inside the spray cabinet. The sprayed alloy sheets were then machined on a milling machine to the required thicknesses as shown in Figure 9.10. Machining the alloy revealed no inconsistency in the sprayed layers such as porosity or cracks that might influence the density of the material during transmission measurements. A 1 mm, two 2 mm, one 5 mm, one 10 mm and one 20 mm sheet were fabricated as shown in Figure 9.11.

Figure 9.10 Machining a sheet of sprayed Wood's alloy to the required thicknesses

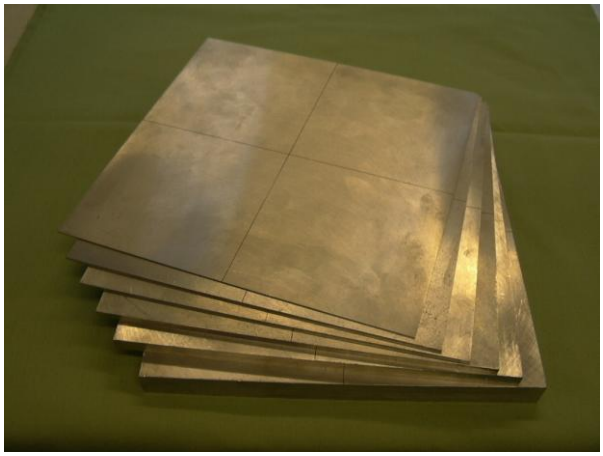

Figure 9.11 Complete set of sheets produced for transmission measurements

By selectively stacking these sheets on top of one another, any thickness of Wood's alloy can be produced from 1-40 mm in 1 mm increments. Ionization measurements to determine radiation transmission through the sheets of Wood's alloy were made using a (0.35 cm^3 PTW) Roos™ parallel-plate ionization chamber Type 34001 with a PTW Unidos™ dose meter. The author also manufactured a Perspex™ phantom for use with the Roos™ chamber as shown in Figure 9.12. The chamber fits flush with the surface of the phantom into a precisely machined hole. The close fit between the chamber and phantom ensures that there will be no air gap around the chamber that may influence the ionization readings. The phantom was positioned on additional Perspex™ plates on the linac's table where the purpose of the plates was to produce back scatter conditions during irradiation. A 10 x 10 cm^2 electron applicator was attached to the linac's radiation head and the treatment table was raised for the applicator to touch the phantom. An open field ionization measurement (no Wood's alloy in the beam) was taken with the linac set at 4 MeV for 200 MU. The couch was lowered and a 1 mm sheet of

Wood's alloy was placed on the phantom. The table was raised for the applicator to touch the alloy sheet as shown in Figure 9.13.

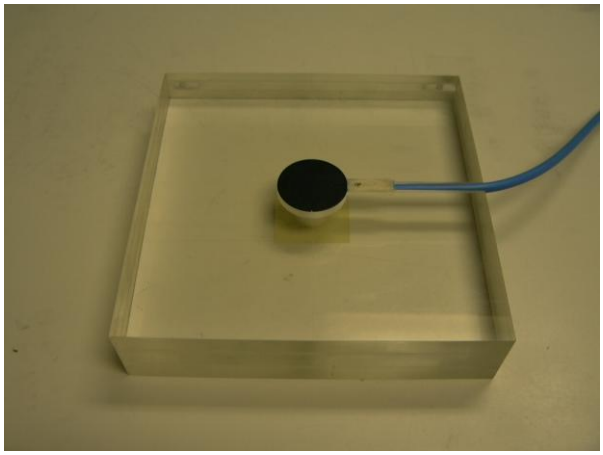

Figure 9.12 Phantom produced for the Roos™ ionization chamber

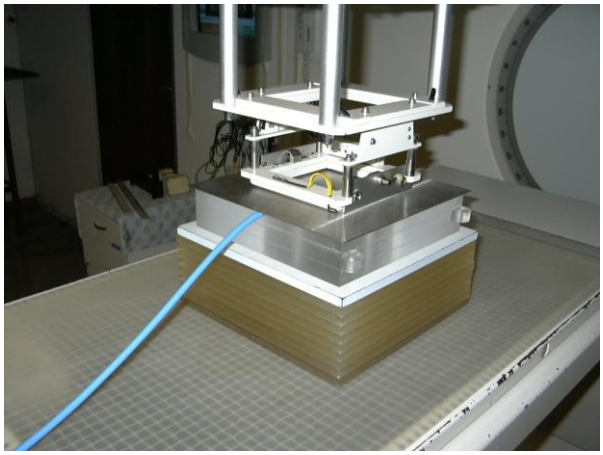

Figure 9.13 Linac setup for transmission measurements

Another ionization measurement was taken at the same radiation energy for the same number of monitor units. This procedure was repeated with 1 mm of alloy added for each measurement until the difference between consecutive ionization measurements became negligible. A radiation energy of 6 MeV was selected on the linac and an open field measurement was taken followed by transmission measurements of the Wood's alloy in 1 mm increments. This procedure was repeated for the remaining electron energies up to 20 MeV. The 10 x 10 cm^2 applicator was replaced with the 20 x 20 cm^2 applicator and the measurement procedure was repeated for all the radiation energies. Measurements as described here were taken to determine the percentage of radiation that would be transmitted through a given thickness of Wood's alloy. Since the sheets of Wood's alloy were placed directly on the ionization chamber, the measurements were effectively taken at skin level. To determine if there would be any sizeable difference between transmission measurements taken at and below skin level, all the measurements were repeated with the ionization chamber at the depth

of D_{max}. Table 9.1 shows the thicknesses of buildup required to be able to do ionization measurements at the depth of D_{max}

Table 9.1 Thickness of buildup required to attain D_{max} at different electron energies for ionization measurements

Electron energy (MeV)	4	6	8	10	12	15	18	20
Buildup thickness (mm)	8	8	16	20	20	20	20	20

The required buildup for each radiation energy was placed on the phantom and the different thicknesses of Wood's alloy were placed on the buildup. Transmission measurements were taken using this setup for all the radiation energies and field sizes.

9.3.1.2 Results from measurements

All transmission ionization measurements taken for the different thicknesses of sprayed Wood's alloy for each radiation energy, field size and measurement depth are presented in Addendum B1. Also shown are the ionization measurements normalized to the open beam ionization measurement for each thickness of Wood's alloy. The relative percentage ionization measurements are shown against thickness of sprayed Wood's alloy in graph form in Addendum B2. From the graphs it can be determined what the thicknesses of Wood's alloy field shaping masks need to be to reduce the open beam dose by 90% and 95% for the different radiation energies, field sizes and measurement depths. To determine alloy thickness for a dose reduction of 95%, for example, a line is drawn through 5% transmission on the y-axis. Where it coincides with the transmission curves of the different radiation energies the thicknesses of alloy is read from the x-axis. The required thicknesses are listed in Tables 9.2 and 9.3.

Table 9.2 Thickness of sprayed Wood's alloy required to attenuate the open beam dose by 95% at different electron energies, measurement levels and field sizes

Field size (cm x cm)	Measurement level	Radiation energy (MeV) Thickness (mm)							
		4	6	8	10	12	15	18	20
10 x 10	Skin	2.00	3.15	4.05	5.00	7.00	14.6	21.6	26.6
10 x 10	Dmax	1.60	2.45	2.55	3.05	4.50	9.10	14.6	19.5
20 x 20	Skin	1.95	3.05	4.10	5.05	7.25	15.5	22.3	27.5
20 x 20	Dmax	1.55	2.50	2.60	3.10	4.65	10.1	16.1	21.0

Table 9.3 Thickness of sprayed Wood's alloy required to attenuate the open beam dose by 90% at different electron energies, measurement levels and field sizes

Field size (cm x cm)	Measurement level	Radiation energy (MeV) Thickness (mm)							
		4	6	8	10	12	15	18	20
10 x 10	Skin	1.85	2.80	3.60	4.30	5.40	7.05	9.25	11.9
10 x 10	Dmax	1.25	2.05	2.05	2.45	3.60	5.10	6.80	8.05
20 x 20	Skin	1.85	2.70	3.60	4.35	5.45	7.30	9.50	12.4
20 x 20	Dmax	1.20	2.05	2.05	2.50	3.70	5.20	7.00	8.30

9.3.1.3 Discussion on measurements

- The determined thicknesses of sprayed Wood's alloy to attenuate the open beam by 90% or 95% shown in Tables 9.2 and 9.3 compares favourably with that determined

by Purdy *et al* [42, pp. 251-253]. The latter authors performed transmission measurements for Cerrobend™ (which is a trade name for Wood's alloy) at similar radiation energies to the ones used by the author at the depth of D_{max}.

- There is a significant difference in alloy thickness required to attenuate the open beam dose to acceptable levels that was determined through transmission measurements performed at skin level and at the level of D_{max}. This is affirmed by Khan *et al* [25, pp. 712-713] who performed transmission measurements at various depths for lead at a radiation energy of 13 MeV, concluding that the thickness of a shielding material determined through percentage transmission data depends greatly on measurement depth.
- The thickness of sprayed Wood's alloy to reduce the open beam to the required percentiles increases with field size for all electron energies. This is because smaller field sizes cause more electron scatter than larger field sizes.
- The initial buildup shown in the percentage transmission curves in Addendum B2, which is due to scattered radiation, also increases with field size. This buildup effect is also much more prominent with percentage transmission measurements taken at skin level than at D_{max}.
- An important observation from Tables 9.1 and 9.2 is that a considerable thickness of Wood's alloy is required to reduce the open beam dose to 5% for radiation energies of 15, 18 and 20 MeV. This is because of the fact that beyond the lower turning point of the percentage transmission curve, the radiation is essentially bremsstrahlung photons [23, p. 317]. Bremsstrahlung is the effect whereby photons are produced when electrons are absorbed by a material with a high atomic number such as lead or Wood's alloy. For the higher electron energies, the weight of the field shaping mask becomes a serious consideration. With these higher energies a compromise should be made between the mask weight the patient can bear and the reduction in dose that is

desired. A reasonable thickness of shielding material can be determined from the percentage transmission curves at about the lower turning point of each curve. Additional shielding material beyond this area is much less effective for further dose reduction since this is the bremsstrahlung region.

9.3.2 Mask thickness for low energy X-irradiation

The relative percentage dose reduction for different thicknesses of sprayed Wood's alloy for 100 and 250 kV as produced by a Philips Medical Systems™ RT250 kilovolt unit were also determined. Transmission ionization measurements were made with a 10 x 8 cm^2 and a 15 x 10 cm^2 field size for each energy.

9.3.2.1 Apparatus required and measurement procedure

The sheets of Wood's alloy that were produced for transmission measurements on the linac were also used for measurements on the kilovolt unit. Instead of using the parallel-plate ionization chamber for measurements such as on the linac, a thimble type PTW Farmer™ 0.6 cm^3 ionization chamber which is better suited to X-ray measurements was used. Ionization measurements for X-irradiation were done in air with nothing in close proximity behind the ionization chamber that may cause back scatter and influence the reading. The ionization chamber was clamped in a retort stand and the stand was placed on a table. The kilovolt unit's radiation head was turned horizontal and a 10 x 8 cm^2 applicator was attached to the unit's radiation head. The kilovolt unit and stand were positioned such as to bring the graphite tip of the ionization chamber into contact with the center of the applicator's plastic cover as shown in Figure 9.14. A radiation energy of 100 kV was selected on the kilovolt unit and the ionization chamber was irradiated for 2 minutes where after an ionization measurement was

taken on a PTW Unidos™ dose meter. A 1 mm sheet of Wood's alloy was placed in front of the kilovolt unit's applicator and was kept upright by clamping it to two angle plates as shown in Figure 9.15. The ionization chamber was taped to the back of the Wood's alloy sheet in such a way that the tip of the chamber was positioned over the center of the applicator.

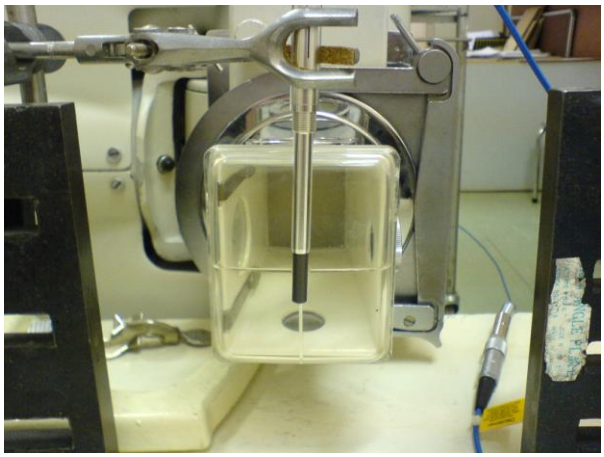

Figure 9.14 Kilovolt unit setup for open field ionization measurement

Figure 9.15 Transmission measurement for a sheet of Wood's alloy

An ionization measurement was taken at the same radiation energy and exposure time. This procedure was repeated for increasing thickness of Wood's alloy until there was no significant difference in measured ionization from measurement to measurement. The 10 x 8 cm^2 applicator was replaced with the 15 x 10 cm^2 applicator and the measurements were repeated at the same energy and exposure time. Measurements were also taken at 250 kV for both applicators. There was no need to repeat the measurements at any level below skin level, such as with electrons, since D_{max} is attained at skin level with X-rays.

9.3.2.2 Results from measurements

All the transmission ionization measurements taken on the kilovolt unit for the different thicknesses of sprayed Wood's alloy at the two radiation energies are presented in Addendum B1. The ionization measurements normalized to the open beam ionization measurement are shown for each thickness of Wood's alloy. The relative percentage ionization measurements are shown against thickness of sprayed Wood's alloy in graph form in Addendum B2. The data are used to determined what the thickness of sprayed Wood's alloy needs to be to reduce the open field dose by 90, 95 and 98% for the two radiation energies and field sizes. The required thicknesses are listed in Table 9.4.

Table 9.4 Thickness of sprayed Wood's alloy required to attenuate the open beam dose by 90, 95 and 98% at two X-ray energies and field sizes

Field size (cm x cm)	**Attenuation %**	**Radiation energy (kV) Thickness (mm)**	
		100	**250**
10 x 8	98.0	0.98	1.39
15 x 10	98.0	0.98	1.39
10 x 8	95.0	0.94	1.13
15 x 10	95.0	0.94	1.13
10 x 8	90.0	0.86	0.99
15 x 10	90.0	0.86	0.99

9.3.2.3 Discussion on measurements

- There is very little difference between transmission measurements taken at the two different field sizes shown in Addendum B1. The required thicknesses of sprayed Wood's alloy to attenuate the open X-ray beam to the percentiles indicated are consequently shown the same for the two field sizes in Table 9.4. Field size does not

have such a significant effect on the transmission measurements for X-rays as it has on electrons.

- The percentage transmission curves in Addendum B2 for X-rays show a rapid falloff with no initial buildup, such as was observed with the percentage transmission curves for electrons.

9.4 Testing for defects in thermal-sprayed layer of Wood's alloy

An investigation was undertaken to determine whether there are any defects such as cracks or porosity present in thermal-sprayed layers of Wood's alloy. Any of these defects may negatively affect the shielding ability of masks produced through the technique. X-ray imaging was chosen as the means through which the thermal-sprayed masks were inspected. An Elekta™ Precise linac equipped with an iViewGT™ portal imaging system as shown in Figure 9.16 was employed to this end. A portal imaging system is generally used to verify patient setup before a dose of radiation is administered to a patient. The system however also proved useful in the application described here. Any defects within a sprayed sheet of Wood's alloy will show up as variation in density of the material under X-ray imaging.

Figure 9.16 Elekta™ Precise linac equipped with an iViewGT™ portal imaging system

To check for uniformity in density across a sprayed sheet, it is important for the sheet to be uniform in thickness. Any variation in thickness may be mistaken for variation in density within the sheet. The Wood's alloy sheets that were used to determine the required thickness of thermal-sprayed masks in section 9.3 were also used in this experiment. The thicknesses of these sheets were verified by the author to be uniform at the time that they were fabricated. A thermal-sprayed Wood's alloy step wedge as shown in Figure 9.17 was also fabricated. This was done by spraying the alloy onto a strip of aluminum. The sprayed layer of alloy was then machined on a milling machine to thicknesses of 1-6 millimeters in 0.5 mm increments. The treatment table was adjusted to isocentric height and the field size to 20 x 20 cm^2 which is the maximum field size detectable by the portal imager.

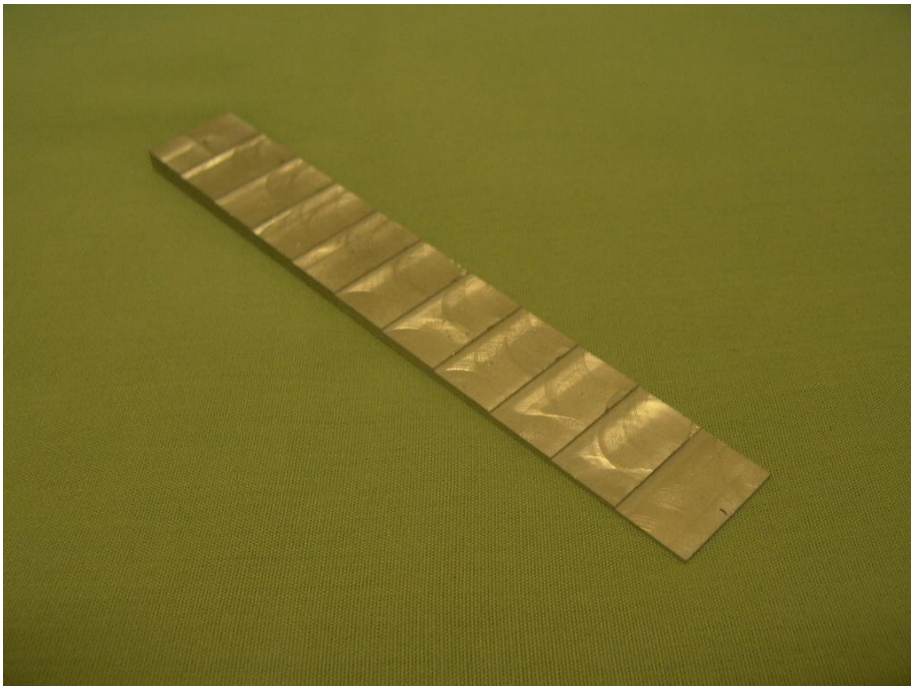

Figure 9.17 Thermal-sprayed Wood's alloy step wedge

The step wedge was positioned in the center of the field on the table and the linac was set at a radiation energy of 8 MV. The step wedge was irradiated while the image of the radiation transmission through the wedge was simultaneously captured on the portal imager. The portal imager's computer automatically switches off the linac when the imager receives a pre-set dose of radiation. This dose is sufficient to create an image on the portal imager without overexposing the unit. Any object placed in the radiation field will cause radiation absorption requiring the linac to produce a higher radiation dose before the portal imager threshold dose value is reached. The higher the density of the object placed in the field the higher the radiation dose needs to be before the imager switches off the linac. With the wedge placed in the radiation field, the required dose delivered by the linac is determined by the open field surrounding the wedge. If the linac is to deliver the same dose with the alloy sheets, an area of open field also needs to be present when the images of the sheets are taken. For this reason each of the sheets were positioned such that a 2 cm gap was left between the edge of the field

and the edge of each sheet when the images of the sheets were taken. Since the wedge and the sheets were exposed to the same dose of radiation when the images were taken, it is possible to compare the images. The gray scale images produced by the iViewGT™ software were converted to colour images using the Osiris™ software introduced in section 9.2.3. The Osiris™ software allows different colours to be allocated to different densities. By placing the coloured image of the step wedge next to the images of the sheets of Wood's alloy (as presented in Addendum C), variation in the densities of the sheets can be identified. Radiation scatter from the linac's collimation system that defines the field size distorts the edges of the 20 x 20 cm² portal image. For this reason only a 10 x 10 cm² area of each sheet of Wood's alloy is shown. The image of the step wedge allows for comparison with the alloy sheets with thicknesses of 1, 2 and 5 mm since the wedge is only 6 mm thick at its highest step. To determine variation in density for the 10 mm sheet an image was taken of the wedge placed on top of the two 2 mm sheets. This places the wedge's highest step at a thickness of 10 mm. By comparing this image of the step wedge with the image of the 10 mm sheet, density variation of up to 5 mm can be observed within the sheet. This procedure was repeated with the wedge positioned on top of the sheets that were stacked to a thickness of 14 mm thereby placing the wedge's highest step at 20 mm. This image of the wedge was then compared with the image of the 20 mm alloy sheet.

9.4.1 Discussion on portal X-ray images

The colour images of the sheets of Wood's alloy shows slight variation in colour from the center to the corners of each radiation field. This variation in colour can be attributed to non-uniformity in delivered radiation dose (field flatness) by the linac rather than variation in density of the sheets of alloy. Consequent measurements with test equipment confirmed slight variation in dose delivered across the treatment plane to coincide with the variation in dose

observed with the portal X-ray images. The variation in dose was however still well within acceptable limits for treatment as set by international standards. Also contributing to the colour variation is the slightly greater thickness a photon has to traverse through the corners of the sheet compared to the center if one considers that the radiation originates from a point source. None of the images shows abrupt colour changes signifying non-uniformity in density and thus indicating defects such as air pockets, cracks or porosity. From this it can be concluded that thermal-sprayed layers of Wood's alloy shows no unexpected internal defects and can be safely used to produce radiation field shaping masks for patients.

CHAPTER 10

CONCLUSION TO THE RESEARCH PROJECT

10.1 Conclusion

The purpose of the research project was to implement an improved field shaping technique for low energy radiation in radiotherapy. Through the introduction of a new low temperature thermal-spray field shaping technique this goal was met. Field shaping masks produced through the thermal-spray technique show some clear advantages over the traditional techniques. This statement is motivated with reference to Table 10.1.

Producing radiation field shaping masks through thermal-spraying onto plaster models is much less labor intensive and faster than producing field shaping shields through the traditional lead mask or wax casting techniques[1]. This is to the advantage of both the technologist who fabricates the shields as well as patients who require field shaping during radiation treatment. A patient that has to attend a radiotherapy centre from a rural area (for a cancerous skin lesion in an early stage as an example) will be able to have a field shaping mask prepared and receive radiation treatment within the same day. This saves the patient the inconvenience and cost of having to stay over for a day or more to have the field shaping mask prepared through the traditional techniques.

[1] see disadvantages of the lead mask and wax casting field shaping techniques in sections 5.2.1 and 5.2.2 respectively

Producing thermal-sprayed masks from LS or CNC milled models presents the patient with some unique advantages in comparison with plaster models. The 3D laser scanner used to capture the treatment area geometry for the model fabrication techniques requires no physical contact with the patient. This procedure appears to be less traumatic for the patient than the plaster bandage impression required for the plaster models. This is particularly the case if the impression needs to be taken in the facial area or if the treatment area involves open wounds. The fast scanning speed of the scanners also makes it ideal to determine treatment area contours of areas prone to movement such as experienced on small children for example. The high cost involved in producing a LS model is unfortunately a disadvantage. The price shown in Table 10.1 is for growing a single model. Should more than one model be grown simultaneously, the production price will be reduced significantly.

Masks produced from CNC milled models prove to be the most effective of all the radiation field shaping techniques. The masks can be produced at a relative low cost and within a reasonable time frame when compared to the other techniques. The initial procurement cost in obtaining a 3D laser scanner and CNC milling machine may be considered too high. The cost of these devices should however be measured against the benefits they will bring to patients. It is also possible for a radiotherapy centre equipped with a CNC milling machine to service other centres without such a device since the treatment area geometry file is easily transferable via the internet over any distance.

Experimental work carried out to evaluate the thermal-spray radiation field shaping technique showed that the shielding ability of masks produced through the technique compared favourably with those produced through the wax casting technique. The thermal-sprayed field shaping masks also showed a marked improvement over field shaping shields produced through the shaped end-frame technique. Although these shields are relatively cheap and

quick to produce, they make no provision for any curvature of the treatment area. Additional experiments showed that there are no defects within thermal-sprayed layers of Wood's alloy that may negatively affect the shielding ability of masks produced through the technique.

The equipment used to produce thermal-spray masks fulfil the criteria (section 7.1) set for the equipment at the onset of the research project well. Field shaping masks are safely and cleanly produced at reasonable cost (depending on the process) within an acceptable time frame using the thermal-spray equipment described in this thesis. The thermal-spray equipment was manufactured from affordable components using locally available tools and equipment. The weight of masks produced for patients were found to be acceptable with an average weight of 676 g measured for 14 facial masks. At present, technologists only produce masks for patients who receive X-ray treatment in the orthovoltage range at the Department of Oncotherapy at National Hospital, Bloemfontein where the thermal-spray field shaping technique is implemented.

10.2 Further research proposals

Towards the end of the study, the author learned of an alloy that can be used instead of Wood's alloy to produce field shaping masks through thermal-spraying. The alloy commercially known as Field's alloy [9] has approximately the same melting point as Wood's alloy but contains no lead or cadmium. Producing masks without these harmful substances will be safer for the technologist and patient. Radiation transmission measurements of the alloy will have to be carried out to determine the required thicknesses of masks produced using the alloy for different radiation energies.

A second proposal is to use wax instead of polyurethane foam as a medium for machining a model of the patient using a CNC milling machine. Waxes are available with a melting point

higher than that of Wood's alloy which will be ideal for the thermal-spray radiation field shaping technique. The wax shavings from milling, together with the produced model can be remelted and cast into a block ready for machining a new model. Since both the shielding and model fabrication materials are recyclable, masks can be produced at low cost. Keeping in mind that the polyurethane model is discarded after use and polyurethane dust is produced during milling, the wax model technique is also more environmentally friendly.

REFERENCES

1. Andrew, J.W. & Aldrich, J.E. A video-based patient contour acquisition system for the design of radiotherapy compensators. Medical Physics, vol. 16, no. 3, 1989, pp. 425-430

2. Azomaterials (2000) Thermal spray coatings – Processes and properties Available from: <http://www.azom.com/details.asp?ArticleID=1581> [Accessed 8 November 2002]

3. Azomaterials (2000) Thermal spray technology Available from: <http://www.azom.com/features.asp> [Accessed 28 October 2002]

4. Baiker, L. Apparatus for spraying of thermo-plastic materials. Patent Nr. 297507, 1954

5. Blazdell, P. & Kuroda, S. Thermal spraying in the new millennium. Materials World, vol. 7, no. 4, 1999, pp. 205-207

6. Boyer, A.L., Fullerton, G.D. & Mira, J.G. An electron beam pseudoarc technique for irradiation of large areas of chest wall and other curved surfaces. International Journal of Radiation Oncology, Biology, Physics, vol. 8, no. 11, 1982, pp. 1969-1974

7. Boyer, A.L. & Goitein, M. Simulator mounted Moiré topography camera for constructing compensating filters. Medical Physics, vol. 7, no. 1, 1980, pp. 19-26

8. Brennan, J.B. Method and apparatus for melting metals. Patent Nr. 2322787, 1943

9. Dirac Delta Consultants Limited (2001) Fields metal Available from: <http://www.diracdelta.co.uk/science/source/f/i/fields%20metal/source.html> [Accessed 8 November 2007]

10. Dollinger, M., Rosenbaum, E.H. & Gable, G. Everyone's Guide to Cancer Therapy. 3rd. Edition. Kansas City: Andrew McMeel Publishing, 1997

11. Duncan Hynd Associates Limited (2000) Laser contouring Available from: <http://www.dha.co.uk/laser_contouring2.html> [Accessed 25 April 2004]

12. Fentiman, I.S. Detection and Treatment of early Breast Cancer. London: Martin Dunitz Ltd, 1990

13. Filt Air (2004) HEPA filters Available from: <http://www.filt-air.com/Resources/Articles/hepa/hepa_filters.aspx> [Accessed 14 August 2005]

14. Flame Spray Incorporated (2001) Thermal spray coatings Available from: <http://www.flamesprayinc.com> [Accessed 8 November 2002]

15. Gerbi, B.J. Compensating filter design using radiographic stereo shift information. Medical Physics, vol. 12, 1985, p. 646

16. Giarratano, J.C., Duerkes, R.J. & Almond, P.R. Lead shielding thickness for dose

reduction of 7 to 28 Mév electrons. Medical Physics, vol. 2, 1975, p. 336

17. Goede, M.R., Gooden, D.S., Ellis, R.G. & Brickner, T.J. A versatile electron collimation system to be used with electron cones supplied with Varian's Clinac 18. International Journal of Radiation Oncology, Biology, Physics, vol. 2, no. 7, 1977, pp. 791-795

18. Greene, D. & Williams, P.C. Linear Accelerators for Radiation Therapy. 2nd. Edition. Manchester: Institute of Physics Publishing, 1997

19. Griffiths, S.E. & Short, C.A. Radiotherapy: Principles to Practice. Edinburgh: Churchhill Livingstone, 1994

20. Gross, K. (2000) Thermal Spraying – An introduction Available from: <http://www.azom.com/details.asp?ArticleID=542> [Accessed 28 October 2002]

21. Horwich, A. Oncology A multidisciplinary textbook. London: Chapman & Hall Medical, 1995

22. Johns, H.E. & Cunningham, J.R. The Physics of Radiology. 4th. Edition. Illinois: Charles Thomas Publishers, 1983

23. Khan, F.M. The Physics of Radiation Therapy. 3rd. Edition. Philidelphia: Lippencott, Williams and Wilkins, 2003

24. Khan, F.M., Moore, V.C. & Levitt, S.H. Field shaping in electron beam therapy. British Journal of Radiology, vol. 49, 1976, p. 883

25. Khan, F.M., Werner, B.L. & Deibel, F.C. Lead shielding for electrons. Medical Physics, vol. 8, no. 5, 1981, pp. 712-713

26. Konica Minolta (2000) VI-910 Non-contact 3D digitizer Available from: <http://www.minolta-3d.com> [Accessed 25 April 2003]

27. Laursen, J.F., Andersen, H.C. & Hansen, H.P. 3D thin lead sheet compensating system. Medical Physics, vol. 9, no. 5, 1982, pp. 741-745

28. Leavitt, D.D., Peacock, LM., Gibbs, F.A. & Stewart, J.R. Electron arc therapy: Physical measurements and treatment planning techniques. International Journal of Radiation Oncology, Biology, Physics, vol. 11, no. 5, 1985, pp. 987-999

29. Levitt, S.H., Khan, F.M. & Potish, R.A. Technological Basis of Radiation Therapy. 2nd. Edition. Malvern: Lea & Febiger, 1992

30. MCG3D (2004) How does a 3D scanning machine based on laser technology work? Available from: <http://www.mcg3d.com/article.php3?id_article=33> [Accessed 25 April 2004]

31. McNeely, L.K., Jacobson, G.M., Leavitt, D.D. & Stewart, J.R. Electron arc therapy: Chest wall irradiation of breast cancer patients. International Journal of Radiation Oncology, Biology, Physics, vol. 14, no. 6, 1988, pp. 1287-1294

32. Miller, W.R. Estrogen and Breast Cancer. Austin, Texas: R.G. Landes Company, 1996

33. Mok, E.C. & Boyer, A.L. Compensator filters made with compact Moiré camera and computer. Medical Physics, vol. 11, no. 4, 1984, pp. 513-515

34. MSS Worldwide (1999) Metal spray Available from: <http://www.metal-spray.co.nz> [Accessed 8 November 2002]

35. Myung, C.C., Purdy, J.A., Gerbi, B., Abrath, F.G. & Glasgow, G.P. Variation in output factor caused by secondary blocking for 7-16 MeV electron beams. Medical Physics, vol. 6, no. 2, 1979, pp. 137-139

36. Payne, P.H. Metal spraying apparatus. Patent Nr. 3776462, 1973

37. Peacock, LM., Leavitt, D.D., Gibbs, F.A. & Stewart, J.R. Electron arc therapy: Clinical experience with chest wall irradiation. International Journal of Radiation Oncology, Biology, Physics, vol. 10, no. 11, 1984, pp. 2149-2153

38. Perez, C.A. & Brady, L.W. Principals and Practice of Radiation Oncology. 2nd. Edition. Philadelphia: J.B. Lippincott Company, 1992

39. Plane, J.H. & Usher, C. A rapid method of production of irregular-shaped fields for use with patients receiving electron radiotherapy. British Journal of Radiology, vol. 63, no. 755, 1990, pp. 882-883

40. Precise Treatment System Corrective Maintenance Manual. Linac House, Crawley, West Sussex, UK: Elekta Limited, 2003

41. ProtoCAM (2002) Selective Laser Sintering Available from: <http://www.protocam.com/html/sls.html> [Accessed 19 May 2005]

42. Purdy, J.A. & Choi, C. Lipowitz metal shielding thickness for dose reduction of 6-20 MeV electrons. Medical Physics, vol. 7, no. 3, 1980, pp. 251-253

43. Reade Advanced Materials (1997) Wood's metal alloy Available from: <http://www.reade.com/Products/Alloys/wood's_metal.html> [Accessed 4 June 2004]

44. Rippey, J.J. General Pathology. Pretoria: Witwatersrand University Press, 1994

45. Siemens AG, Medical solutions (2006) Computed Tomography History and Technology Available from: <http://www.scribd.com/doc/3986451/Computed-Tomography-History-and-Technology-MIND-4561699-2> [Accessed 8 March 2007]

46. Smith, P.B. Irregular-shaped fields in electron radiation. British Journal of Radiology, vol. 64, no. 762, 1991, p. 561

47. Souhami, R.L. & Tobias, J. Cancer and its Management. 2nd. Edition. Oxford: Blackwell Science Ltd, 1995

48. Spiritus Temporis (2003) Cerrobend Available from: <http://www.spiritus-temporis.com/cerrobend> [Accessed 4 June 2004]

49. Tobias, J.S. & Thomas, P.R.M. Current Radiation Oncology. vol. 1, London: Edward Arnold, 1994

50. Underwood, J.C.E. General and Systematic Pathology. 4th. Edition. Sheffield: Elsevier Limited, 2004

51. Walter, J. Cancer and Radiotherapy. 2nd. Edition. Edinburgh: Churchhill Livingstone, 1977

52. Wohlers, T.T. Wohlers Report 2004. Colorado: Wohlers associates, 2004

ADDENDUM A1

ISODENSITY CHARTS

Arbitrary field shape

Printing scale: 1:1.92

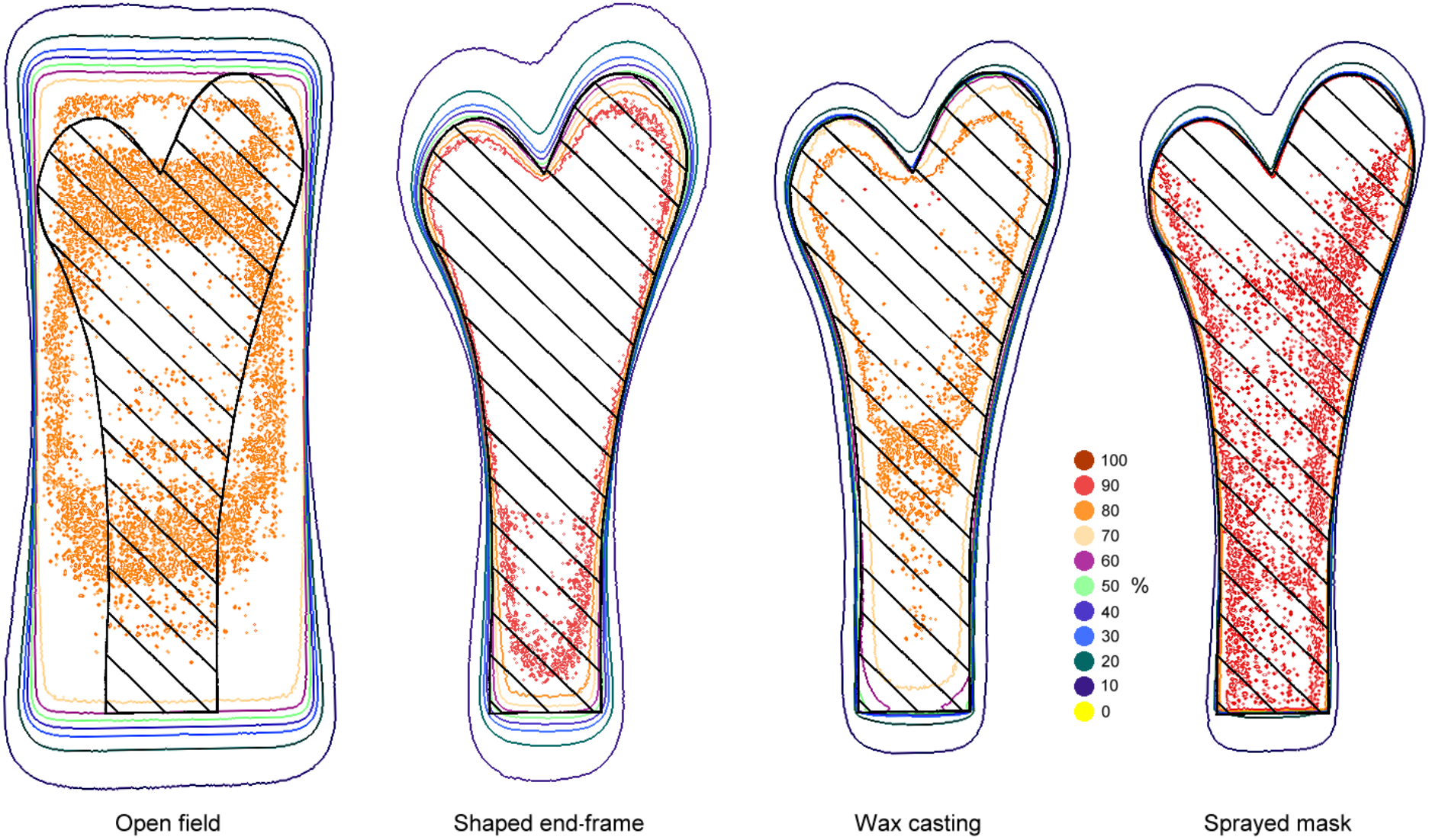

A1.1 Arbitrary field shape isodensity curves 4 MeV (Surface)

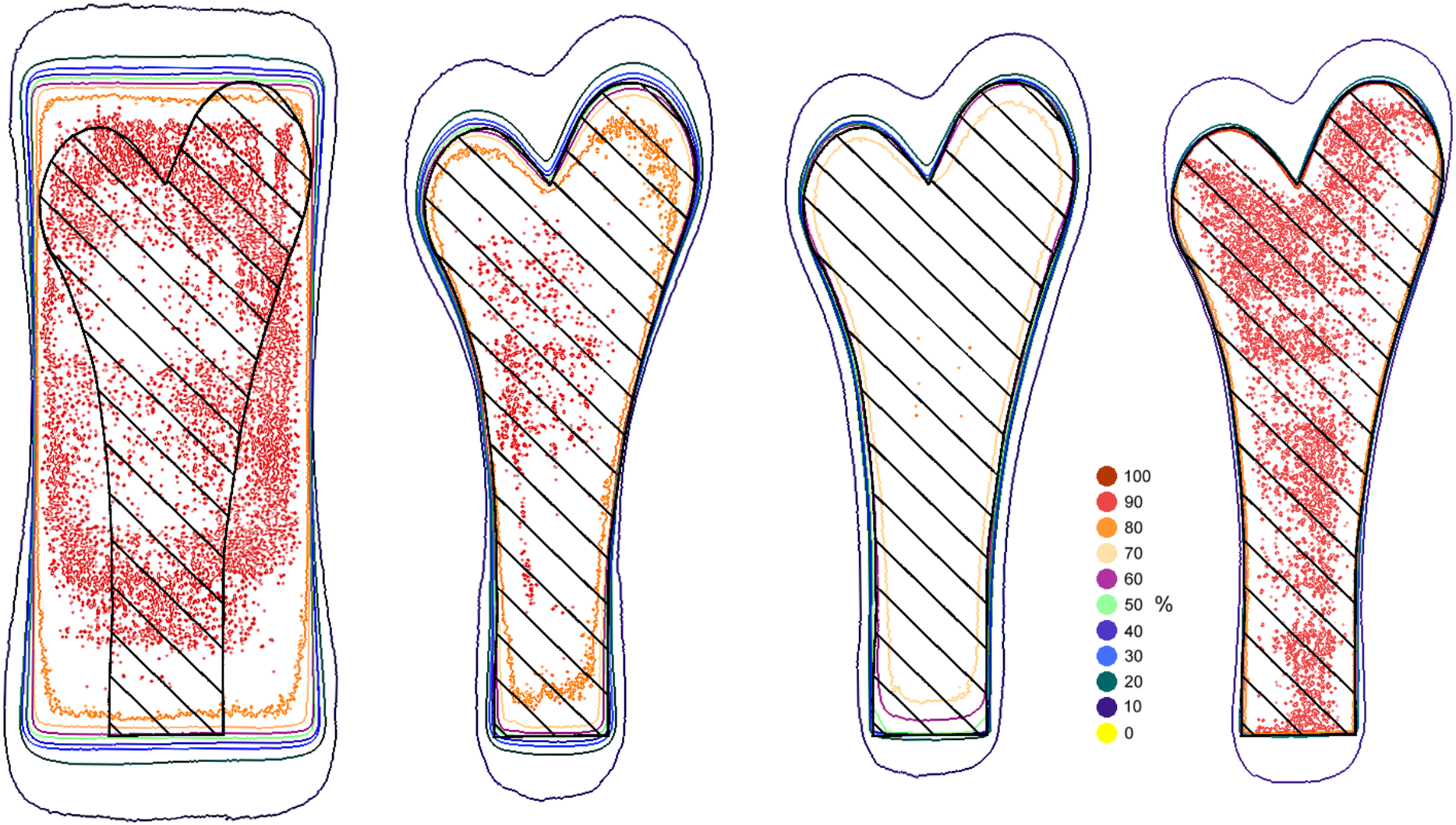

A1.2 Arbitrary field shape isodensity curves 6 MeV (Surface)

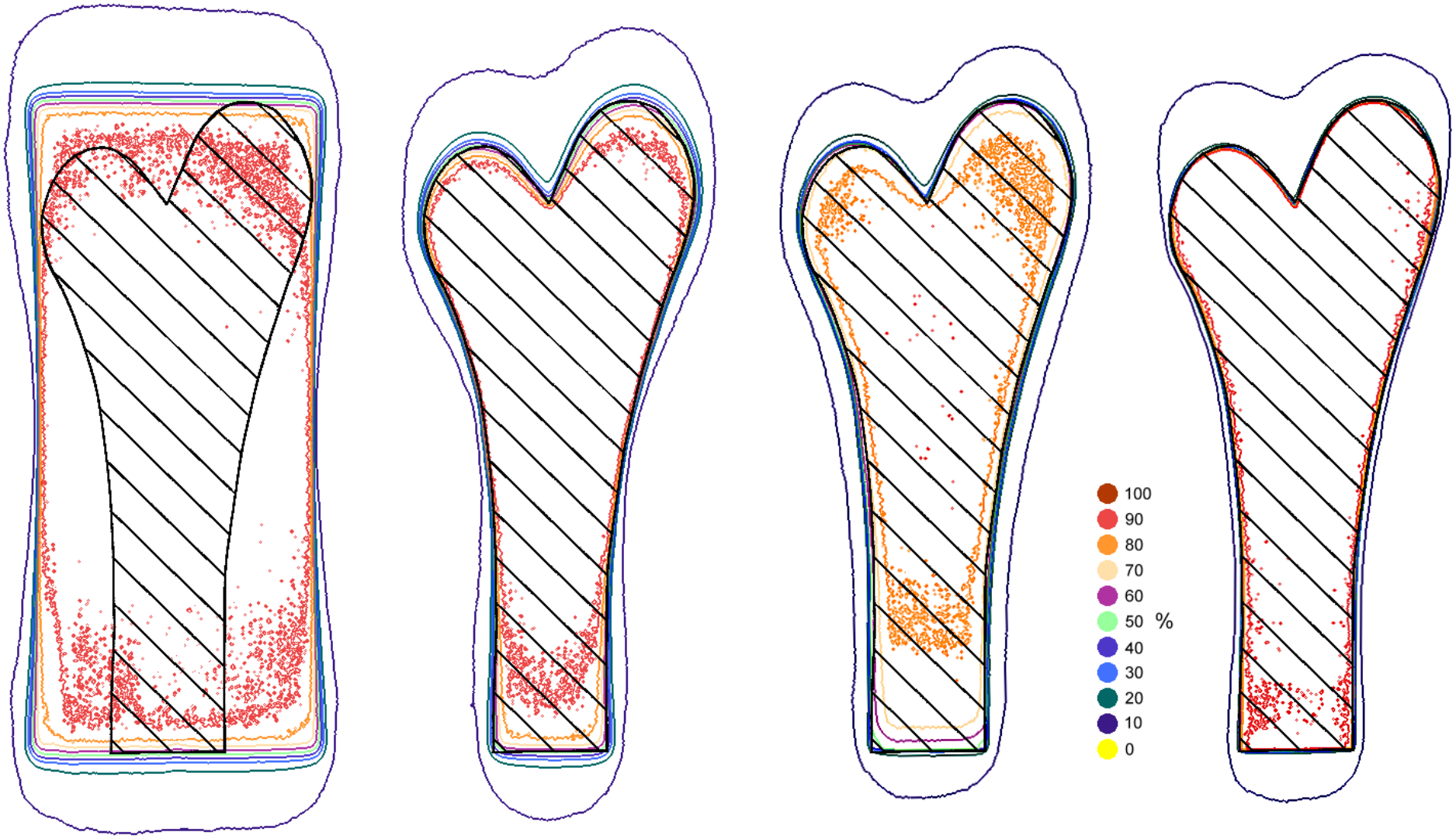

A1.3 Arbitrary field shape isodensity curves 8 MeV (Surface)

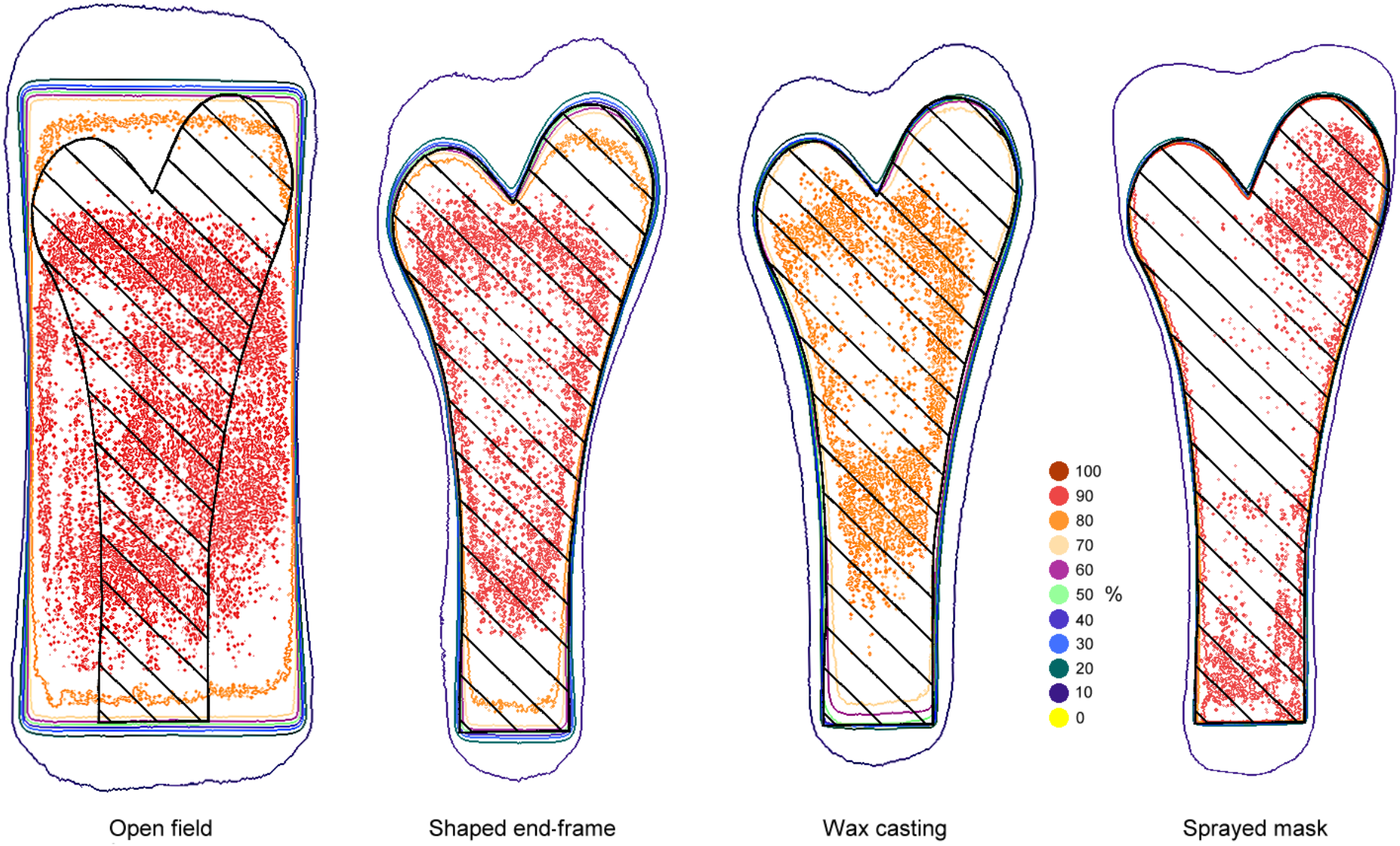

A1.4 Arbitrary field shape isodensity curves 10 MeV (Surface)

ADDENDUM A2

ISODENSITY CHARTS

20 x 10 cm² field

Printing scale: Surface charts: 1:2.1
Cross-sectional charts: 1:1.9

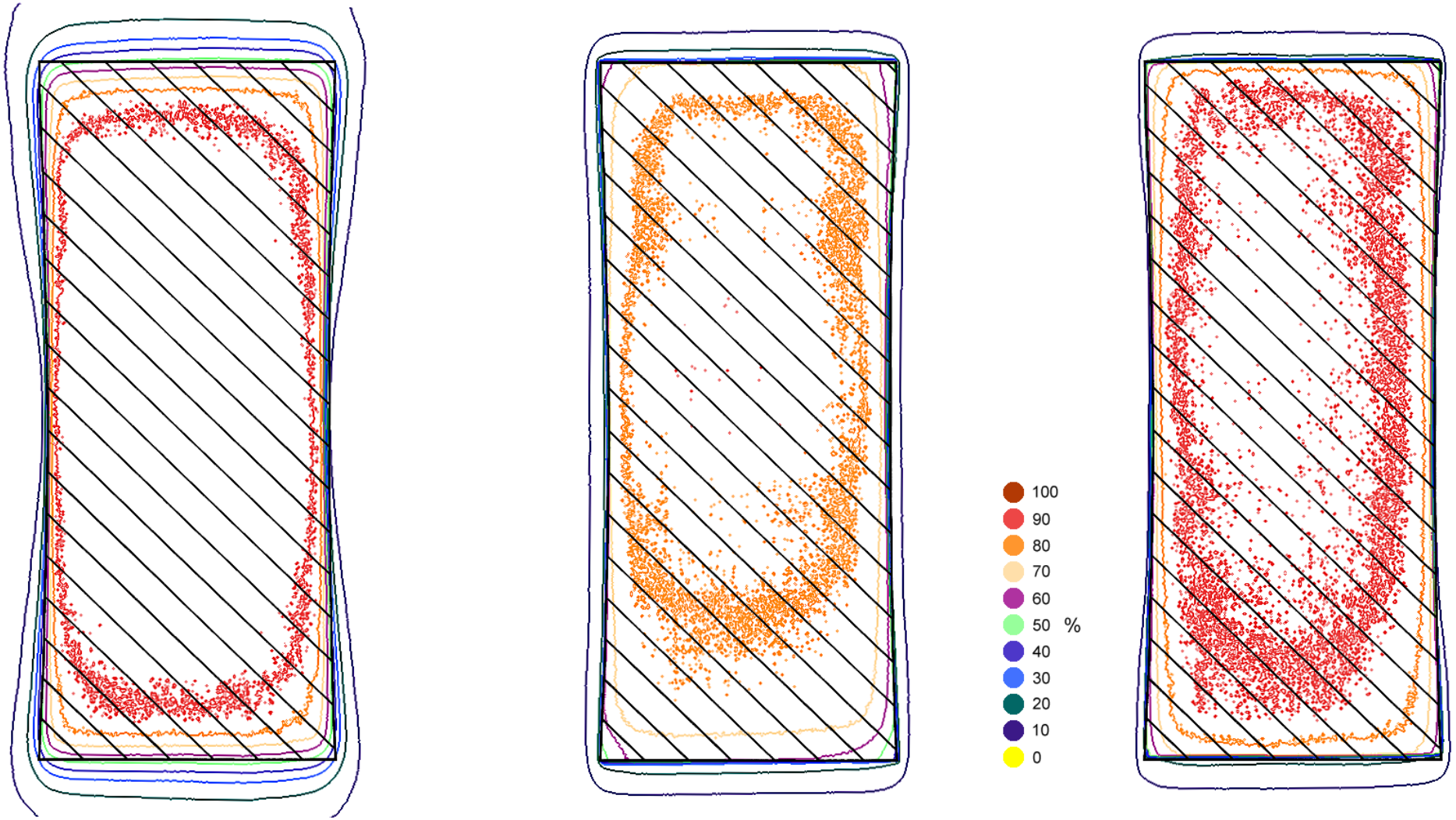

A2.1.1 20 x 10 cm² field isodensity curves 4 MeV (Surface)

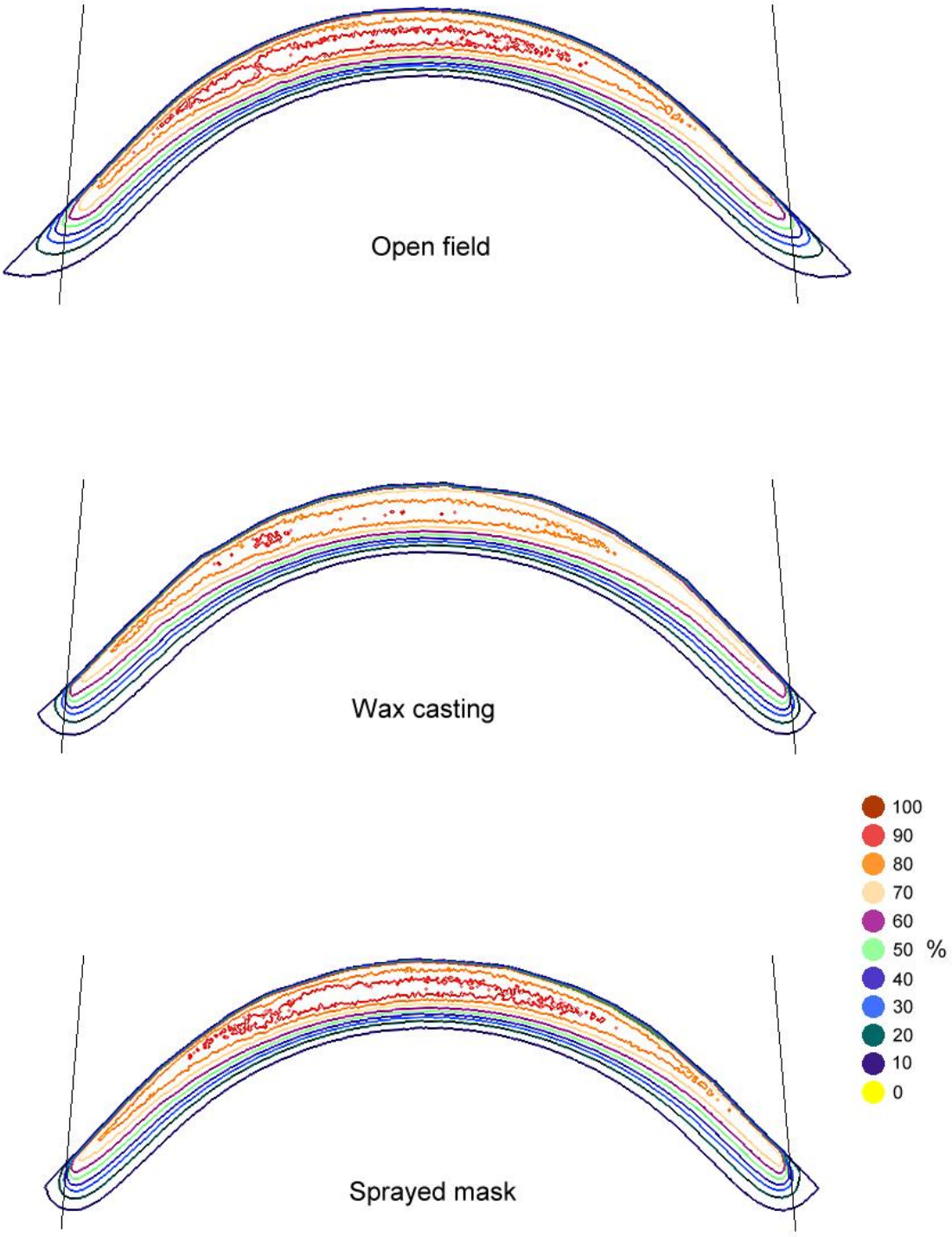

A2.1.2 20 x 10 cm² field isodensity curves 4 MeV (Cross-section)

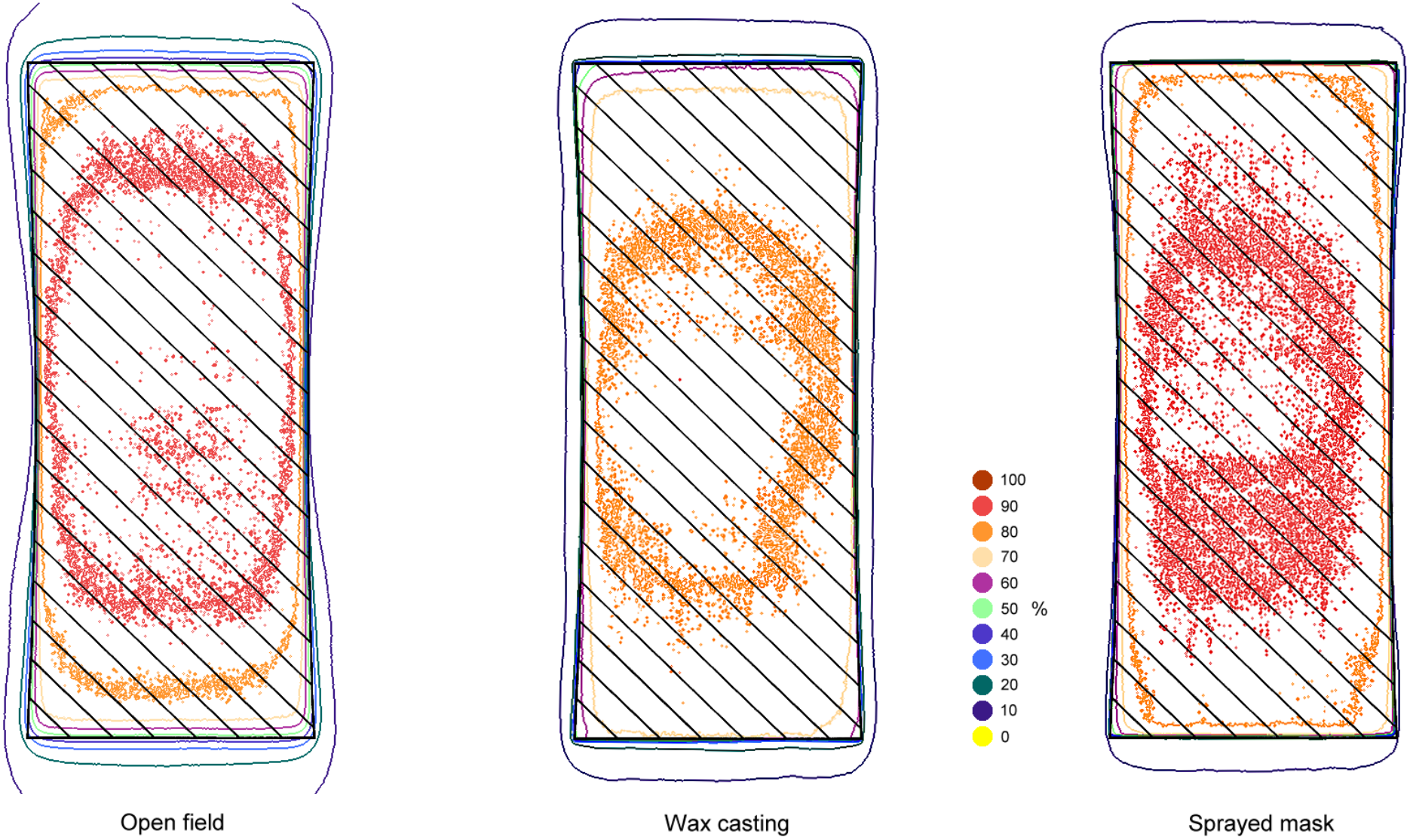

A2.2.1 20 x 10 cm² field isodensity curves 6 MeV (Surface)

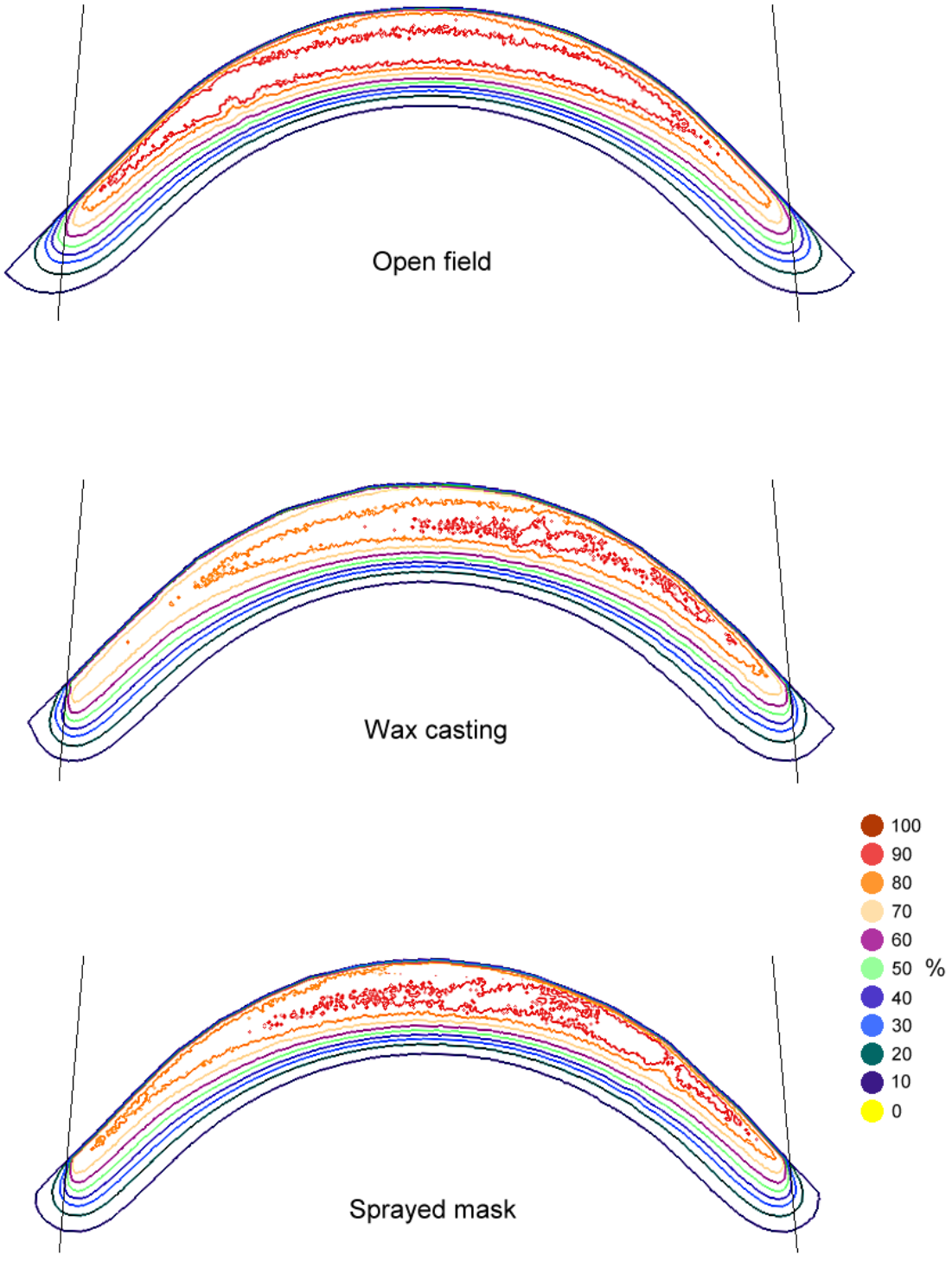

A2.2.2 20 x 10 cm² field isodensity curves 6 MeV (Cross-section)

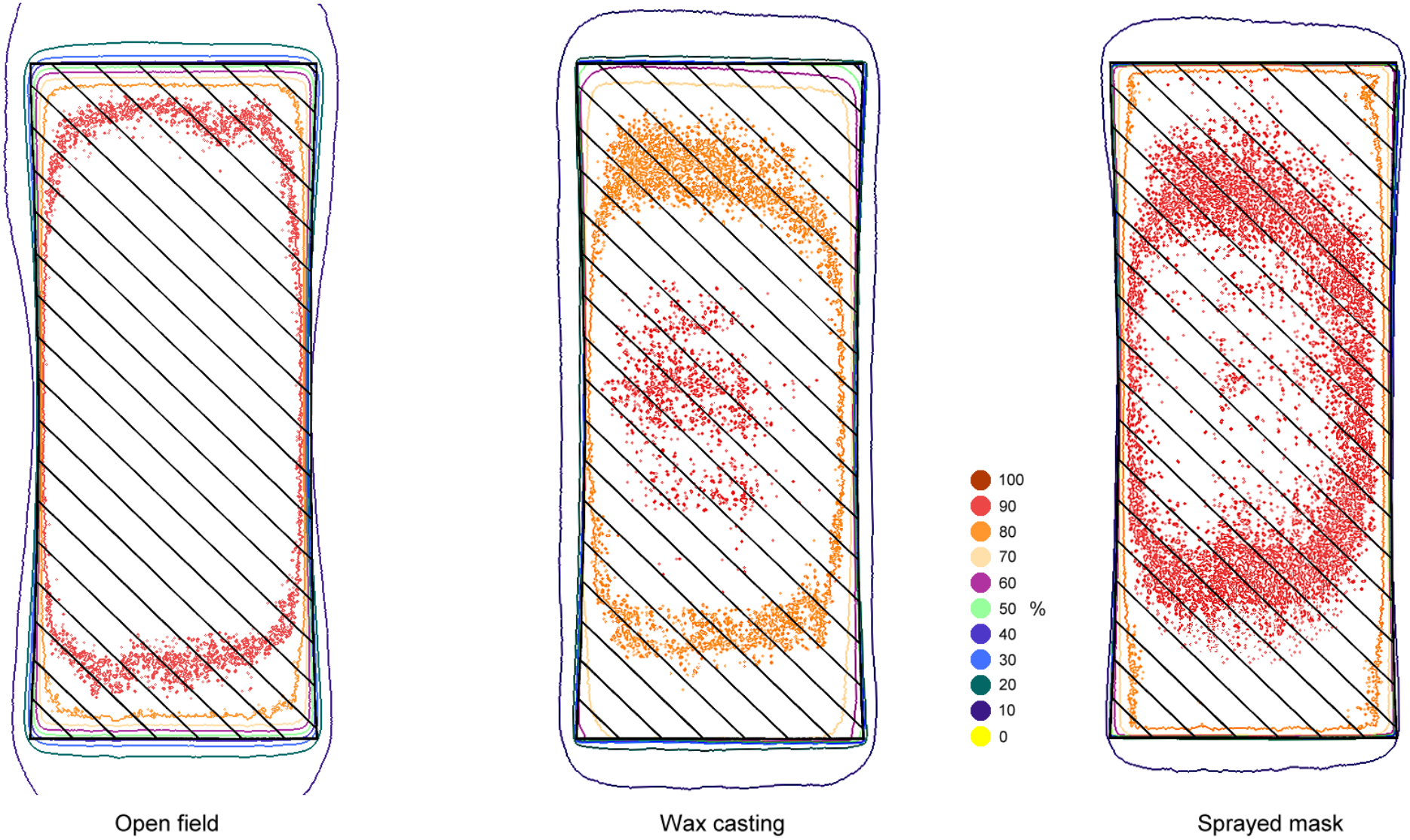

A2.3.1 20 x 10 cm² field isodensity curves 8 MeV (Surface)

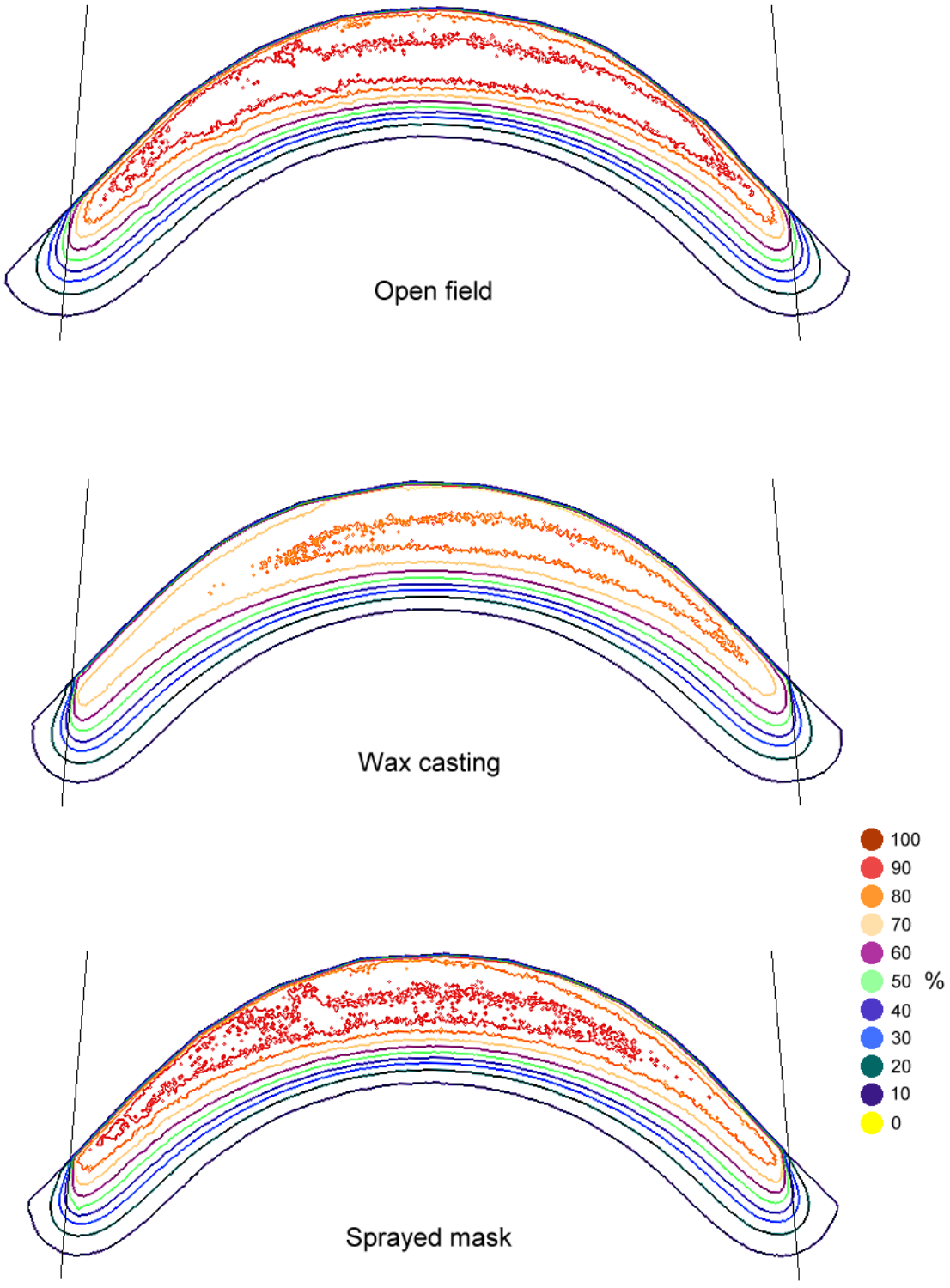

A2.3.2 20 x 10 cm² field isodensity curves 8 MeV (Cross-section)

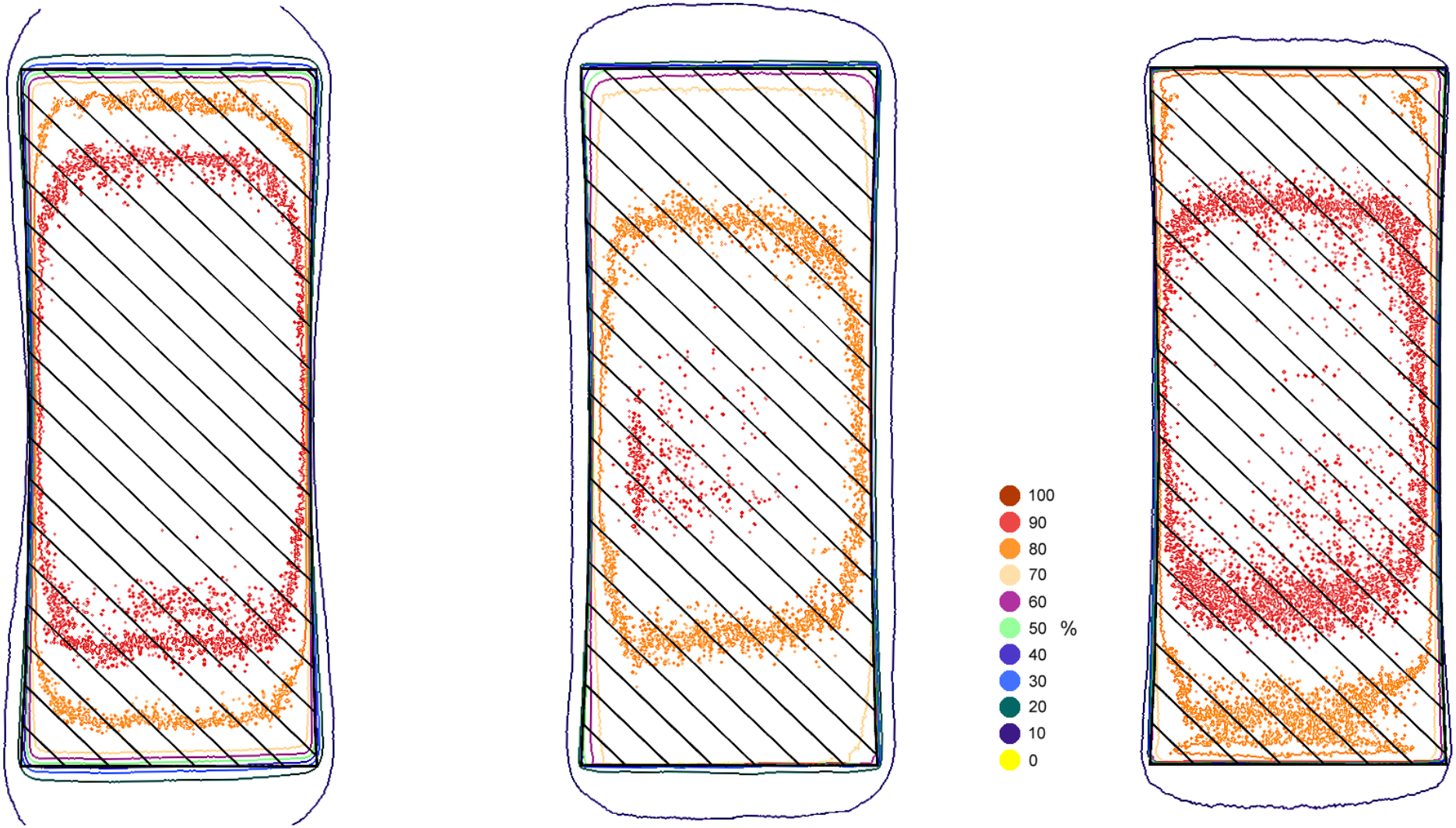

A2.4.1 20 x 10 cm² field isodensity curves 10 MeV (Surface)

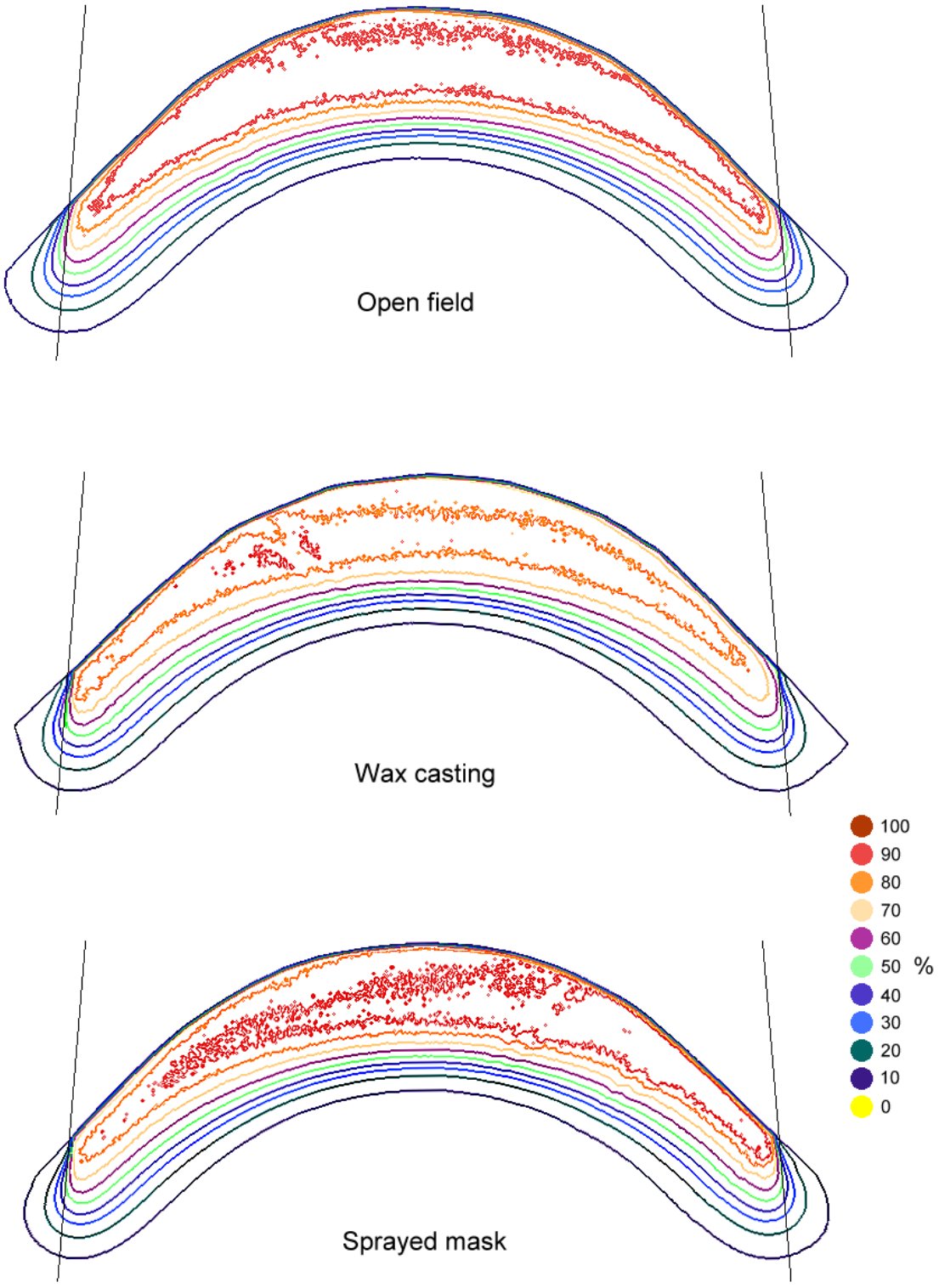

A2.4.2 20 x 10 cm² field isodensity curves 10 MeV (Cross-section)

ADDENDUM A3

ISODENSITY CHARTS

Rotational electron beam field

Printing scale: Surface charts: 1:2.1
Cross-sectional charts: 1:1.9

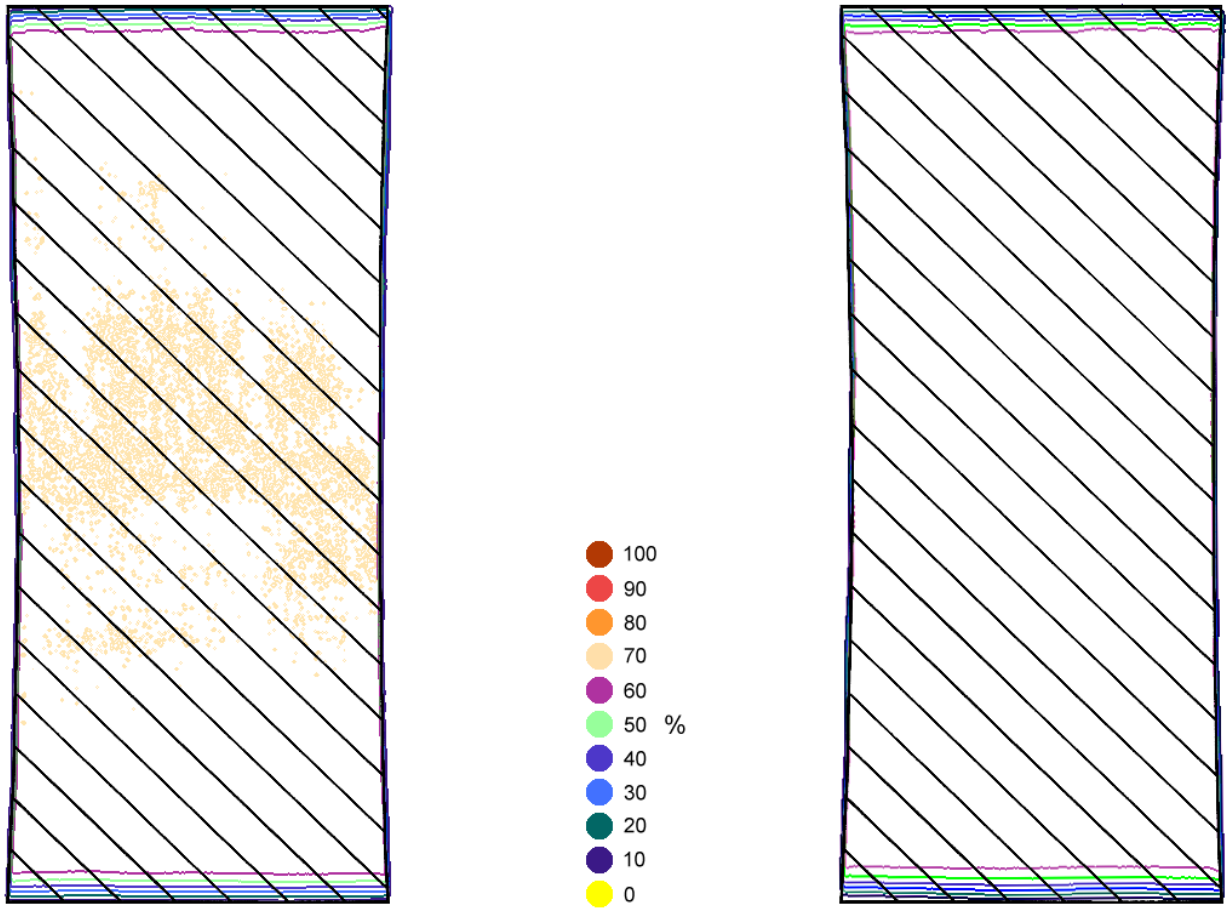

A3.1.1 20 x 10 cm² field isodensity curves (Electron arc surface)

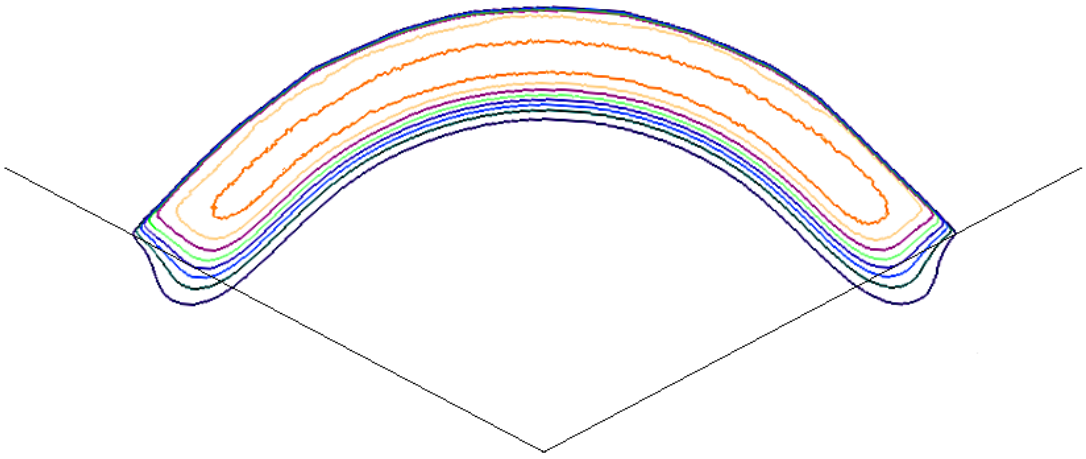

6 MeV

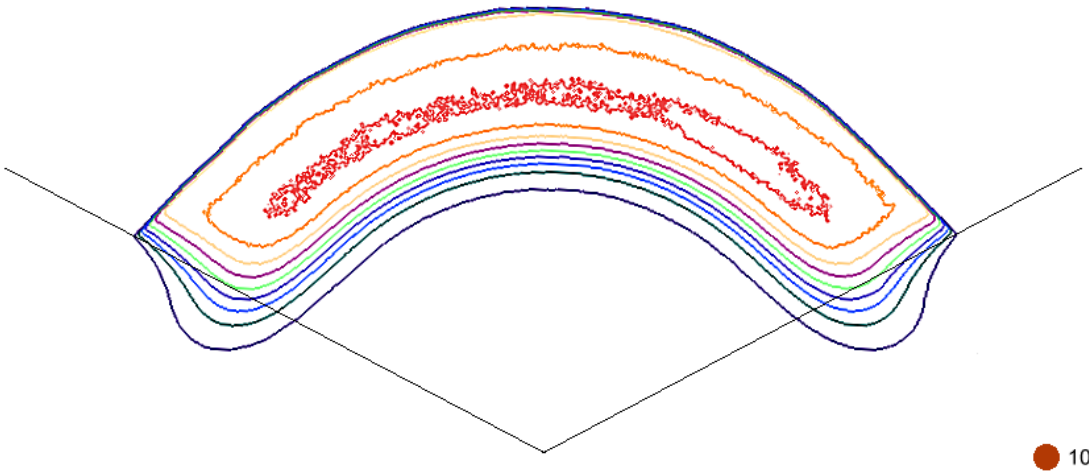

10 MeV

A3.1.2 20 x 10 cm² field isodensity curves (Electron arc cross-section)

ADDENDUM B1

REQUIRED THICKNESS OF THERMAL-SPRAYED MASKS

Transmission ionization measurements

B1.1.1 Measurements at 4 MeV, 10 x 10 cm² Field size, Skin dose

mm alloy	measured ionization	% of open field
0	2027	100.0
1	1313	64.78
2	101.5	5.007
3	21.38	1.055
4	17.96	0.886
5	16.12	0.795

B1.1.2 Measurements at 6 MeV, 10 x 10 cm² Field size, Skin dose

mm alloy	measured ionization	% of open field
0	2109	100.0
1	2379	112.8
2	746.1	35.38
3	141.9	6.728
4	39.62	1.879
5	33.76	1.601
6	31.00	1.470

B1.1.3 Measurements at 8 MeV, 10 x 10 cm² Field size, Skin dose

mm alloy	measured ionization	% of open field
0	2246	100.0
1	2847	126.8
2	1476	65.72
3	523.1	23.29
4	122.7	5.463
5	67.56	3.008
6	60.54	2.695
7	55.08	2.452
8	51.60	2.297

B1.1.4 Measurements at 10 MeV, 10 x 10 cm² Field size, Skin dose

mm alloy	measured ionization	% of open field
0	2294	100.0
1	3015	131.4
2	2113	92.11
3	1053	45.90
4	325.5	14.19
5	117.9	5.139
6	80.68	3.517
7	70.54	3.075
8	65.90	2.873
9	61.56	2.684
10	57.48	2.506

B1.1.5 Measurements at 12 MeV, 10 x 10 cm² Field size, Skin dose

mm alloy	measured ionization	% of open field
0	2385	100.0
1	3021	126.7
2	2676	112.2
3	1737	72.83
4	792.3	33.22
5	329.3	13.81
6	171.9	7.208
7	119.7	5.019
8	107.8	4.520
9	100.7	4.222
10	93.96	3.940
11	89.22	3.741
12	83.92	3.519
13	79.90	3.350
14	74.76	3.135
15	70.58	2.959
16	67.26	2.820

B1.1.6 Measurements at 15 MeV, 10 x 10 cm² Field size, Skin dose

mm alloy	measured ionization	% of open field
0	2515	100.0
1	3001	119.3
2	3046	121.1
3	2416	96.06
4	1470	58.45
5	799.0	31.77
6	451.7	17.96
7	257.2	10.23
8	200.0	7.952
9	177.8	7.070
10	164.3	6.533
11	156.8	6.235
12	148.2	5.893
13	140.8	5.598
14	132.6	5.272
15	126.4	5.026
16	120.4	4.787
17	113.8	4.525
18	108.5	4.314
19	103.8	4.127
20	99.44	3.954

B1.1.7 Measurements at 18 MeV, 10 x 10 cm² Field size, Skin dose

mm alloy	measured ionization	% of open field
0	2616	100.0
1	2964	113.3
2	3188	121.9
3	2891	110.5
4	2133	81.54
5	1404	53.67
6	903.0	34.52
7	521.5	19.94
8	362.4	13.85
9	277.7	10.62
10	238.6	9.121
11	221.9	8.482
12	208.9	7.985
13	198.9	7.603
14	187.5	7.167
15	178.4	6.820
16	170.2	6.506
17	161.2	6.162
18	154.2	5.894
19	146.9	5.615
20	140.6	5.375
21	136.3	5.210
22	130.2	4.977
23	124.9	4.774
24	118.6	4.534
25	113.4	4.335
26	108.5	4.148

B1.1.8 Measurements at 20 MeV, 10 x 10 cm² Field size, Skin dose

mm alloy	measured ionization	% of open field
0	2622	100.0
1	2921	111.4
2	3160	120.5
3	2987	113.9
4	2355	89.82
5	1669	63.65
6	1183	45.12
7	731.3	27.89
8	507.8	19.37
9	374.7	14.29
10	307.0	11.71
11	279.6	10.66
12	261.3	9.966
13	248.3	9.470
14	234.3	8.936
15	222.5	8.486
16	213.1	8.127
17	202.1	7.708
18	193.0	7.361
19	184.0	7.018
20	179.0	6.827
21	171.6	6.545
22	163.8	6.247
23	157.2	5.995
24	149.4	5.698
25	142.4	5.431
26	137.0	5.225
27	130.3	4.969
28	125.0	4.767
29	119.2	4.546
30	114.5	4.367

B1.2.1 Measurements at 4 MeV 10 x 10 cm² Field size, D_{max}

mm alloy	measured ionization	% of open field
0	2480	100.0
1	411.0	16.57
2	22.52	0.908
3	18.70	0.754
4	17.16	0.692

B1.2.2 Measurements at 6 MeV, 10 x 10 cm² Field size, D_{max}

mm alloy	measured ionization	% of open field
0	2391	100.0
1	1538	64.32
2	253.6	10.61
3	51.46	2.152
4	35.84	1.499
5	32.78	1.371

B1.2.3 Measurements at 8 MeV, 10 x 10 cm² Field size, D_{max}

mm alloy	measured ionization	% of open field
0	2520	100.0
1	1249	49.56
2	264.7	10.50
3	80.90	3.210
4	59.42	2.358
5	56.04	2.224
6	52.48	2.083

B1.2.4 Measurements at 10 MeV, 10 x 10 cm² Field size, D_{max}

mm alloy	measured ionization	% of open field
0	2549	100.0
1	1565	61.40
2	454.6	17.83
3	137.9	5.410
4	71.56	2.807
5	63.68	2.498
6	59.72	2.343
7	56.72	2.225

B1.2.5 Measurements at 12 MeV, 10 x 10 cm² Field size, D_{max}

mm alloy	measured ionization	% of open field
0	2573	100.0
1	2199	85.46
2	1064	41.35
3	462.9	17.99
4	181.1	7.038
5	108.1	4.201
6	93.92	3.650
7	89.28	3.470
8	84.46	3.283
9	80.00	3.109

B1.2.6 Measurements at 15 MeV, 10 x 10 cm² Field size, D_{max}

mm alloy	measured ionization	% of open field
0	2651	100.0
1	2600	98.08
2	1802	67.97
3	1090	41.12
4	551.5	20.80
5	283.5	10.69
6	188.8	7.122
7	155.2	5.854
8	144.0	5.432
9	135.3	5.104
10	127.5	4.810
11	122.1	4.606
12	115.7	4.364
13	111.0	4.187

B1.2.7 Measurements at 18 MeV, 10 x 10 cm² Field size, D_{max}

mm alloy	measured ionization	% of open field
0	2715	100.0
1	2767	101.9
2	2308	85.01
3	1691	62.28
4	1055	38.86
5	607.6	22.38
6	376.5	13.87
7	254.6	9.378
8	207.7	7.650
9	184.8	6.807
10	172.4	6.350
11	164.9	6.074
12	156.1	5.750
13	149.6	5.510
14	142.5	5.249
15	136.3	5.020
16	130.1	4.792
17	124.8	4.597
18	119.4	4.398
19	114.8	4.228
20	110.2	4.059

B1.2.8 Measurements at 20 MeV, 10 x 10 cm² Field size, D_{max}

mm alloy	measured ionization	% of open field
0	2733	100.0
1	2770	101.4
2	2468	90.30
3	1953	71.46
4	1339	48.99
5	838.5	30.68
6	541.3	19.81
7	359.1	13.14
8	276.4	10.11
9	232.8	8.518
10	213.7	7.819
11	203.5	7.446
12	193.0	7.062
13	184.6	6.754
14	176.2	6.447
15	168.6	6.169
16	160.9	5.887
17	154.3	5.646
18	147.7	5.404
19	142.2	5.203
20	136.7	5.002
21	130.8	4.786
22	124.8	4.566
23	119.8	4.383
24	114.7	4.197

B1.3.1 Measurements at 4 MeV, 20 x 20 cm² Field size, Skin dose

mm alloy	measured ionization	% of open field
0	2130	100.0
1	1393	65.40
2	77.10	3.620
3	22.36	1.050
4	19.04	0.894
5	16.88	0.792

B1.3.2 Measurements at 6 MeV, 20 x 20 cm² Field size, Skin dose

mm alloy	measured ionization	% of open field
0	2129	100.0
1	2480	116.5
2	663.8	31.18
3	121.5	5.707
4	41.94	1.970
5	35.18	1.652
6	32.48	1.526

B1.3.3 Measurements at 8 MeV, 20 x 20 cm² Field size, Skin dose

mm alloy	measured ionization	% of open field
0	2235	100.0
1	2915	130.4
2	1389	62.15
3	473.3	21.18
4	126.6	5.664
5	68.26	3.054
6	61.62	2.757
7	57.20	2.559
8	54.40	2.434

B1.3.4 Measurements at 10 MeV, 20 x 20 cm² Field size, Skin dose

mm alloy	measured ionization	% of open field
0	2180	100.0
1	2992	137.2
2	1999	91.70
3	959.9	44.03
4	324.9	14.90
5	117.3	5.381
6	79.48	3.646
7	70.52	3.235
8	65.30	2.995
9	60.52	2.776
10	56.18	2.577

B1.3.5 Measurements at 12 MeV, 20 x 20 cm² Field size, Skin dose

mm alloy	measured ionization	% of open field
0	2294	100.0
1	3020	131.6
2	2605	113.6
3	1657	72.23
4	799.8	34.86
5	331.7	14.46
6	173.8	7.576
7	122.1	5.323
8	109.0	4.752
9	99.82	4.351
10	93.62	4.081
11	88.26	3.847
12	82.02	3.575

B1.3.6 Measurements at 15 MeV, 20 x 20 cm² Field size, Skin dose

mm alloy	measured ionization	% of open field
0	2407	100.0
1	2983	123.9
2	3028	125.8
3	2366	98.30
4	1497	62.19
5	825.6	34.30
6	465.5	19.34
7	276.2	11.47
8	207.4	8.617
9	177.8	7.387
10	164.6	6.838
11	156.0	6.481
12	146.5	6.086
13	138.7	5.762
14	131.6	5.467
15	125.9	5.231
16	120.1	4.990
17	114.8	4.769
18	109.4	4.545
19	105.3	4.375
20	101.1	4.200

B1.3.7 Measurements at 18 MeV, 20 x 20 cm² Field size, Skin dose

mm alloy	measured ionization	% of open field
0	2464	100.0
1	2918	118.4
2	3181	129.1
3	2853	115.8
4	2145	87.05
5	1410	57.22
6	907.1	36.81
7	551.3	22.37
8	373.7	15.17
9	273.7	11.11
10	234.3	9.509
11	218.4	8.864
12	203.5	8.259
13	194.0	7.873
14	183.9	7.463
15	174.4	7.078
16	167.2	6.786
17	159.7	6.481
18	152.2	6.177
19	146.3	5.938
20	140.3	5.694
21	133.9	5.434
22	127.5	5.175
23	122.2	4.959
24	116.9	4.744
25	111.9	4.541
26	106.9	4.338

B1.3.8 Measurements at 20 MeV, 20 x 20 cm² Field size, Skin dose

mm alloy	measured ionization	% of open field
0	2493	100.0
1	2889	115.9
2	3183	127.7
3	2996	120.2
4	2424	97.23
5	1727	69.27
6	1195	47.93
7	769.9	30.88
8	529.9	21.26
9	373.6	14.99
10	305.6	12.26
11	278.0	11.15
12	256.7	10.30
13	244.1	9.791
14	232.3	9.318
15	220.4	8.841
16	210.9	8.460
17	201.6	8.087
18	192.2	7.710
19	181.5	7.280
20	177.8	7.132
21	169.9	6.815
22	161.9	6.494
23	155.0	6.217
24	148.1	5.941
25	141.8	5.688
26	135.4	5.431
27	129.9	5.211
28	124.3	4.986
29	118.8	4.765
30	113.2	4.541

B1.4.1 Measurements at 4 MeV, 20 x 20 cm² Field size, D_{max}

mm alloy	measured ionization	% of open field
0	2594	100.0
1	417.6	16.10
2	24.76	0.955
3	20.38	0.786
4	18.28	0.705

B1.4.2 Measurements at 6MeV, 20 x 20 cm² Field size, D_{max}

mm alloy	measured ionization	% of open field
0	2417	100.0
1	1556	64.38
2	266.0	11.01
3	53.98	2.233
4	37.68	1.559
5	34.64	1.433

B1.4.3 Measurements at 8 MeV, 20 x 20 cm² Field size, D_{max}

mm alloy	measured ionization	% of open field
0	2550	100.0
1	1269	49.76
2	274.4	10.76
3	86.98	3.411
4	63.36	2.485
5	58.46	2.293
6	55.14	2.162

B1.4.4 Measurements at 10 MeV, 20 x 20 cm² Field size, D_{max}

mm alloy	measured ionization	% of open field
0	2482	100.0
1	1539	62.01
2	454.4	18.31
3	144.0	5.802
4	74.14	2.987
5	66.94	2.697
6	62.92	2.535
7	59.08	2.380

B1.4.5 Measurements at 12 MeV, 20 x 20 cm² Field size, D_{max}

mm alloy	measured ionization	% of open field
0	2507	100.0
1	2176	86.80
2	1075	42.88
3	472.5	18.85
4	188.1	7.503
5	113.8	4.539
6	99.98	3.988
7	93.60	3.734
8	88.64	3.536
9	83.48	3.330

B1.4.6 Measurements at 15 MeV, 20 x 20 cm² Field size, D_{max}

mm alloy	measured ionization	% of open field
0	2567	100.0
1	2560	99.73
2	1795	69.93
3	1092	42.54
4	554.9	21.62
5	288.2	11.23
6	193.2	7.526
7	159.7	6.221
8	148.1	5.769
9	139.6	5.438
10	131.9	5.138
11	126.0	4.908
12	119.7	4.663
13	114.3	4.453

B1.4.7 Measurements at 18 MeV, 20 x 20 cm² Field size, D_{max}

mm alloy	measured ionization	% of open field
0	2604	100.0
1	2708	104.0
2	2300	88.33
3	1688	64.82
4	1051	40.36
5	611.3	23.48
6	379.1	14.56
7	258.9	9.942
8	211.4	8.118
9	188.8	7.250
10	176.3	6.770
11	168.4	6.467
12	159.1	6.110
13	152.7	5.864
14	145.1	5.572
15	139.1	5.342
16	133.0	5.108
17	127.2	4.885
18	121.4	4.662
19	117.2	4.501
20	112.9	4.336

B1.4.8 Measurements at 20 MeV, 20 x 20 cm² Field size, D_{max}

mm alloy	measured ionization	% of open field
0	2623	100
1	2729	104.0
2	2468	94.09
3	1944	74.11
4	1339	51.05
5	837.5	31.93
6	545.6	20.80
7	361.5	13.78
8	281.1	10.72
9	237.4	9.051
10	218.5	8.330
11	207.0	7.892
12	196.5	7.491
13	187.7	7.156
14	179.7	6.851
15	171.7	6.546
16	163.7	6.241
17	157.1	5.989
18	150.4	5.734
19	144.9	5.524
20	139.4	5.315
21	133.7	5.097
22	127.9	4.876
23	122.7	4.678
24	117.5	4.480

B1.5.1 Measurements at 100 kV, 10 x 8 cm² Field size

mm alloy	measured ionization	% of open field
0	1740	100.0
1	22.11	0.892
2	0.940	0.038

B1.5.2 Measurements at 100 kV, 15 x 10 cm² Field size

mm alloy	measured ionization	% of open field
0	1708	100.0
1	22.52	0.942
2	0.960	0.040

B1.6.1 Measurements at 250 kV, 10 x 8 cm² Field size

mm alloy	measured ionization	% of open field
0	871.1	100.0
1	238.8	9.476
2	76.28	3.027
3	35.39	1.404
4	16.48	0.654
5	8.460	0.336
6	4.000	0.159

B1.6.2 Measurements at 250 kV, 15 x 10 cm² Field size

mm alloy	measured ionization	% of open field
0	787.6	100.0
1	240.5	9.433
2	76.09	2.985
3	35.68	1.400
4	16.73	0.656
5	8.490	0.333
6	4.040	0.158

ADDENDUM B2

REQUIRED THICKNESS OF THERMAL-SPRAYED MASKS

Percentage transmission curves

B2.1 Thickness of sprayed Wood's alloy required for shielding electrons
Measurement depth: Skin level, 10 x 10 cm^2 Field size

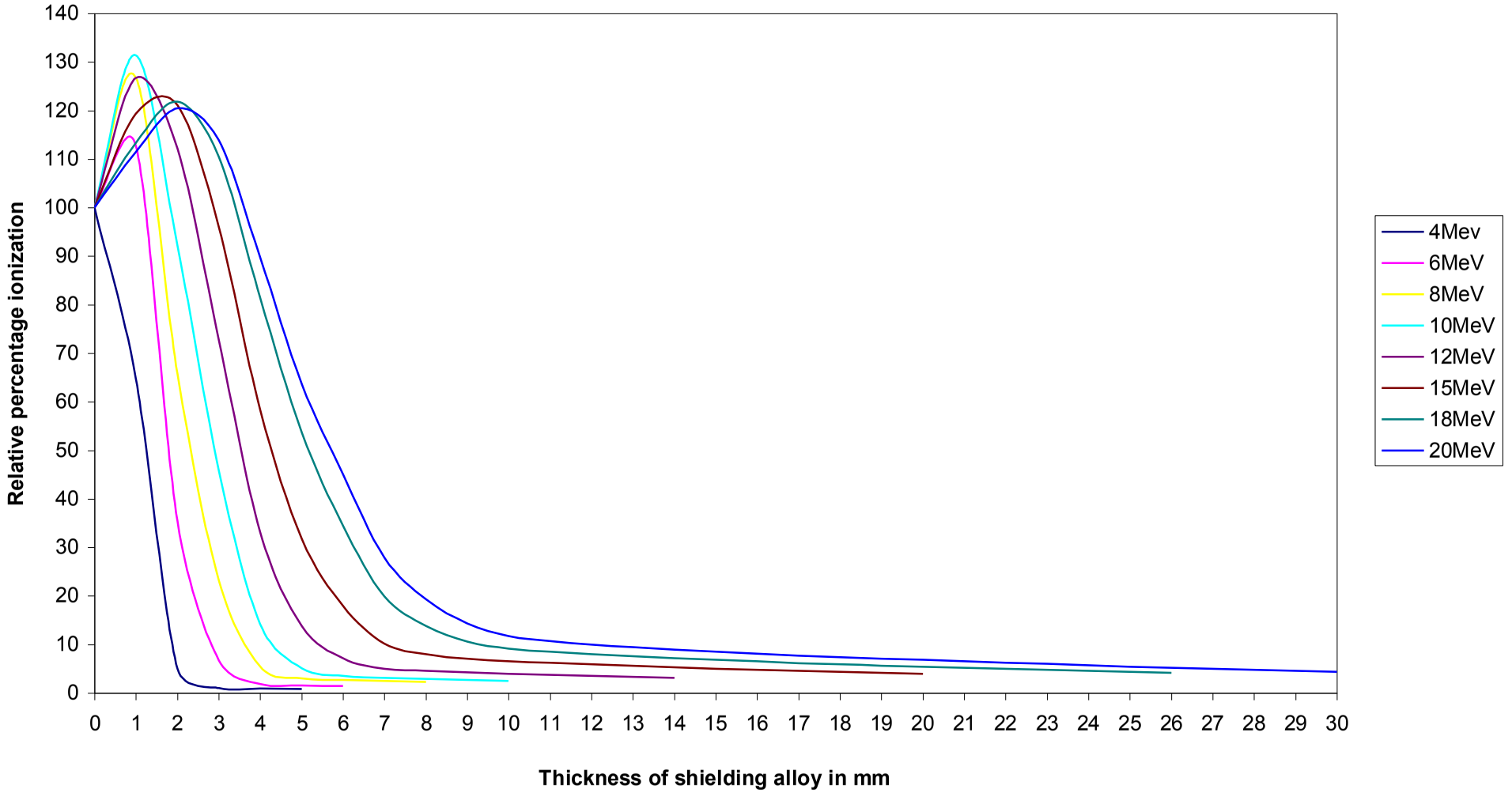

B2.2 Thickness of sprayed Wood's alloy required for shielding electrons
Measurement depth: D_{max}, 10 x 10 cm^2 Field size

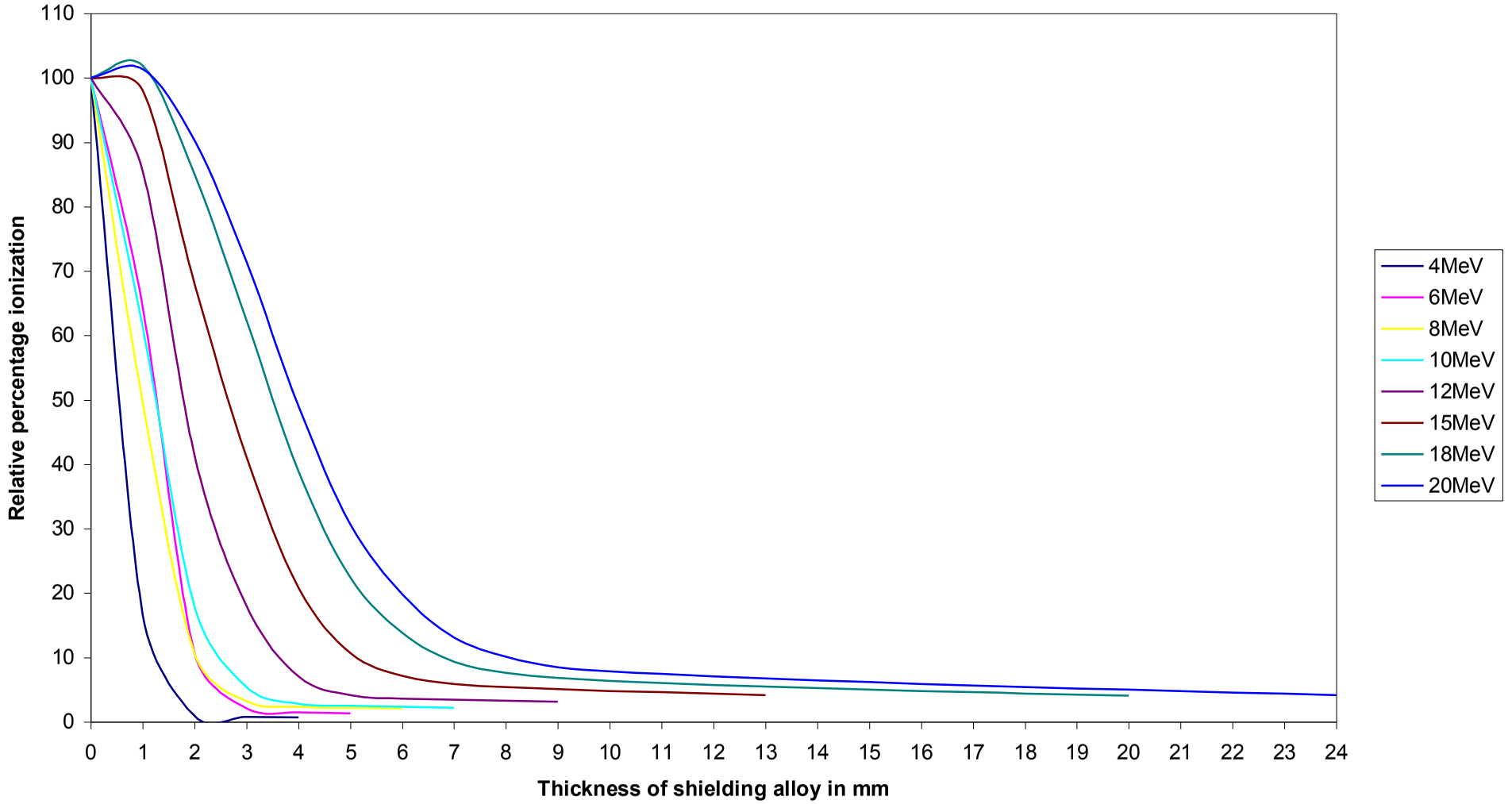

B2.3 Thickness of sprayed Wood's alloy required for shielding electrons
Measurement depth: Skin level, 20 x 20 cm^2 Field size

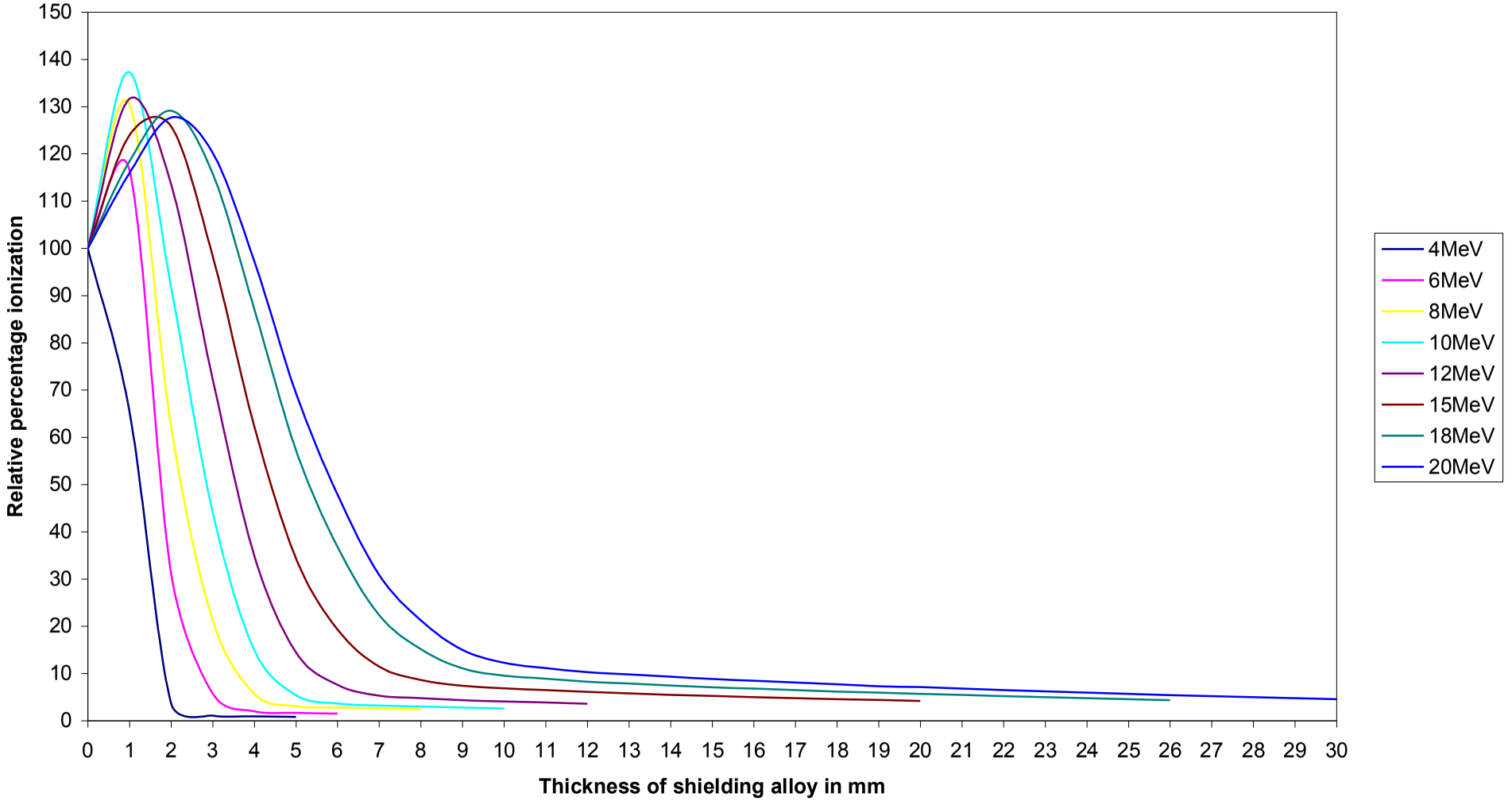

B2.4 Thickness of sprayed Wood's alloy required for shielding electrons

Measurement level: D_{max}, 20 x 20 cm^2 Field size

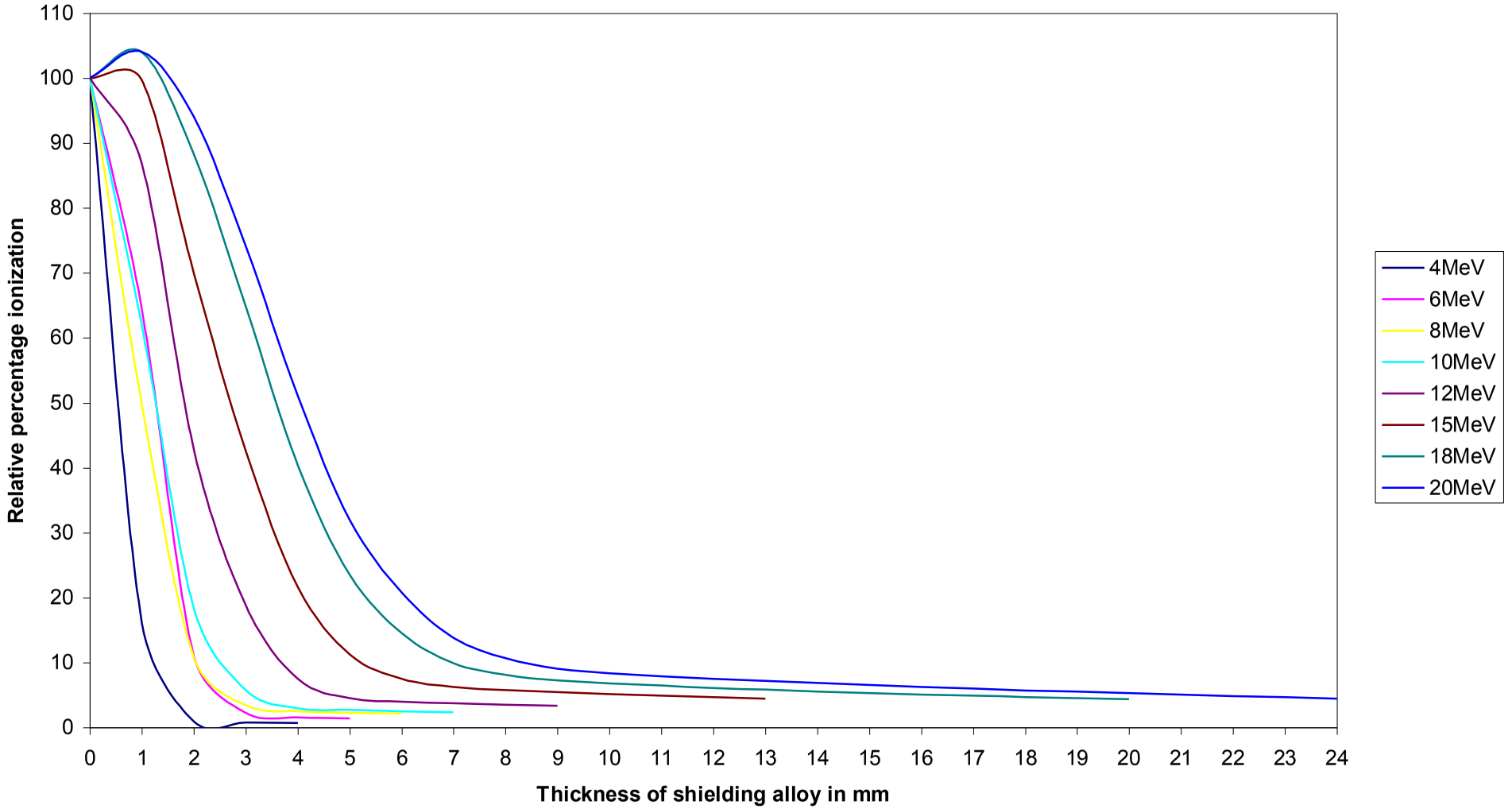

B2.5 Thickness of sprayed Wood's alloy required for shielding low energy X-rays

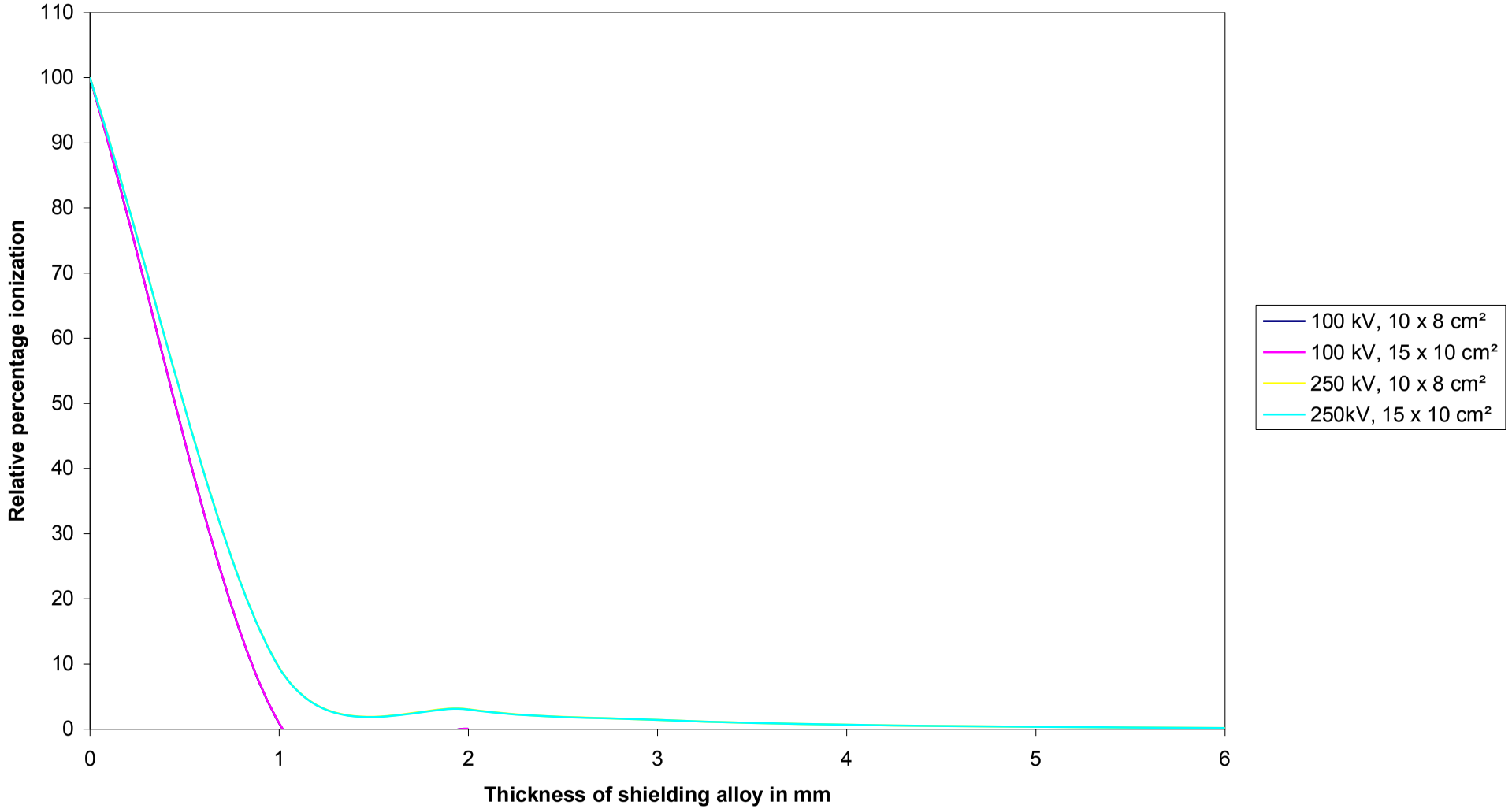

ADDENDUM C

TESTING FOR DEFECTS IN THERMAL-SPRAYED SHEETS OF WOOD'S ALLOY

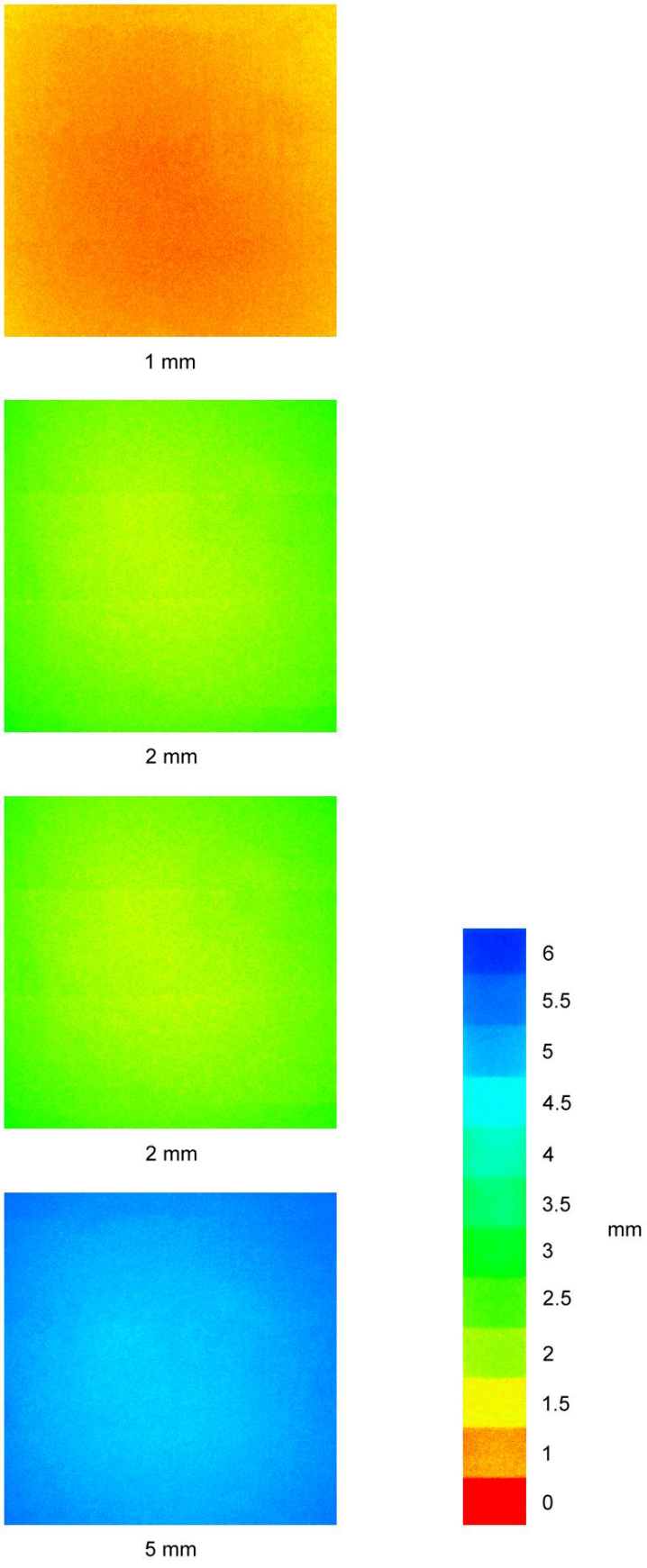

C1 Testing for defects in 1, 2 and 5 mm thermal-sprayed sheets of Wood's alloy

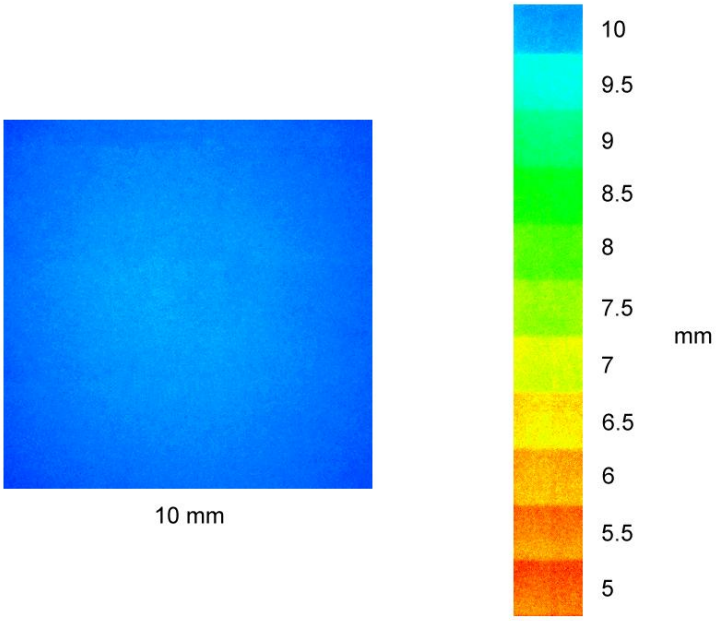

10 mm

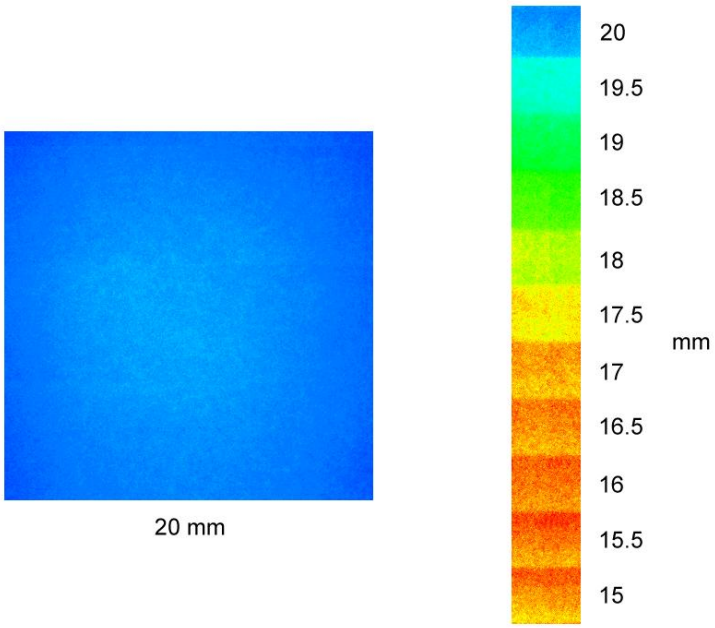

20 mm

C2 Testing for defects in 10 and 20 mm thermal-sprayed sheets of Wood's alloy

ADDENDUM D

PATENT DOCUMENT

REPUBLIC OF SOUTH AFRICA

REPUBLIEK VAN SUID AFRIKA

PATENTS ACT, 1978

CERTIFICATE

In accordance with section 44 (1) of the Patents Act, No. 57 of 1978, it is hereby certified that

CENTRAL UNIVERSITY OF TECHNOLOGY, FREE STATE

has been granted a patent in respect of an invention described and claimed in complete specification deposited at the Patent Office under the number

2005/6444

A copy of the complete specification is annexed, together with the relevant Form P2.

In testimony thereof, the seal of the Patent Office has been affixed at Pretoria with effect from the **24th** day of **July 2006**

Registrar of Patents

FORM P2

MRF Ref: P.20747/DD

REPUBLIC OF SOUTH AFRICA

PATENTS ACT, 1978

REGISTER OF PATENTS

Official Application No.	Lodging date: Provisional	Acceptance date:
21 01 2005/06444	22	47 10-03-06
International classification	**Lodging date: Complete**	**Granted date:**
51	23 23 AUGUST 2005	24-06-06

Full name(s) of applicant(s)/Patentee(s)

71 CENTRAL UNIVERSITY OF TECHNOLOGY, FREE STATE

Applicant(s) substituted:	Date Registered:
71	

Assignee(s):	Date Registered:
71	

Full name(s) of inventor(s)

72 DE BEER, Deon Johan; VAN DER WALT, Jacobus Gert; BARNARD, Ludrick Johannes

Priority claimed	Country		Number		Date	
Note:	33	ZA	31	2003/1770	32	1 March 2003
Use International	33		31		32	
Abbreviation for Country	33		31		32	

Title of Invention:

54 A SPRAY APPARATUS AND METHOD

Address of applicant(s)/patentee(s)

Cor Kolbe Avenue and Victoria Road, Bloemfontein, 9300

Address for Service:

74 **McCALLUM, RADEMEYER & FREIMOND, Maclyn House, 7 June Avenue, Bordeaux, Randburg • P.O. Box 1130, Randburg 2125**

Patent of Addition to Patent No.:	Date of any change:	
61		
Fresh Application based on:	Date of any change:	

A SPRAY APPARATUS AND METHOD

BACKGROUND OF THE INVENTION

[0001] This invention relates to a spray apparatus used for the spraying of molten metal material as well as a method of spraying molten metal material making use of the spray apparatus.

[0002] Skin cancer is treated by radiation with low energy x-rays (100-250kV) or electrons (4-6MeV). Low energy x-rays are produced by a kilovolt unit and electrons with a linear electron accelerator. The size of the electron field is determined by a square or rectangular applicator that attaches to the radiation unit.

[0003] Radiation of a cancerous growth often affects healthy skin between the cancerous growth and the edge of the radiation field. It is known to protect healthy skin from radiation by manufacturing a lead mask which is placed over a part of a patient's anatomy which is to be treated. A cut out, in the form of the cancerous growth, is made in the mask to limit radiation to the area of the cancerous growth.

[0004] The manufacture of the mask is an onerous, time consuming and costly operation. An impression of the affected area on the patient's anatomy is taken by means of plaster of Paris bandages and a female mould is made of the affected area. Once removed the female mould is filled with stone plaster in order to form a male mould of the affected area. The stone plaster is allowed to set and the female mould is removed. A lead sheet with an appropriate thickness, which depends on the intensity of the radiation to be applied, is beaten over the male mould in order for the lead sheet to take the shape of the affected area. The size, shape and location of the cancerous growth is

marked on the lead sheet and a saw is used to cut a hole in the lead sheet which corresponds to the cancerous growth. The completed mask is coated with bee's wax to prevent metal to skin contact during radiation. During treatment the mask is placed over the affected area in order for radiation of healthy skin to be restricted.

[0005] The manufacture of the mask requires skill, effort and is time consuming especially where the lead sheet is thicker than 2mm. The cost of the stone plaster is significant and the mask can only be made once the stone plaster has set completely in order to prevent the disintegration of the male mould during the working of the lead sheet over the male mould.

[0006] As the shape and size of each mask are unique each mask must be custom made for the relevant patient. The recycling of used masks requires that the masks must be melted, the molten material rolled into sheets and that the sheets be cut into appropriate sizes. The recovery process of used masks is in itself a lengthy and costly exercise.

SUMMARY OF INVENTION

[0007] This invention aims to provide a spray apparatus with which molten metal material can be sprayed as well as a method of spraying molten metal material which may be used to manufacture a metal mask for use in the radiation of cancerous growths on the skin of a patient.

[0008] The invention provides a spray apparatus for applying molten metal material to an object which includes an atomizer, feeder means connected to the atomizer to supply the material to the atomizer, which feeder means has a furnace member wherein the material is produced and a conduit formation connected to both the furnace member and the

atomizer through which the material is delivered to the atomizer, and heating means engaged with the feeder means and connectable to a power supply.

[0009] Preferably the atomizer includes a spray gun which pneumatically atomizes the material.

[0010] The heating means may include a first heating element engaged with the furnace member and a second heating element in the form of a coiled wire resistor which is engaged with the conduit formation.

[0011] The spray apparatus may include a third heating element which is engaged with the atomizer.

[0012] The spray apparatus may include a first heat sensor engaged with the atomizer, a second heat sensor engaged with the conduit formation and a third heat sensor engaged with the furnace member.

[0013] The spray apparatus may include a control circuit which is connected to the heating means and the first, second and third heat sensors.

[0014] Preferably the spray apparatus includes air supply means connected to the atomizer. The air supply means may include a compressor, an air tube which extends between the compressor and the atomizer, an air pressure regulator which is connected to the air tube and a valve connected to the air tube.

[0015] The spray apparatus may include a fourth heating element engaged with the air supply means.

[0016] The spray apparatus may include a housing wherein the atomizer is located. The housing may include a sealable cavity formation. The cavity formation may include a drain and an air vent.

[0017] The housing preferably includes a transparent lid member and a switch which is actuated by the lid member.

[0018] The spray apparatus may include a filtration device which is in communication with the cavity formation.

[0019] The filtration device may include a vacuum pump and a boiler. A hose may be attached to the boiler and a circulation pump may be connected to the hose.

[0020] The spray apparatus may include a stand which is insertable into the cavity formation. The stand may include at least one rail with which a runner is movably engaged. The stand may include a rotation means. The rotation means may be a ball and cup joint, alternatively a bearing member.

[0021] The stand may include a holder which may include a platform or a cradle.

[0022] The invention also provides a method of applying a cover to an object which includes the steps of:

a. feeding molten metal material by way of a feeder means to a pneumatic atomizer, which feeder means includes a furnace member wherein the material is produced and a conduit formation connected to both the feeder means and the atomizer through which the material is delivered to the atomizer;

b. heating the material in the feeder means by way of a heating means;

c. atomizing the material by means of the atomizer;

d. and spraying the material onto the object

[0023] The method may include the step of making a mould of an article and of covering at least part of the mould with the material to form the cover over the mould.

[0024] The method may include the step of allowing the material to solidify on the mould to form the cover. The cover may include a mask. Preferably a spray apparatus for applying molten metal material to an object of the aforementioned kind is used in the method.

BRIEF DESCRIPTION OF THE DRAWINGS

[0025] The invention is further described by way of examples with reference to the accompanying drawings in which:

Figure 1 is a perspective top view of a spray apparatus according the invention;

Figure 2 is a schematic representation of the spray apparatus of Figure 1;

Figure 3 is a schematic cross-sectional side view of the spray apparatus of Figure 1; and

Figures 4A and 4B are perspective views of two alternative stands used in the spray apparatus of Figure 1.

DESCRIPTION OF PREFERRED EMBODIMENTS

[0026] Figures 1, 2 and 3 illustrate a spray apparatus 10 for spraying molten metal material 12 which has a housing 14, an open ended cavity 16 in the housing 14, a transparent lid 18 which is hinged to the housing 14 and which lockingly seals the cavity 16, a pneumatic atomizer 20 in the form of a spray gun located in the cavity 16 and housing 14 and a feeder means or arrangement 22 which is connected to the spray gun 20 and which supplies the material 12 to the spray gun 20.

[0027] The housing 14 has two access openings 24A, B which extend into the cavity 16. A left hand glove 26A is attached to the opening 24A and a right hand glove 26B is attached to the opening 24B in order to allow a user (not shown) to extend his hands and arms at least partially into the cavity 16 through the gloves 26. The user can in this manner handle and manipulate the spray gun 20, a stand 28 and an object 30 inside the cavity 16.

[0028] A compartment 32 is formed in the housing 14 below the cavity 16, which compartment 32 is accessible by way of hinged doors 34. The housing 14 is made in a known manner from metal tubing and sheeting. The cavity 16 is made from galvanized steel and is in the form of a square shaped container with a sump plate 36 at its lower end. The sump plate 36 depends downwardly towards a drain hole 38.

[0029] The lid 18 has a metal frame 40 and a transparent Perspex™ sheet 42 is attached to the frame 40. The lid 18 seals the cavity 16 and is lockable to the housing 14 by way of clamp locks 41.

[0030] An air inlet 44 with an air filter 46 is formed through side walls of the housing 14 and cavity 16 and allows airflow from an outside of the housing 14 into the cavity 16.

[0031] The feeder 22 has a furnace or melting vessel 48 which is attached to the housing 14. The vessel 48 has an outer cover 50 which is insulated from an internal holder 52. A first heating element 54 is located inside the holder 52 which is used to melt metal 56 placed in the holder 52. The molten metal material 12 is fed to the spray gun 20 through a flexible metal conduit 58 which extends between the vessel 48 and the spray gun 20. A second heating member 60 in the form of a nickel chrome resistance wire is coiled around the conduit 58.

[0032] The spray gun 20 is of known construction and has a third heating element 62 to heat the material 12 in the spray gun 20.

[0033] The first, second and third heating elements 54, 60, 62 are connected to a control circuit 64 which is fed with electrical power from a power source 66. Sensors 68A, B, C are respectively attached to the spray gun 20, conduit 58 and vessel 48 and are also connected to the control circuit 64. The control circuit 64 measures the temperature of the material 12 in the vessel 48, conduit 58 and spray gun 20 and depending on requirements increases power supply to the first, second and third heating elements 56, 60, 62. This ensures that the material 12 reaches the spray gun 20 at the correct temperature.

[0034] An air supply arrangement 66 is connected to the spray gun 20. The air supply arrangement 66 consists of an air tube 68 and a compressor 70 which is connected to the air gun 20 by the tube 68. An air pressure regulator 72 of known construction is fitted to the tube 68. A solenoid valve 74 is connected to the tube 68 between the compressor

70 and the spray gun 20. The compressor 70 is connected to the power source 66 and generates compressed air in a known manner which is fed to the spray gun 20.

[0035] A drainage pipe 76 is fixed to the drain hole 38 and extends from the cavity 16 into the compartment 32. A particle trap and boiler 78 sits in the compartment 32 and the drain pipe 76 extends into the boiler 78. The boiler 78 has a cup-shaped body 80 which is sealingly closed by a removable cap 82. A horizontally extending buffer plate 84 extends at least partially across the interior of the body 80. A metal water trap 86 stands inside the body 80 below the buffer plate 84 and the drainage pipe 76 extends into the water trap 86. The body 80 is at least partially filled with an appropriate liquid 88 such as for example water. It is important to note that there is enough water 88 in the body 80 to allow the drainage pipe 76 to extend into the water 88 in the water trap 86. A fourth heating element 89 is attached to the cap 82 and extends into the water 88. The fourth heating element 89 is connected to the power source 66.

[0036] A hose 90 is attached to and extends from the body 80 through the cap 82 and into the cavity 16. A circulation pump 92 is connected to the hose 90 to pump heated water 88 from the body 80 into the cavity 16.

[0037] A ventilation pipe 94 extends from the cap 82 to a vacuum pump 96. The vacuum pump 96 is of conventional design and includes known wet and dry particle filters. The vacuum pump 96 is in communication with the boiler 78 and the cavity 16 and withdraws air from the boiler 78 and expels excess air to atmosphere through an outlet 98.

[0038] A contact switch 100 which is actuated by the lid 18 is attached to the housing 14. The switch 100 is connected to the power source 66 as well as the solenoid valve 74 and the vacuum pump 96. When the lid 18 is closed the switch 100 allows the

activation of the vacuum pump 96 and the opening of the solenoid valve 74.

[0039] A stand 28A shown in Figure 4A is used when a small object is sprayed with the material 12 inside the cavity 16 and a stand 28B shown in Figure 4E3 is used in the cavity 16 when a large object is sprayed with the material 12. The stand 28A has a base 102A with two elongate parallel rails 104A. A runner 106A is movingly engaged with the rails 104A and a rotatable and pivotable holder in the form of a turntable 108 is attached to the runner 106A by way of a universal or ball and cup joint 110. The stand 286 has a base 102B with two elongate parallel rails 104B with which a runner 106B is movably engaged. A holder in the form of a cradle 112 is rotatably attached to the runner 106B by way of a bearing member 114. The cradle 112 has a beam 116 which is attached to the bearing member 114 and two spaced apart arms 118 which are movably connected to the beam 116.

[0040] In use the metal 56 which has a low melting point of between 70°C and 75°C is inserted into the vessel 48. Metal alloy materials such as those sold under the trade names MCP70™, WOOD'S ALLOY™ or FRY'S METAL™ can be used. Depending on the melting point of the metal 56 the control circuit 64 applies an appropriate power supply to the first heating element 54 to melt the metal 56. The sensors 68A, B, C measure the temperature of the material 12 and the measurements are relayed to the control circuit 64. By controlling the power supplied to the first, second and third heating elements 54, 60, 62 the temperature and liquidity of the material 12 are controlled.

[0041] The appropriate stand 28 is inserted into the cavity 16, the object 30 which is to be covered or sprayed with the material 12 is placed on the stand 28 and the lid 18 is closed, sealed and locked. As the lid 18 is closed the contact switch 100 causes the opening of the solenoid valve 74 and activates the vacuum pump 96.Compressed

air 124 is supplied to the spray gun 20 from the compressor 70 by way of the tube 68. The pressure of the compressed air 124 is regulated by the regulator 72. In the event that the lid 18 is inadvertently opened the switch 100 causes the solenoid valve 74 to close and the supply of compressed air 124 to the spray gun 20 is interrupted.

[0042] The vacuum pump 96 withdraws air from the boiler 78 by way of the ventilation pipe 94. In order to fill the vacuum created in the boiler 78 air is drawn from the cavity 16 through the drain hole 38 and drain pipe 76 into the boiler 78. Air drawn from the cavity 16 is fed through the water 88 in the water trap 86. The buffer plate 84 prevents water 88 from splashing out of the body 80 into the ventilation pipe 94.

[0043] The vacuum created in the cavity 16 is filled by air which is drawn from atmosphere through the inlet 44 and filter 46 or fed through the spray gun 20 from the compressor 70.

[0044] In order to operate the spray gun 20 a user grips the spray gun 20 by means of his hands which are inserted into the cavity 16 through the gloves 26A, B. The spray gun 20 is operated and the material 12 is atomized and sprayed onto the object 30. The number of layers of material 12 sprayed onto the object 30 depends on the required thickness of a metal cover 130 formed over the object 30. The second and third heating elements 60, 62 ensure that the material 12 atomized by the spray gun 20 is in the molten state. Once the material 12 is sprayed onto the object 30 the material 12 cools, solidifies and sets to form the cover 130 on the object 30.

[0045] Once the cover 130 has reached its desired thickness the spray gun 20 is deactivated and set aside and the compressor 70 is switched off. The user removes the object 30 and cover 130 from the holder 28 and activates the circulation pump 92. The fourth heating element 89 heats the water 86 to boiling point and the boiling water 88 is

delivered to the cavity 16 by way of the hose 90. The user uses the hose 90 and water 88 to clean all contact surfaces inside the cavity 16. Any excess metal 56 in the cavity 16 is melted by the water 88 and washed away along the sump plate 36 and through the drain hole 38 and drain pipe 76 into the water trap 86. In this manner any material 56 which remains in the cavity 16 is removed, scrubbed and trapped in the water trap 86 and boiler 78. The wet and dry particle filters in the vacuum pump 96 remove any particles which might escape the water trap 86 and boiler 78. The waste metal 56 trapped in the water trap 86, boiler 78 and vacuum pump 96 is recovered for re-use.

[0046] Once the cavity 16 is cleaned the lid 18 is opened in order to remove the object 30 and cover 130 from the cavity 16. The cover 130 is removed from the object 30 and processed as required.

[0047] In this example cold compressed air 124 is fed to the spray gun 20 from the compressor 70. It is however possible to attach a fifth heating element 132 in the form of a heat radiator to either the compressor 70 or inline on the tube 68. It is also possible to combine the compressor 70 and vacuum pump 96 in order to form a closed circuit for air movement through the spray apparatus 10.

[0048] An important application of the spray apparatus 10 is the manufacture of metal masks used in radiation treatment of cancerous skin growths. In order to manufacture such a mask a female mould (not shown) is taken of the relevant area of the patient's anatomy. This female mould is made from plaster of Paris bandages. Once the female mould has set the mould is removed and a male mould made from plaster of Paris is cast inside the female mould. Once set, the male mould is removed and used as the object 30. The cover 130 applied to the male mould 30 is in the form of a metal mask. The mask 130 is removed from the male mould 30 and an appropriately sized and shaped

aperture is burnt through the mask 130 through which the cancerous growth can be radiated. As a final step a clear lacquer is applied to the mask 130 to prevent metal to skin contact. The mask 130 is thereafter used in the conventional manner.

[OO49] When the mask 130 is discarded the mask 130 is broken into appropriate sized pieces to provide a source of the metal 56 which is re-used.

[0050] By limiting the use of hardened settable materials such as stone plaster which takes time to set, the manufacture of the male mould and the production time of the mask 130 are reduced. The use of softer materials for the male mould also results in cost savings. Recovery of the metal 56 from which the mask 130 is made is also improved.

[0051] The material 12 is sprayed onto the object 30 in the sealed cavity 16 in order to prevent accidental inhalation of the atomized material 12 by the user as this could be damaging to the user's health. For the same reason the air and excess material 12 in the cavity 16 are and withdrawn therefrom, and are washed, scrubbed and filtered

CLAIMS

1. A spray apparatus [10] for applying molten metal material [12] to an object [30] which includes an atomizer [20], feeder means [22] connected to the atomizer to supply the material to the atomizer, which feeder means has a furnace member (50] wherein the material is produced and a conduit formation [58] connected to both the furnace member and the atomizer through which the material is delivered to the atomizer, heating means [54,60] engaged with the feeder means and connectable to a power supply [66] and characterised in a housing [14] which has a sealable cavity formation [16] wherein the atomizer is located.

2. A spray apparatus according to claim 1 characterised therein that the atomizer includes a spray gun [20].

3. A spray apparatus according to claim 1 or 2 characterised therein that the heating means includes a first heating element [54] engaged with the furnace member.

4. A spray apparatus according to claim 1, 2 or 3 characterised therein that the heating means includes a second heating element [60] which is engaged with the conduit formation.

5. A spray apparatus according to claim 4 characterised therein that the second heating element includes a coiled wire resistor [60].

6. A spray apparatus according to any one of claims 1 to 5 characterised therein that it includes a third heating element [62] engaged with the atomizer.

7. A spray apparatus according to any one of claims 1 to 6 characterised therein that it includes a first heat sensor (68A) engaged with the atomizer.

8. A spray apparatus according to any one of claims 1 to 7 characterised therein that it includes a second heat sensor [68B] engaged with the conduit formation.

9. A spray apparatus according to any one of claims 1 to 8 characterised therein that it includes a third heat sensor [68C] engaged with the furnace member.

10. A spray apparatus according to any one of claims 1 to 9 characterised therein that it includes a control circuit [64] connected to the heating means.

11. A spray apparatus according to any one of claims 1 to 10 characterised therein that it includes air supply means [66] connected to the atomizer.

12. A spray apparatus according to claim 11 characterised therein that the air supply means includes a compressor [70].

13. A spray apparatus according to claim 12 characterised therein that the air supply means includes an air tube [68] which extends between the compressor and the atomizer.

14. A spray apparatus according to claim 13, characterised therein that the air supply means includes an air pressure regulator [72] which is fitted to the air tube.

15. A spray apparatus according to claim 13 or 14 characterised therein that the air supply means includes a valve [74] connected to the air tube.

16. A spray apparatus according to any one of claims 11 to 15 characterised therein that it includes a fourth heating element [132] engaged with the air supply means.

17. A spray apparatus according to any one of claims 1 to 16 characterised therein that the cavity formation includes a drain [38].

18. A spray apparatus according to any one of claims 1 to 17 characterised therein that the cavity formation includes an air vent [44].

19. A spray apparatus according to any one of claims 1 to 18 characterised therein that the housing includes a transparent lid member [18].

20. A spray apparatus according to claim 19 characterised therein that the housing includes a switch [100] which is actuated by the lid member.

21. A spray apparatus according to any one of claims 1 to 20 characterised therein that it includes a filtration device [78,86,96] in communication with the cavity formation.

22. A spray apparatus according to claim 21 characterised therein that the filtration device includes a vacuum pump [96].

23. A spray apparatus according to claim 21 or 22 characterised therein that filtration device includes a water trap [78,86].

24. A spray apparatus according to claim 21, 22 or 23 characterised therein that the filtration device includes a boiler [78].

25. A spray apparatus according to claim 24 characterised therein that it includes a hose [90] attached to the boiler and a circulation pump [92] connected to the hose.

26. A spray apparatus according to any one of claims 1 to 25 characterised therein that it includes a stand [28] which is insertable into the cavity formation.

27. A spray apparatus according to claim 26 characterised therein that the stand includes at least one rail [104] with which a runner [106] is movably engaged.

28. A spray apparatus according to claim 26 or 27 characterised therein that the stand includes a rotation means [110,114].

29. A spray apparatus according to claim 28 characterised therein that the rotation means includes a ball and cup joint [110].

30. A spray apparatus according to claim 28 characterised therein that the rotation means includes a bearing member [114].

31. A spray apparatus according to any one claims 26 to 30 characterised therein that the stand includes a holder [108,118].

32. A spray apparatus according to claim 31 characterised therein that the holder includes a platform [110].

33. A spray apparatus according to claim 31 characterised therein that the holder includes a cradle [118].

34. A method of applying a cover [130] to an object [30] which includes the steps of:

a. making a mould of an article to form the object;

b. feeding molten metal material to a pneumatic atomizer [20] by way of a feeder means [22], which feeder means includes a furnace member [50] wherein the material is produced and a conduit formation [58] connected to both the feeder means and the atomizer through which the material is delivered to the atomizer;

c. heating the material in the feeder means by way of a heating means [54,60,62];

d. atomising the material by means of the atomizer; and

e. spraying the material over the object,

35. A method of applying a cover according to claim 34 characterised therein that it includes the step of allowing the material to solidify on the object to form the cover.

36. A method of applying a cover according to claim 34 or 35 characterised therein that the cover includes a mask [130].

37. A method of applying a cover according to claim 36 characterised therein that the mask is used for the radiation treatment of cancerous skin growths.

FIG 1

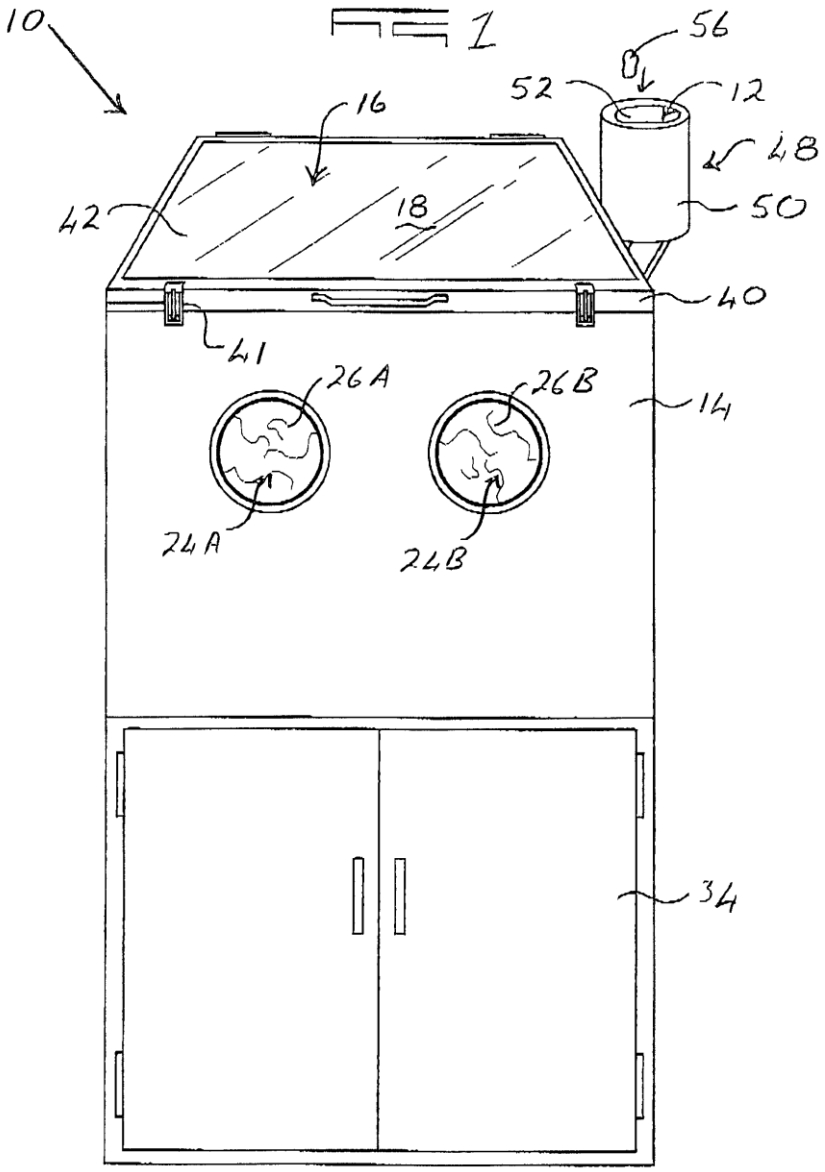

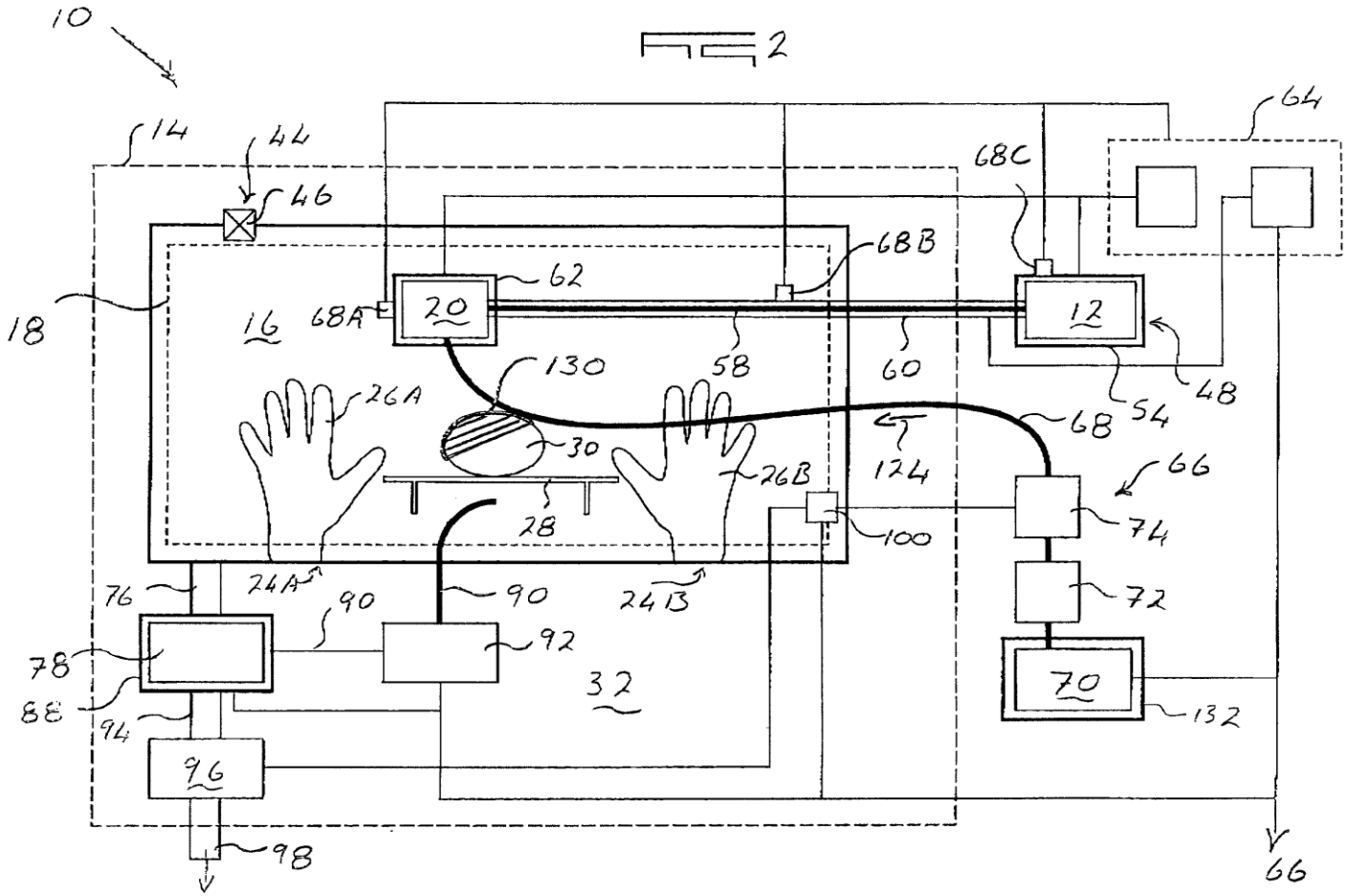
10
FIG 2
14
44
46
64
68C
68B
62
18
16
68A
20
12
58
60
54
48
130
26A
68
124
30
26B
66
28
100
74
76
24A
90
90
24B
72
78
92
32
70
88
94
132
96
98
66

FIG 3

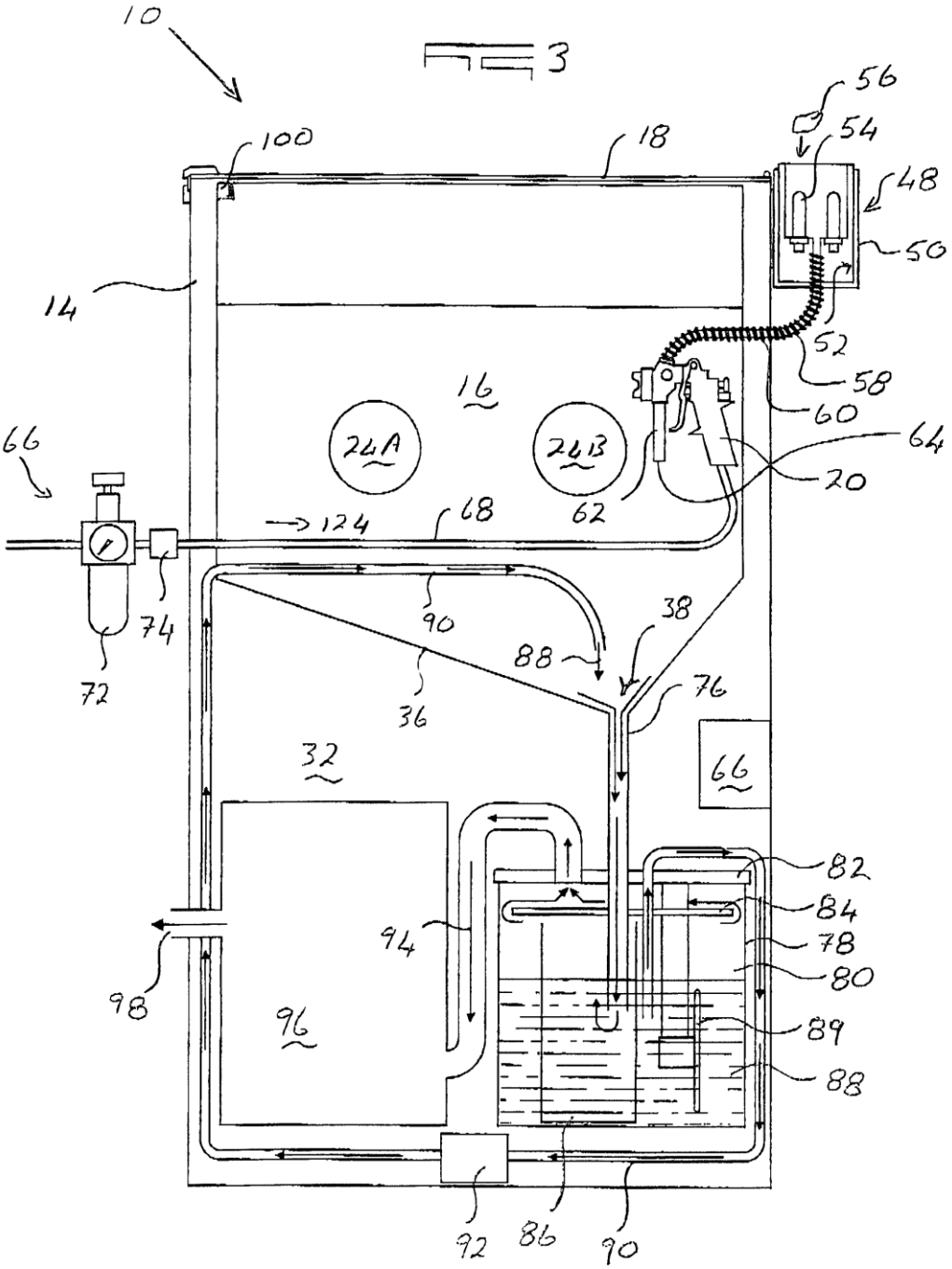
10
100
18
56
54
48
50
14
52
58
60
16
24A
24B
62
64
20
66
124
68
74
72
90
38
88
36
76
66
32
82
84
78
80
94
98
89
96
88
92
86
90

FIG 4

FIG 4A

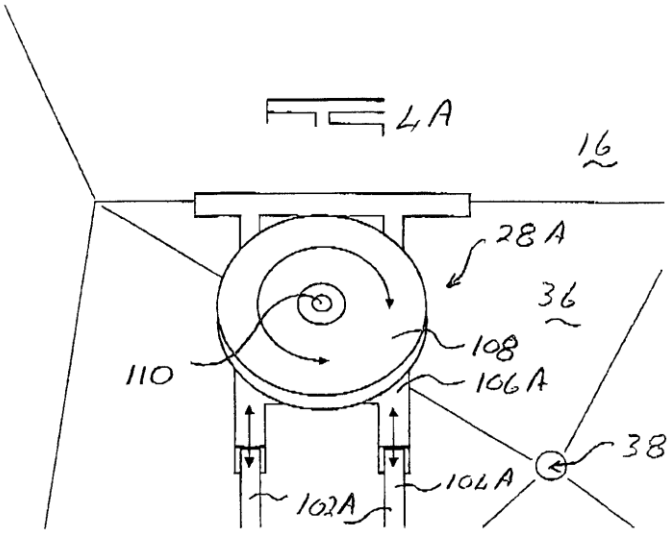
16
28A
36
108
110
106A
38
104A
102A

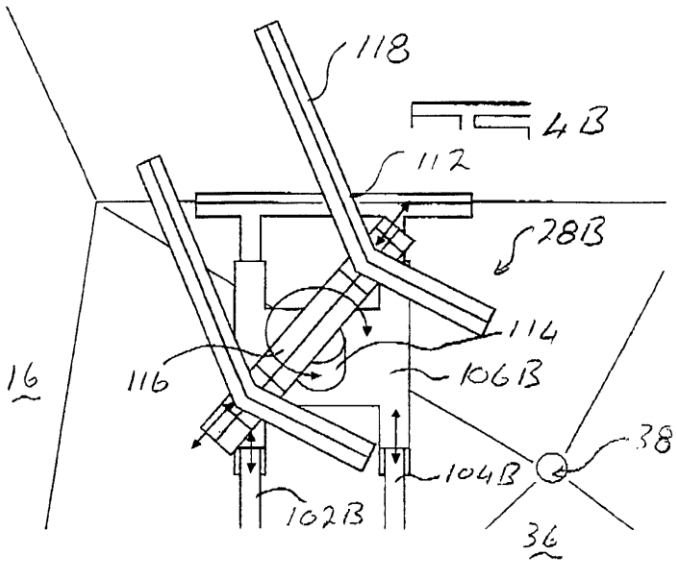
118
FIG 4B
112
28B
114
16
116
106B
38
104B
102B
36

ADDENDUM E

PUBLISHED ARTICLE

ISSN 1355-2546
Volume 11 Number 5 2005

Rapid Prototyping Journal

The international journal on technologies for rapid product development and direct manufacturing

www.emeraldinsight.com

Emerald

Rapid Prototyping Journal

Volume 11, Number 5, 2005

ISSN 1355-2546

Contents

Rapid manufacturing of patient-specific shielding masks, using RP in parallel with metal spraying

Deon J. de Beer, Michéle Truscott, Gerrie J. Booysen, Ludrick J. Barnard and Jakobus G. van der Walt
Central University of Technology, Free State, Bloemfontein, South Africa

Abstract
Purpose – The purpose of the present work is to develop a methodology to manufacture patient-specific models (lead masks) to be used as protective shields during cancer treatment, using 3D photography, rapid prototyping (RP) and metal spraying. It is also intended to reduce the trauma experienced by the patient, by removing any physical contact as with conventional methods, and also to reduce the manufacturing lead time.
Design/methodology/approach – Patient-specific data are collected using 3D photography. The data are converted to.STL files, and then prepared for building with an LS 380 in nylon polyamide. Next, the sculpted model is used as the mould in a newly patented metal-spraying device, spraying liquid metal on to the sculpted surface.
Findings – Intricate body geometries can be reproduced to effectively create metal shields, to be used in radiography applications. The models created fit the patients more accurately than through conventional methods, reducing the trauma experienced by the patient, and in a reduced time-frame, at similar costs to conventional methods. The new process and its materials management are less of a an environmental risk than conventional methods.
Research limitations/implications – Access to 3D photography apparatus will be necessary, as well as to RP or CNC equipment. Using this approach, files can be transferred to a central manufacturing facility, i.e. hospitals or treatment units do not need their own facilities. Added implications are the design of jigs and fixtures, which will ensure accuracy in reuse.
Practical implications – Metal shields can be created with ease and great accuracy using RP machines. It takes less time without inflated costs. Models are more accurately and easy to use, with less trauma experienced by the patient during the manufacturing phase.
Originality/value – Novel applications, combined with a new process. The research expands the fast-growing field of medical applications of RP technologies. Its practical application will benefit patients on a daily basis.

Keywords Cancer, Lead, Lasers, Sintering, Metals, Spraying

Paper type Case study

1. Introduction

The *Concise Encyclopaedia of Science and Technology* (Yule, 1985) describes cancer as

> A group of diseases in which some body cells change their nature, start to divide uncontrollably and may revert to an undifferentiated type. They may form a malignant tumour, which enlarges and may spread to adjacent tissues. In many cases cancer cells enter the blood or lymph system and are carried to distant parts of the body.

Although the mortality rate due to skin cancer is high, treatment can be curative in some instances if carried out in the early stages. Caccialanza *et al.* (2004) reviewed 115 cases in 108 patients and report complete remission in 96.52 per cent cases. Treatments include surgical excision, radiation therapy, chemotherapy or combinations of these. The latter of the two methods are used to destroy or slow down the growth of cancerous cells. The difficulty, however, is to do so without also damaging healthy tissue. Sanghera *et al.* (2001) discussed the manufacturing of shields from plaster of paris moulds, and described the process as crude and unpleasant for the patient. Rapid prototyping (RP) offers numerous possibilities to support the medical profession, some of which may impact positively on the conventional approaches.

In radiotherapy, it is necessary to differentiate between superficial and deep cancer treatment. Radiation of skin cancer (commonly found amongst fair skinned people in countries with a high intensity of sunshine) is a typical example of superficial cancer treatment while deep treatment will involve radiation treatment of internal organs, glands and so forth. This paper focuses on the use of 3D photography, RP and a customised metal spraying process to "manufacture" shields to protect healthy tissue during the treatment of superficial cancer infiltration.

2. Treatment procedure

The radiation treatment required for superficial infiltration depends on the degree of cancer infiltration required. For very

The Emerald Research Register for this journal is available at
www.emeraldinsight.com/researchregister

The current issue and full text archive of this journal is available at
www.emeraldinsight.com/1355-2546.htm

Rapid Prototyping Journal
11/5 (2005) 298–303

[DOI 10.1108/13552540510623611]

Received: 17 December 2004
Revised: 17 June 2005
Accepted: 23 June 2005

superficial infiltration, low energy X-rays ((100-250 kV) or electrons (4-10 MeV)), as produced by a kilovolt unit, will be sufficient. Once the degree of infiltration has been determined and the level of radiation energy selected for treatment, a radiation field size needs to be decided upon. Each treatment unit is equipped with a number of standard applicators that determines the field sizes available from which therapists can select a suitable applicator.

A typical problem is that applicators produce either a rectangular, square or round field shapes, while the cancerous growths normally are irregular in shape as shown in Figure 1. There will thus always be an area of healthy tissue between the edges of the growth and the field's edges. Physicians create blocking devices to shield the healthy tissue surrounding the tumour from radiation. The shields are normally made from alloys of which the density is close to that of lead, but easier to mould, due to a lower melting temperature, and the need to be individualised for each patient (Cancer Research, 2005; Lowell, 2005; Willis-Knighton, 2004).

Furthermore, the part of the applicator making contact with the patient's skin is flat, as shown in Figure 2. Should the exposed area be large and curved, there will be a considerable amount of scattering past the field's edges. This is especially problematic with electron treatments since the electrons scatter past the edges of the treatment field, resulting in a larger area being irradiated than intended – exposing a larger part of the patient's body (normally healthy flesh) to radiation.

Figure 1 Irregular shaped cancerous growth in rectangular treatment field

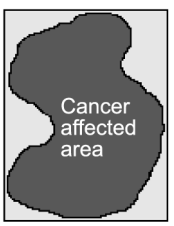

Figure 2 Electron applicator in contact with patient's skin

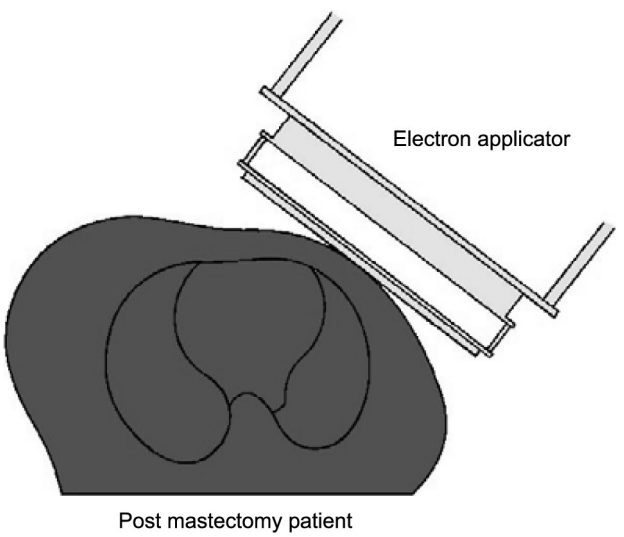

Plate 1 shows a film, placed on a curved phantom and which was irradiated with electrons to simulate a patient's treatment. (Note: A phantom is a term that is used in radiography for an object that will closely resemble the shape of a human body, or part of the body, and which is normally manufactured from a medium that also has the same density as human tissue, for radiography purposes.)

The original treatment field size is shown by the rectangle, thereby highlighting the degree of scatter past the field's edges.

2.1 Traditional shielding methods

The traditional way to reduce the degree of scatter is to shield the healthy tissue, surrounding the cancerous growth, by means of a lead mask or a wax mould. A lead mask would typically be used for skin cancer. In order to fabricate such masks, an impression of the cancer-affected area on the patient needs to be taken by means of plaster bandages. When the plaster bandages have set, they are removed from the patient and Yellow-Stone™ plaster is moulded into the negative impression they create. After the plaster has set, the bandages are removed to release a positive impression of the patient. Next, a lead sheet with a thickness corresponding to the intensity of the radiation to be applied during treatment is formed onto the impression with a special hammer. Lastly, a hole is sawn into the mask, according to the position of the cancerous growth on the patient, allowing radiation only to pass through the selected area during treatment. Plate 2 shows a lead mask on a plaster impression of the patient.

2.2 Disadvantages of the lead mask technique

The following are disadvantages of the lead mask technique:

- The Yellow-Stone™ plaster has to be left at least overnight to harden sufficiently to prevent it from breaking up while forming the lead sheet on it. A technologist can thus at earliest, only start fabricating the mask a day after the plaster bandage impression was taken.
- The technique of forming the lead sheet on the model requires a great deal of skill, effort and time – especially if the lead sheet is thicker than 2 mm.
- It is difficult to recycle the lead since it has to be melted and rolled into a sheet to be used again. Radiotherapy departments subsequently seldom do this, which makes the lead mask technique expensive, and it contributes to environmentally unfriendly waste.

Plate 1 Film taken on curved phantom

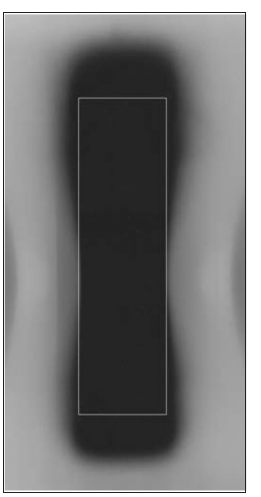

Plate 2 Lead mask

- The procedure of taking a plaster bandage impression of a patient, especially in the facial area, is often traumatic and uncomfortable for the already traumatised patient.

Various data sources consulted, mention the practice of manufacturing a lead shield on an individual (customised) basis, according to patient/physician needs. The process, however, is not well described or published, except for remarks that it is a crude and an unpleasant process for the patient (Sanghera *et al.*, 2001). This work also mentioned the production of waste products, and a messy environment, which necessitates dedicated/facilities for material storage and disposal. Furthermore, face-movement during formation of the positive with a conventional process using Yellow-Stone™ is a recognised problem.

3. Development of the new process

The ideal would therefore be to create a process chain, which can replicate the patient's affected area without physical contact with the patient. Cutting the Yellow-Stone™ plaster out of the process would result in enormous time-savings. It would also contribute to relieve the trauma experienced by patients receiving treatment. Furthermore, the process of forming the lead onto the mask should be replaced by a faster, easier and more controllable method.

As a hypothetical solution, the following process chain was envisaged:

1 *Reverse engineering.* Creation of 3D computer data (.STL) of the patient's affected area through 3D photography.
2 *Rapid prototyping.* A physical model of the 3D data in a suitable RP material through laser sintering.
3 *Metal spraying.* Manufacturing of a lead mask fitting the physical model through the use of metal spraying.

3.1 Reverse engineering

Through the use of a 3D camera (Minolta Vivid 910), the geometry of treatment areas can be captured. The benefit of this process is that no physical contact with the patient is necessary, which means no plaster bandages that need to set, no pipes in a patient's nose, mouth, etc. and no contact with possibly irritated skin. Output formats from the Minolta Vivid 910 supports various commercial software systems including Alias Wavefront/Maya, 3D Studio Max, Raindrop Geomagic, Softimage, Lightwave, RapidForm and is applicable to RP, reverse engineering, CAD/CAM and 3D modelling technologies. Figure 3 shows the steps that are involved in the 3D capturing of facial-data.

3.2 Rapid prototyping

Laser sintering with nylon polyamide was selected as the RP technology, as it offers various advantages over other RP systems available in the research facility, namely:

- No support system is needed, as the powder supports itself, thus reducing post-growing cleanup.
- Thin walled parts can be grown, which will save both time and costs.
- Durability of prototypes which have to be used as a model for the metal to be sprayed upon. Material flexibility will also allow bending/flexing to release the sprayed metal.

3.3 CNC machining

Using the scanned data, either from.STL or IGES format, CNC codes can be generated, to use three axis CNC milling as alternative to produce the facial geometry. As the cutting media, Superwood™ would be used. Various CAD/CAM packages are commercially available to execute the operation, using.STL files as input. Except for undercuts that may occur in the nose and ear environments, the milling is an easy operation, and should be a mere formality for any experienced CNC operator.

3.4 Metal spraying

To overcome some of the disadvantages of the lead mask and wax mould techniques, the possibility of using a custom-designed metal spray technique to fabricate shielding masks was investigated.

The design criteria for the metal spray equipment were:

- The metal spraying process needs to be clean, since the equipment will be used in a hospital set-up.
- The equipment should be user friendly and not expose the operator or the immediate environment to hazardous metal dust or gasses.
- The metal used in the process should be recoverable in order to make the technique cost-effective.
- The equipment should be able to lay down low melt alloy up to a thickness of 12 mm on a field size of $400 \times 400\,mm^2$ in a reasonably short time-frame.
- It should be possible to fabricate the metal spray equipment with locally available tools and machinery from affordable components to make the project financially viable.

Figure 3 Process of 3D photograph assembly

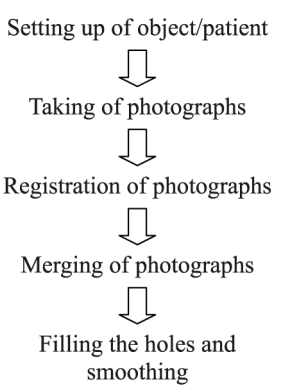

3.5 Low melting point alloys

The alloy considered for fabricating the masks was commercially available under the trade names of Wood's alloy™, MCP 70™ or Fry's metal™. These alloys are commonly used for shielding radiation sensitive areas during high-energy radiation in radiotherapy. It is cast in 9 cm blocks according to the shape of the area to be shielded, and is placed in the radiation field during treatment. The alloys consist of mixtures of bismuth, tin, lead and cadmium and have a melting points within the region of 70°C.

Because of its low melting point, it was considered to use it in a liquid state. This would be a less complex procedure to feed the alloy to the spray gun, as opposed to the solid or powder form as is done with commercially available metal spray equipment. The technique would offer a high metal flow-rate, resulting in a rapid build-up of metal on the substrate during spraying.

4. Results

4.1 3D scanning

Using a Minolta scanner, facial-data can be scanned, and manipulated through a few easy steps. Plates 3 and 4 show the scanning and image processing, whilst Plates 5 and 6 show the STL data obtained through Magics RP.

4.2 Rapid prototyping

Laser sintering, applied through an EOS P380 machine was selected as the method of prototyping. Nylon polyamide was used due to its thin walled characteristics. Horizontal growing of a face image in 2.5 mm wall-thickness (119 mm diameter and a highest point of 50 mm high, weighing 30 g, and with total material volume of 32,006 mm^3) was achieved in 3.5 h. Growing the model upright, would take 6.25 h.

4.3 Metal spraying

Through a newly patented metal spraying process (PCT/04/00021), the metal is sprayed in an enclosed cabinet, operated by a spray gun, accessed through rubber gloves. The spray gun is similar to that used for spray paint purposes but was modified by attaching a heating element to its frame.

Molten metal is fed from a double walled (insulated) melting pot attached to the outside of the cabinet by means of

Plate 3 Scanning process

Plate 4 Image processing

Plate 5 .STL data processing

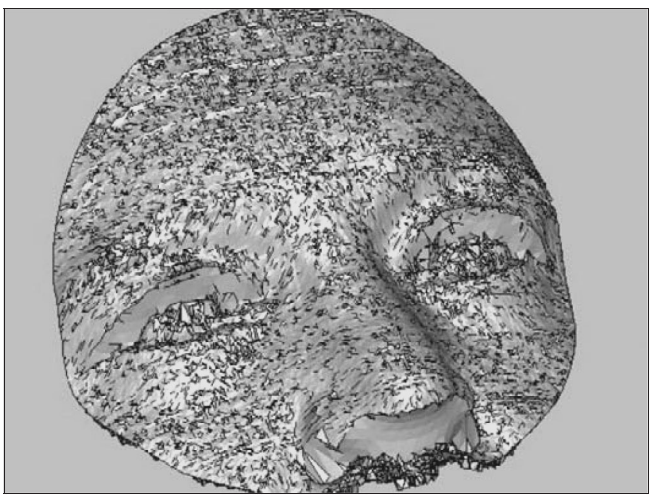

Plate 6 .STL data processing

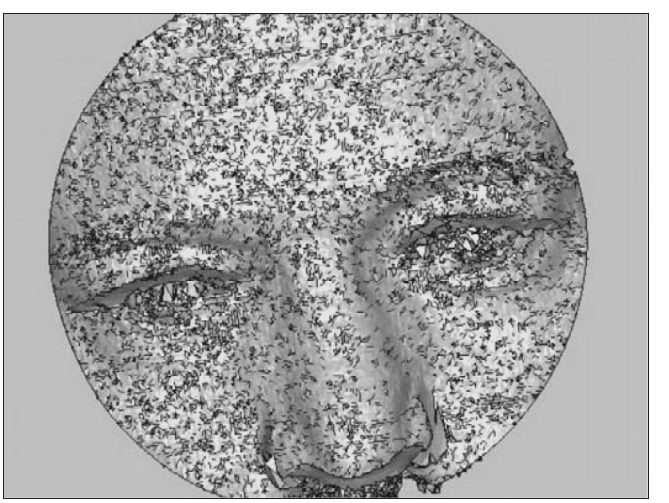

a heated feeding tube, to prevent the metal from cooling and setting while passing through the tube. Compressed air is supplied to the spray gun via a pressure regulator/water trap to ensure a constant flow of clean air. A 4 mm thick mask, weighing 629 g, was achieved in 2.5 h.

Plate 7 shows the initial mask, manufactured on traditional Yellow-Stone™ plaster mould, whilst Plate 8 shows the RP and sprayed metal mask.

Table I gives a comparison between the traditional masking technique and the newly developed metal spray masks. In order to do a complete comparison, time and cost estimation is included for the conventional method and for RP using SL.

5. Conclusions

Contrary to the conventional process, data capturing with 3D photography proved to be an effective method, both in time taken, as well as the fact that no physical contact with the patient was necessary. RP, although fast and efficient, unfortunately is far more expensive than the conventional method. However, if patient trauma and production costs (man hours), skills needed or specialised storage/material wastes are taken into account, RP costs become less of a factor. The high degree of accuracy and speed involved in the 3D photography/RP process eliminates previous problems such as inaccuracy due to movement during casting or setting of the plaster bandages, and offers better treatment/isolation due to improved definition of face edges, such as the chin. Due to the nature of the combined RP/3D photography method, radiography units not having access to biomedical engineering support may be serviced over any given distance. The recycling of material also becomes a much more environmentally-friendly process, which further impacts on hospital facilities, and may impact on the evaluation of the RP costs.

A further "mechanical" advantage of the new process is having the face data in a 3D format, which allows "construction" or modelling and addition of features in CAD to include fixation accessories or other needs, prior to RP model fabrication. Other medical benefits include

Plate 7 Initial mask manufactured on Yellow-Stone™ plaster mould

Plate 8 RP and sprayed metal mask

Table I Comparison between traditional masking techniques and metal spray masks

Manufacturing method	Production time	Cost	Comments
Lead mask	48 h	Lead: R185/kg Approximately 2 kg of Yellow-Stone™ used at R10/kg Human inputs/costs: Approximately R1500	To withstand the lead-forming process, the plaster needs to be completely dry
RP	3.5 h	Nylon: R2300	Although initially expensive, costs are limited because the alloys can be recycled. Also, if facility management is such that more than one mask can be grown simultaneously, costs will drastically come down
Metal spraying	2.5 h	Approximately 1 kg of material melted, to produce a 629 g mask Human inputs/costs less that R300	
CNC	3 h	Using Superwood™: R1850	Probably the fastest method, but less easy to use for undercuts
Metal spraying		Same as above	

the possibility that the radiologist can mark exact areas on the patient's face or body to be treated, with "markers" which can be transferred to CAD through the reverse engineering process. Next, precise geometry can be modelled in CAD, which may be turned into a positive "feature" that will "prevent" metal to be sprayed on a well-defined geometry. Through the use of specialised software such as MedCad from materialise, modelling can be done in the.STL environment.

Initial investigations into the use of CNC milling as an alternative to produce the external geometry of the face mask, has shown that it would take approximately 2 h to prepare the CNC file, together with another 2 h to execute the milling, making this the fastest prototyping route. Costs compare favourably to RP costs (about 80 per cent of the costs involved for the growing of one mask). These estimates have been added to Table I. However, it should be borne in mind that the price used is for the growing of one mask. Should two or more masks be grown simultaneously, the RP cost is lowered drastically, and might outperform any of the other processes. Furthermore, the addition of devices such as fixtures, buckles, etc. may not be as easy in CNC. It is, however, acknowledged that further research into the combination of 3D/CNC and customised CNC machines/processes may impact on the manufacturing costs and delivery time.

References

Caccialanza, M., Piccinno, R., Kolesnikova, L. and Gnecchi, L. (2004), "Radiotheraphy of skin carcinomas of the pinna: a study of 115 lesions in 108 patients", *International Journal of Dermatology*.

Cancer Research (2005), *Treating Skin Cancer*, Cancer Research, Lincoln's Inn Field, London, PO Box 123, available at: www.cancerhelp.org.uk/help/default.asp?page = 4313 (accessed 7 July 2005).

Lowell General Hospital (2005), *Services and Specialities: The Cancer Center – Radiation Oncology*, Lowell General Hospital, Amherst, MA, available at: www.lowellgeneral.org/features/services/cancercenter/radiation.asp (accessed 8 July 2005).

Sanghera, B., Naique, S., Papaharilaou, Y. and Amis, A. (2001), "Preliminary study of rapid prototype medical models", *Rapid Prototyping Journal*, Vol. 7 No. 5, pp. 275-84.

Willis-Knighton (2004), *Available Treatments*, Willis-Knighton Cancer Center, Department of Radiation Oncology, Shreveport, LA, available at: www.wkmc.com/cancerftr/treat.html (accessed 8 February 2004)

Yule, J.D. (1985), *Concise Encyclopaedia of Science and Technology*, Peerage Books, London, 59 Grosvenor Street, W1.